2.13 Measuring High-Pressure Electronic and Magnetic Properties

RJ Hemley and VV Struzhkin, Carnegie Institution of Washington, Washington, DC, USA
RE Cohen, Carnegie Institution of Washington, Washington, DC, USA; University College London, London, UK
G Shen, Carnegie Institution of Washington, Argonne, IL, USA

This chapter is a revision of the previous edition chapter by R H Genketm, V V Struzhkin, and R E Cohen, Volume 2, pp. 293–367, © 2007, Elsevier B.V.

Glossary

Bonding in deep Earth materials Description of the binding between atoms and molecules in substances that comprise the interior of the planet, typically the mantle and core.

Bonding under high *P–T* conditions Description of the binding between atoms and molecules at high pressures and temperatures such as those that characterize the Earth and other planets.

Brillouin and Rayleigh scattering Inelastic light-scattering technique in which light is scattered off areas of altered density caused by acoustic waves in a material.

Charge transfer Excitations or bonding states derived by promotion of an electron from one atom or molecule to another atom or molecule.

Compton scattering (CS) Inelastic scattering of x-ray radiation typically used to probe electron momentum distributions.

Conventional bonding classification The description of binding forces in atoms and molecules found in gases, solids, and liquids under ambient or near-ambient conditions, specifically covalent, ionic, metallic, van der Waals, and hydrogen-bonding.

Crystal field transitions Excitations between quantum states of an atom, ion, and molecule inside a crystal where the states are perturbed (e.g., degeneracies lifted) by the symmetry of the site of the crystal.

de Haas–van Alphen Technique for measuring Fermi surfaces of metals in a magnetic field.

Defect excitations Transitions or spectral features arising from defects in the material, including color centers.

Dielectric functions The response of a material to an applied electric field.

Elastic neutron scattering Scattering of neutron without a change in particle energy, as in typical neutron diffraction.

Elastic x-ray scattering Scattering of x-rays without changes in photon energy as in typical x-ray diffraction, may be either coherent or incoherent.

Electrical conductivity Movement of charge in a system in response to an applied electric field (static or frequency-dependent) and can be intrinsic or extrinsic, electronic or ionic.

Electron paramagnetic resonance (EPR) Technique that involves resonant microwave absorption between electronic energy levels split in a magnetic field (the Zeeman effect).

Electronic inelastic x-ray scattering (EIXS) Technique to probe electronic excitations such as core level, plasmons, and electronic bands, using x-rays, including momentum q dependence.

Electronic structure Quantum description of electrons in an atom, molecule, or condensed phase (i.e., crystal, liquid, fluid, or glass).

Excitons Well-defined quantum excitations or quasi-particles such as bound electron–hole pairs in crystals.

Extended excitations Spectral transitions that involve electronic states that are coherent over long distances, as in a metal.

High *P–T* CARS Coherent anti-Stokes Raman scattering, a nonlinear optical technique whereby a pump beam ω_P and a Stokes beam ω_s are mixed via third-order susceptibility, typically used to study vibrational transitions.

Inelastic x-ray scattering spectroscopy (IXSS) General class of techniques that measure excitation spectra, probes the dynamical structure factor.

Infrared spectroscopy Class of techniques that use radiation from 10 to 10 000 cm^{-1} in absorption, emission, or reflectivity and used to study vibrational, electronic, and magnetic excitations.

Iron and iron alloys Soft, silver-colored metal with an atomic number of 26; the most abundant transition element in the solar system; iron alloys are a mixture of iron and other elements.

Kramers–Kronig analysis Mathematical treatment that uses causality to determine the full set of optical constants of a material as a function of frequency to its complete spectrum (e.g., absorption and reflectivity).

Luminescence Light emitted by materials; includes both fluorescence (short-lived) and phosphorescence (long-lived).

Magnetic excitations Transitions between magnetic states in materials, such as magnons.

Magnetic properties Properties arising from the presence of unpaired electrons and giving rise to a magnetic field or the response of a material to an external magnetic field.

Nonlinear optical methods Optical techniques in which the response of the material under study involves the nonlinear response (susceptibility) or, in other words, more than photon.

Nuclear magnetic resonance (NMR) Technique that uses radio-frequency radiation to probe transitions associated with nuclei that split in a magnetic field.

Nuclear resonance forward scattering (NRFS) Time-domain technique that uses synchrotron radiation to probe the Mössbauer effect in materials.

Nuclear resonant inelastic x-ray scattering (NRIXS) Synchrotron radiation technique that probes phonon spectra associated with the excitation of the Mössbauer-active nuclei.
Olivine $(Mg,Fe)_2SiO_4$; is a magnesium iron silicate, one of the most common minerals in the Earth's upper mantle.
Optical absorption and reflectivity Techniques used to study transitions in the infrared–visible–ultraviolet spectral range from transmission of light through the material (absorption) or from the light reflected from the surface.
Oscillator fits Analyses of spectra that employ one or more excitations to comprise the spectra profile, often used for modeling dielectric function.
Phonon inelastic x-ray scattering (PIXS) Technique to probe vibrational excitations, including their momentum q dependence, using x-rays.
Raman scattering Inelastic light-scattering technique that measures transitions to an excited state from the ground state (Stokes scattering) and to the ground state from a thermally excited state (anti-Stokes scattering).
Rayleigh scattering Quasi-elastic scattering spectroscopy technique, typically used to explore relaxation phenomena in materials.
Resonance methods Techniques that probe materials by measuring the response through a characteristic frequency or frequencies.
Resonant inelastic x-ray spectroscopy (RIXS) Technique to probe electronic excitations using x-rays scattered at energies that are different from the incident x-rays and where the incident radiation is tuned through core-level excitations.
Silicate perovskite and postperovskite High-pressure silicate phases with the stoichiometry $ASiO_3$, where A is a metal ion (e.g., Mg, Fe, and Ca). Silicate perovskite represents the dominant class of phase of the Earth's lower mantle.
Silicate postperovskite Dense pressure phase of the same stoichiometry as silicate perovskite having the $CaIO_3$ structure and stable at P–T conditions of the base of the mantle.
Transition metal oxides Compounds with the general formula $M^i_aM^j_bO_z$, where M^i_a is a transition metal in a particular oxidation and O is oxygen.
Transport measurements Experiments that quantify the transport of charge (electrons, protons, or ions) and of heat (thermal conductivity).
Volatiles Low boiling point compounds usually associated with a planet's atmosphere or crust, including hydrogen, H_2O, CO_2, methane, and ammonia; also the components of these materials that can be bound in high-pressure phases.
x-Ray absorption spectroscopy (XAS) Technique in which incident x-rays are absorbed when energy exceeds the excitation energy of core electrons of a specific element, typically causing an atomic edge-like spectrum.
x-Ray emission spectroscopy (XES) Technique in which core electrons are excited by x-ray and then the core holes decay through a radiative process.
x-Ray inelastic near-edge spectroscopy (XINES) Technique in which an incident x-ray is scattered at a lower energy of a core excitation (e.g., K-edge) of a material; typically used to probe structure containing information on bonding states.
x-Ray magnetic circular dichroism (XMCD) Technique to measure the spin polarization of an electronic excitation of materials by the use of circularly polarized x-rays.

Abbreviations

CS	Compton scattering
EIXS	Electronic inelastic x-ray scattering
EPR	Electron paramagnetic resonance
IXSS	Inelastic x-ray scattering spectroscopy
NMR	Nuclear magnetic resonance
NRFS	Nuclear resonance forward scattering
NRIXS	Nuclear resonant inelastic x-ray scattering
PIXS	Phonon inelastic x-ray scattering
RIXS	Resonant inelastic x-ray spectroscopy
XAS	x-Ray absorption spectroscopy
XES	x-Ray emission spectroscopy
XINES	x-Ray inelastic near-edge spectroscopy
XMCD	x-Ray magnetic circular dichroism

2.13.1 Introduction

Electronic and magnetic properties directly influence large-scale global phenomena ranging from the initial differentiation of the planet, the formation and transmission of the Earth's magnetic field, the propagation of seismic waves, to the upwelling and downwelling of mass through the mantle. The properties of deep Earth materials are not readily familiar to us, owing to their distance, both physically and conceptually, from the near-surface environment of the planet. Over the range of pressures encountered with the Earth, rock-forming oxides and silicates compress by factors of two to three. Even the many incompressible materials are compressed by 50%. Volatiles such as rare gases and molecular species can be compressed by over an order of magnitude. With the large reduction in interatomic distances produced by these conditions, dramatic alterations of electronic and magnetic properties give rise to myriad transformations. Discrete electronic and magnetic transformations can occur, such as metallization of insulators and magnetic collapse. More commonly, these changes are associated with, and drive, other transformations such as structural phase transitions, as well as controlling chemical reactions. Materials considered volatiles under near-surface conditions can be structurally bound in dense,

high-pressure phases (e.g., hydrogen in ice, mantle silicates, and ferrous alloys). Gases and H_2O become refractory (high melting-point) materials at high pressures (Lin et al., 2005a). The heavy rare gases metallize (Eremets et al., 2000; Goettel et al., 1989; Reichlin et al., 1989). Ions such as Fe^{2+} and Mg^{2+}, which almost always can substitute completely for each other at low pressures, partition into separate phases at depth (Mao et al., 1997), whereas incompatible elements such as Fe and K may form alloys (Parker and Badding, 1996). Noble gases form new classes of compounds (Sanloup et al., 2002b; Vos et al., 1992).

This chapter constitutes an overview of measurements of high-pressure electronic and magnetic properties of Earth materials. The chapter draws largely on a pedagogical review written in 1998 (Hemley et al., 1998b), including numerous updates as a result of considerable advances in the field, particularly in the area of synchrotron techniques. The article focuses on in situ high P–T techniques and selected applications in geophysics. We begin with a short review of fundamental properties, with emphasis on how these are altered under very high pressures and temperatures of the Earth's deep interior. This is followed by a discussion of different classes of electronic and magnetic excitations. We then provide a short description of various techniques that are currently used for high-pressure studies. We then selected examples, showing how the use of a combination of different techniques reveals insight into high P–T phenomena.

2.13.2 Overview of Fundamentals

2.13.2.1 Bonding in Deep Earth Materials

2.13.2.1.1 Conventional bonding classification

The binding forces that hold the atoms together are generally electrostatic in origin. The forces that keep the atoms from collapsing into each other arise from increased kinetic energy as atoms are brought closer together, the Pauli exclusion principle that keeps electrons apart, the electrostatic repulsion between electrons, and ultimately, as the atoms are brought closer and closer together, the electrostatic repulsion of the nuclei. Crystals can be characterized by the primary source of their binding energy. Following the conventional classifications set out by Pauling (1960), we describe for the purposes of the present chapter the following bonding types: ionic, covalent, metallic, van der Waals, and hydrogen bonding. As pressures increase, the problem changes from understanding the cohesion of crystals to understanding how electronics and nuclei rearrange in order to minimize repulsive forces.

In ionic crystals, the primary source of binding is from the electrostatic attraction among ions. Prototypical examples are NaCl (Na^+Cl^-) and MgO ($Mg^{2+}O^{2-}$). This ionicity is driven by the increased stability of an ion when it has a filled shell of electrons. For example, oxygen has a nuclear charge $Z=8$, which means that it would have two 1s, two 2s, and four 2p electrons, but a filled p shell has six electrons. In a covalent bond, charge concentrates in the bonding region, increasing the potential and kinetic energy of interaction between electrons but reducing the energy through the electron–nuclear interactions (since each electron is now on average close to both nuclei). Covalent bonds tend to be directional since they are formed from linear combinations of directional orbitals on the two atoms. It is straightforward to develop models for such covalent materials, and such models have ranged from models with empirical parameters to those with parameters obtained from first principles. The high-pressure behavior of metals, and in particular iron and iron alloys, is of paramount importance for understanding the nature of the Earth's core. The bonding in metals is often thought of as a positive ion core embedded in a sea of electrons, the negative electrons holding the ions together. Under pressure, the conductivity may increase or decrease: in some cases (e.g., carbon) pressure may drive a transition from a metallic phase (graphite) to an insulator (diamond).

One must also consider weaker bonding interactions. Dispersion, or van der Waals forces, arises from fluctuating dipoles on separated atoms or molecules. Separated, nonoverlapping charge densities have such an attractive force between them, and it varies as $1/r^6$ and higher-order terms at large distances. Even at low pressures, van der Waals forces are largely quenched in solids and become completely insignificant at high pressures. Hydrogen bonds are essentially ionic bonds involving H and O; a hydrogen atom is covalently bonded to an oxygen atom and attracted electrostatically to a neighboring oxygen ion. As such, the three atoms form a linear linkage with a hydrogen atom asymmetrically disposed between the oxygens, a configuration that is ubiquitous in hydrous materials. A range of degrees of hydrogen bonding at ambient pressure are evident in dense hydrous silicates that are candidate mantle phases. In such structures, the application of moderate pressures causes a reduction in oxygen–oxygen distances, which generally enhances bonding between the hydrogen and the more distant oxygen atom. At deep mantle and core pressures, conventional hydrogen bonding is lost, and hydrogens might be symmetrically situated between oxygens.

Many high-pressure minerals exhibit combinations of the types of interactions outlined in the preceding text. The most common are ionic bonding and covalent bonding, both within the same bond and different degrees of each in different bonds present in the material. Silicates are considered about half-ionic and half-covalent. Transition metals such as Fe are both metallic and covalent. A molecular group that contains strong covalent bonds can also be ionically bound to other ions in the crystal. An example is $CaCO_3$, where the C–O bonds are strong and directional, forming a planar triangle in the CO_3^{2-} carbonate group, which is bound ionically to Ca^{2+} ions.

2.13.2.1.2 Bonding under high P–T conditions

The bonding in Earth materials characterized under ambient conditions typically does not reflect their state under conditions of the deep Earth. The contributions from each type are in general strongly pressure-dependent. High pressure favors high density and high temperatures favor phases with higher entropy S. At lower mantle and core conditions, the density terms dominate, with generally small Clapeyron slopes, dP/dT, found for solid for phase transitions. Structures tend to adopt more close-packed configurations with increasing compression. At high pressures, the attractive terms in molecular solids become less and less important, and one could rather think of the atoms as soft spheres. Much of the chemistry and phase

diagrams of such materials can be understood as the packing of spheres of various sizes. However, as pressure is increased, the electronic structure also changes. This happens first in the crystals of heavier rare gases such as Xe, which transforms from the fcc to the hcp structure (Jephcoat et al., 1987) prior to metallization (Eremets et al., 2000; Goettel et al., 1989; Reichlin et al., 1989). On the other hand, the tendency toward close packing is not observed in all cases. There have been a few theoretical treatments of these phenomena (Neaton and Ashcroft, 1999, 2001). In fact, surprisingly complex structures can be adopted, as has been seen in some pure elements (McMahon and Nelmes, 2004). Oxides can also adopt complex structures, driven by subtle pressure-induced changes in orbital hybridization. This is particularly evident in some ferroelectric materials (Wu and Cohen, 2005). In addition, there can be effects of magnetism, or the tendency of electron spins to align: theory and a number of experiments indicate that magnetism tends to decrease and disappear with increasing pressure (Cohen and Mukherjee, 2004; Cohen et al., 2002; Pasternak and Taylor, 2001; Pasternak et al., 1997b; Steinle-Neumann et al., 2003, 2004a,b; Stixrude, 2001).

Changes in bonding also apply to liquids. For the deep Earth, the important systems are silicate and oxide melts and liquid iron alloys of the outer core. There is evidence that silicate melts undergo similar structural transformations such as coordination changes, although not abrupt, and spread out over a range of pressures. Detailed information on the electronic properties of geophysically relevant liquids under extreme conditions is lacking. Insulating materials can also become metallic at high temperatures and pressures, as has been observed and computed in FeO (Ohta et al., 2012).

2.13.2.2 Electronic Structure

Insight into these phenomena must come from examination of the changes in electronic structure induced by materials subjected to extreme P–T conditions. Because of the presence of long-range interactions in condensed phases, the bonding must in general be viewed from an extended point of view, although a local picture is often employed to simplify the problem. For crystals, the eigenstates can be characterized by the wave number k (Kittel, 1996). The interaction between orbitals on different atoms gives rise to energy bands, which are dispersive as functions of k, and the band energies versus k form the band structure. The core states, or deep levels for each atom, remain sharp delta function-like states, which may be raised or lowered in energy relative to their positions in isolated atoms. These core-level shifts are due largely to the screened Coulomb potential from the rest of the atoms in the crystal. The occupied valence and empty conduction states no longer look like atomic states, but are broadened into energy bands. There are often intermediate states between the core levels and the valence states called semicore states that are slightly broadened at low pressures but that become broader and more different from atomic states with increasing pressure. The formation of ions is driven by the increased stability of an ion when it has a filled shell of electrons. The strong attractive electrostatic, or Madelung, interaction between the ions greatly enhances the crystal stability.

This picture now becomes a means for classifying different materials. Metals have partially occupied states at the Fermi level, the highest occupied energy level in a crystal. One can understand the insulating behavior of materials with fully filled bands by considering what happens when one applies an electric field. An electric field raises the potential at one part of the sample relative to another, and one would think that electrons would then flow down that potential gradient. However, in an insulator, the bands are filled, and due to the Pauli exclusion principle, nothing can happen without exciting electrons to states above the gap. This requires a large energy, so there is no current flow for small fields, and thus, the materials have a finite susceptibility and the material is insulating. In a metal, the partially filled states at the Fermi level mean that current will flow for any applied field, and the susceptibility is infinite. Actually, the distinction between metallic and insulating systems involves some subtle physics (Resta, 2002), but in general, the band picture suffices to understand metals and insulators well within their stability fields. Insulator to metal transitions, however, are expected to show complex behavior in some materials (Huscroft et al., 1999). Many transitions found to date seem to involve structural transitions at the same pressure as the metal–insulator transition (e.g., FeO from the rhombohedrally strained rock salt structure to the anti-B8 (inverse NiAs) structure) (Fei, 1996; Gramsch et al., 2003; Mazin et al., 1998; Murakami et al., 2004b), but an isostructural transition has been seen in MnO (Yoo et al., 2005) and FeO (Ohta et al., 2012).

In an insulator, the energy of the highest occupied levels is the valence band, designated E_v, and that at the bottom of the conduction band, E_c. The difference is the bandgap, $E_g = E_c - E_v$. Crystals with bandgaps between occupied and unoccupied states should be insulators, and those with partially filled bands should be metals. Localized states may exist at energies between the valence and conduction bands, and these can have major effects on optical and transport properties. If the gap is small or if the material has such intermediate states (e.g., by chemical doping such that electrons can be excited into the conduction bands or holes in the valence bands), the crystal is considered a semiconductor. In a nonmagnetic system, each band holds two electrons, and thus, a crystal with an odd number of electrons in the unit cell should be a metal since it will have at least one partially filled band. Magnetic crystals that are insulators by virtue of local magnetic moments are known as Mott insulators (Mott, 1990). These materials include transition metal-containing oxides present in the mantle (and considered core components); such materials exhibit intriguing behavior as a function of pressure and temperature.

We should also consider the electronic structure of noncrystalline materials, including liquids. The existence of a bandgap in crystals can be described in terms of the Brillouin zone and Bragg-like reflection of electrons. But a gap does not depend upon the periodicity of the atoms on a lattice. The electrons in the lowest energy states in the conduction band of a noncrystalline material (or disordered crystal) can be localized (Anderson, 1958; Mott, 1990). The difference between the localized and delocalized states is called the mobility edge. These may be important in describing the electronic properties of liquids and amorphous materials formed from deep Earth crystalline materials (e.g., metastably compressed crystalline minerals and dense melts).

2.13.2.3 Magnetic Properties

Magnetism arises from the presence of unpaired electrons. Electrons have magnetic moments, but if they are paired up in states as up and down pairs, there will be no net magnetism in the absence of a magnetic field. However, in open-shelled atoms, there may be a net moment. According to Hund's rules, atoms (or isolated ions) will maximize their net magnetic moment, which lowers their total energy due to a decrease in electrostatic energy. In a crystal, interactions with other atoms and formation of energy bands (hybrid crystalline electronic states) may lead to intermediate- or low-spin magnetic structures.

The behavior of iron (Fe^{3+}, Fe^{2+}, and Fe^{0}) at high pressure is of central importance. Fe^{2+} has six d-electrons, and two end-member situations can be considered. In a site with octahedral symmetry and limited ligand–field interactions, the six d-electrons can be paired to fill three t_{2g} states, forming low-spin, ferrous iron, and there is no net magnetic moment. In high-spin ferrous iron, five up d-states are split in energy from five down d-states by the exchange energy, and five d-electrons go into the three t_{2g} and two e_g lower-energy, majority spin states and one electron into a high-energy t_{2g} state. This gives a net magnetic moment component of $4\mu_B$ (Bohr magnetons). The fully spin-polarized magnetic moment component of Fe^{3+} is $5\mu_B$. In crystals, the 4s states usually dip down in energy with respect to k and are partially occupied, leading to a smaller d-occupation and smaller net moment.

Such open-shell systems have often been discussed in terms of crystal field theory, which has been very successful in rationalizing optical spectra, crystal chemistry, and thermodynamic and magnetic properties of minerals, including their pressure dependencies. The principal assumption of crystal field theory is the existence of localized atomic-like d-orbitals. It has provided a way to rationalize the changes in energy levels in terms of local interactions of the transition metal cations with the coordinating atoms. The symmetry of the coordination polyhedron results in a lifting of the otherwise degenerate d-orbitals. The primary success of crystal field theory arose from symmetry analysis of the splitting of the atomic-like states. These symmetry arguments are rigorous, but the origin of the splitting may not arise from a potential field represented as a point charge lattice, but rather to bonding hybridization. Furthermore, d-states are not pure atomic-like states but are dispersed across the Brillouin zone (energy varies with k).

As shown by Mattheiss (1972), the origin of the crystal field splitting is due largely to hybridization. In the language of quantum mechanics, the $e_g - t_{2g}$ splitting is due to off-diagonal interactions, not shifts in the diagonal elements as would be the case for the conventional electrostatic crystal field interaction. The splitting can be considered a ligand–field effect and does not arise from changes in the electrostatic field at an atomic site. Rather, the splitting is due to d–d interactions between next-nearest neighbors and due to p–d and s–d interactions between neighboring oxygen ions. The d–d interactions led to splittings that vary as $1/r^5$; although the p–d and s–d interactions follow a $1/r^7$ dependence (Harrison, 1980), the metal–metal d–d splittings dominate. Thus, the same $1/r^5$ dependence of the observed splittings is predicted by electrostatic crystal field model (Drickamer and Frank, 1973) and by hybridization (Mattheiss, 1972).

In the low-temperature ground states, moments on individual ions or atoms can be oriented, giving rise to ferromagnetism if they are lined up in the same direction or antiferromagnetism if they are oppositely aligned, which depends on the sign of the magnetic coupling J, which depends on hybridization with other atoms in the crystal. At high temperatures, the moments will disorder, but there are still local moments present. This paramagnetic state is distinguished from the paramagnetic state that arises from loss of local moments (magnetic collapse or a high- to low-spin transition), although the two states merge continuously into each other with increasing pressure. Ferrimagnetism results when the magnetic moments are unequally distributed over different sublattices. A net spontaneous magnetic moment arises from the incomplete cancellation of aligned spins. An example is magnetite, Fe_3O_4, which consists of a sublattice of Fe^{2+} and one of Fe^{2+} and Fe^{3+}. In some materials, such as fcc and possibly iron (Cohen and Mukherjee, 2004), the moments are non-collinear. For ferromagnetic (FM) and antiferromagnetic (AFM) phases, the magnetic moments are aligned below the Curie and Néel temperatures, respectively. The decrease in magnetism with pressure can be understood qualitatively from the increase in electronic bandwidths, which eventually become greater than the exchange splitting. This can be understood more quantitatively with the Stoner and extended Stoner models (Cohen et al., 1997).

2.13.3 Electronic and Magnetic Excitations

Excitations in a system are induced by external (e.g., electronic or magnetic) or internal (e.g., temperature) fields. The coupling of the response to the field is given by the frequency-dependent susceptibility. This can be characterized as the dielectric function $\varepsilon(\omega, k)$, where ω is the frequency and k is the wavevector (the dielectric function is also known as the relative permittivity). The dielectric function is complex, $\varepsilon = \varepsilon_1 + i\varepsilon_2$, where ε_2 contains the contribution from absorption. In general, the response of a crystal to an electric field is dependent on its orientation relative to the crystal axes (which gives rise to properties such as birefringence and optical activity), that is, the dielectric function is a tensorial function). The dielectric tensor is also a function of applied electric field, giving rise to nonlinear optical response (e.g., multiphoton excitations) as described later in the text. Electrons can be excited into extended or itinerant states (i.e., across the band-gap), or the excitations may be local (i.e., forming a localized electron–hole pair, or exciton).

2.13.3.1 Dielectric Functions

The index of refraction is related to the dielectric function ε, as $n^2 = \varepsilon$, which can strongly depend on pressure. In general, there are several different contributions to the dielectric function. In materials that contain polar molecules, the molecules can align. There are three main contributions to the dielectric response in insulators: ionic polarization (displacement of ions) in crystals containing nonpolar atoms or ions, electronic polarization (from the deformation of atomic charge distributions), and charge transfer from atom to atom. The electronic

contribution to the dielectric function of a material is formally determined by the sum of its electronic excitations (Ashcroft and Mermin, 1976). Hence, measurement of the index of refraction of transparent minerals (i.e., below bandgap or absorption edge) can be used to constrain the frequency of higher-energy electronic excitations (e.g., in the ultraviolet spectrum), for example (Eremets, 1996). Optical spectra of oxides and silicates from the near-IR to the vacuum UV are determined by electronic transitions involving the valence (bonding) band, the conduction (antibonding) band, and d-electron levels. Piezoelectric crystals become polarized when subjected to a mechanical stress (compressive or tensile). Quartz is a common example. In ferroelectric phases, the crystals are spontaneously polarized and have very high dielectric constants.

This approach has been useful in high-pressure studies when the window of the high-pressure cell precludes measurements above a critical photon energy (Hemley et al., 1991). For example, diamond anvil cells at zero pressure have an intrinsic absorption threshold of 5.2 eV (i.e., for pure type IIa diamonds). Moreover, type I diamonds contain nitrogen impurities that lower the effective threshold at zero pressure to below 4 eV (depending on the impurities). Although the bandgap of diamond increases under pressure, the absorption threshold of diamond (and most likely the gap) decreases in energy under the stresses due to loading in the cell. Full quantitative information on the dielectric function in the diamond transparency window is hard to obtain, although there exist few applications facilitating data analysis. Two mostly used approaches are oscillator model and the Kramers–Kronig (KK) analysis of the reflectivity data. Several experimental setups have been reported for reflectivity measurements (Goncharov et al., 2000; Syassen and Sonneschein, 1982); however, only relatively few studies have been performed that yield full dielectric function information under pressure (e.g., Goncharov et al., 1996).

The electronic dielectric function including intra- and interband electronic transitions can be computed from first principles within the random phase approximation using, for example, the WIEN2k LAPW code (Ambrosch-Draxl and Sofo, 2006; Schwarz et al., 2002). Predictions for high-pressure hydrogen (Cohen et al., 2013) will be useful for better understanding experimental spectroscopy. These calculations have been used to discriminate solid CO_2 phases (Sharma et al., 2003).

2.13.3.1.1 Oscillator fits

Classical oscillator fits are based on the following expression for the dielectric constant:

$$\varepsilon(\omega)=\varepsilon_1(\omega)+\mathrm{i}\varepsilon_2(\omega)=\varepsilon_\infty+\sum_{j=1}^{m}\frac{\omega_{pj}^2}{\omega_j^2-\omega^2-\mathrm{i}\omega\gamma_j} \quad [1]$$

where ω_i and γ_j are the frequency and line width, respectively, of oscillator j. The real and imaginary parts of the refractive index (omitting the ω dependence) $N=n+\mathrm{i}k$ are related to the dielectric constant by

$$n=\left(\frac{\left(\varepsilon_1^2+\varepsilon_2^2\right)^{1/2}-\varepsilon_1}{2}\right)^{1/2} \quad [2]$$

$$k=\left(\frac{\left(\varepsilon_1^2+\varepsilon_2^2\right)^{1/2}+\varepsilon_1}{2}\right)^{1/2} \quad [3]$$

The following discussion is restricted to the analysis of the normal incidence of light at a sample–diamond interface, which is a good approximation to many experimental conditions. The reflectivity from the sample between diamond anvil cells having a thickness D is given in this case by the following equation, which is equivalent to the formula from Born and Wolf (1980), the only difference being written in complex numbers:

$$R=\left|\frac{(N-N_\mathrm{D})^2(1-\chi)}{(N+N_\mathrm{D})^2-\chi(N-N_\mathrm{D})^2}\right|^2 \quad [4]$$

where N_D is the refractive index of diamond and

$$\chi=\exp(\mathrm{i}2N\omega D)=\exp(\mathrm{i}2n\omega D-2k\omega D) \quad [5]$$

For the case of a strong absorption a sample when the reflectivity from the second sample–diamond interface is negligible, one obtains well-known expression

$$R=|r|^2=\left|\frac{(N-N_\mathrm{D})}{(N+N_\mathrm{D})}\right|^2=\frac{(n-N_\mathrm{D})^2+k^2}{(n+N_\mathrm{D})^2+k^2} \quad [6]$$

2.13.3.1.2 KK analysis

In general, the response function r (eqn [6]) can be determined from the reflectivity R using the KK procedure (Bassani and Altarelli, 1983). One defines

$$\theta(\omega)=-\frac{2\omega}{\pi}P\int_0^\infty \mathrm{d}\omega'\frac{\ln|r(\omega')|}{\omega'^2-\omega^2} \quad [7]$$

where P is the principal part of the integral. From eqns [5] and [7], it is straightforward to calculate

$$n=\frac{N_\mathrm{D}(1-R)}{1+R-2\sqrt{R}\cos(\theta)} \quad [8]$$

$$k=\frac{2N_\mathrm{D}(1-R)\sin(\theta)}{1+R-2\sqrt{R}\cos(\theta)} \quad [9]$$

The dielectric constants are given then by

$$\varepsilon_1=n^2-k^2 \quad [10]$$

$$\varepsilon_2=2nk \quad [11]$$

This procedure works only in the region of strong absorption, where we can use eqn [4] instead of eqn [3]. Although all weak IR bands can often be observed in absorption, it is much more convenient to use Fourier transform techniques to carry out the KK transformation, instead of directly using eqn [7]. The following discussion is based upon the technique outlined in Titchmarsh (1937). The KK transformation is a transformation between the functions connected in the following way (Bassani and Altarelli, 1983):

$$f(x)=-\frac{1}{\pi}P\int_{-\infty}^{\infty}\frac{g(t)}{t-x}\mathrm{d}t,\quad g(x)=\frac{1}{\pi}P\int_{-\infty}^{\infty}\frac{f(t)}{t-x}\mathrm{d}t \quad [12]$$

For the present case, $g(x)$ and $f(x)$ can correspond to dielectric functions $\varepsilon_1(\infty)-\varepsilon_\infty$ and $\varepsilon_2(\omega)$. When calculating the phase of the reflectivity, the matching pair would be

$\ln|r(\omega)|$ and $\theta(\omega)$. Functions $g(x)$ and $f(x)$ are called Hilbert transforms, and their Fourier transforms $F(t)$ and $G(t)$ are coupled by the following relation (Titchmarsh, 1937):

$$G(t) = -iF(t)\mathrm{sgn}(t) \quad [13]$$

where $\mathrm{sgn}(x) = 0$ when $x < 0$ and $\mathrm{sgn}(x) = 1$ when $x \geq 0$. Thus, taking the Fourier transform of $g(x)$ ($G(t)$), we can find the transform of $f(x)$ ($F(t)$) using eqn [13]; the inverse transform of $F(t)$ gives $f(x)$, thereby giving the KK transform of the function $g(x)$. Fast Fourier transform techniques permit the calculation of KK transforms easily and much faster than direct integration of eqn [7]. Formally, the transform should be performed over the frequency range $0 < \omega < \infty$, but experimental data are always limited to a specific frequency range. Procedures are therefore needed to account for missing data, and these procedures will be discussed later in the experimental section. When calculating the KK transform of $\ln|r(\omega)|$ at sample–diamond interface, there may be an additional contribution to the calculated phase shift, which is known as the Blaschke product (Stern, 1963). The phase shift is given by

$$\theta(\omega) = \theta_c(\omega) + \zeta(\omega) \quad [14]$$

where

$$\zeta(\omega) = -i\ \ln[B(\omega)] = 2\sum_n \tan^{-1}\left[(\omega - \mu_n^r)/\mu_n^i\right] \quad [15]$$

Here, the summation runs over all n; r and i stand for the real and imaginary parts of μ_n, and μ_n^r and μ_n^i are determined from the condition

$$r(\mu_n) = 0,\ \ (\mu_n^r + i\mu_n^i = \mu_n) \quad [16]$$

$\theta_c(\omega)$ is a canonical phase shift that results from the KK procedure. The physical reason for the occurrence of the Blaschke product $\zeta(\omega)$ is a zero in reflectivity $r(\omega)$ in the upper half of the complex ω plane (eqn [16]), which introduces a singular point in $\ln|r(\omega)|$ and makes the application of the KK relation unjustified in that case. However, one can define the canonical reflectivity

$$r_c(\omega) = r(\omega)/\left[(\omega - \mu_n)\left(-\omega + \mu_n^*\right)\right] \quad [17]$$

which does not have zeros in the upper half of the complex ω plane. Moreover, on the real ω_r axis, $r(\omega_r) = r_c(\omega_r)$. Thus, the KK relation can be applied to the canonical reflectivity, and the resulting formula for the phase shift will be given exactly by eqn [14]. The Blaschke root μ_n is pure imaginary in this case ($\mu_n^r = 0$), because eqn [16] is satisfied when $n(\omega) + ik(\omega) - N_D = 0$ is fulfilled (which requires $k = 0$). It is known that the refractive index $N(\omega)$ is a complex number everywhere, except on the imaginary ω_i axis. On that axis, we have

$$n(i\omega_i) = (\varepsilon(i\omega_i))^{1/2} = \left(1 + \frac{2}{\pi}\int_0^\infty \frac{x\varepsilon_2(x)dx}{x^2}\right)^{1/2} \quad [18]$$

$n(i\omega_i)$ decreases monotonically from $n(0)$ to 1 when ω_i increases from 0 to infinity (Landau and Lifshitz, 1977). The condition $n(i\omega_i) - N_D = 0$ will be satisfied somewhere on the imaginary axis, if $n(0) > N_D$. As shown later in the experimental section, this condition is satisfied for ices at high pressures. Modifications needed to apply the KK procedure correctly will be discussed later in the text. It is useful to point out here that a very simple way to account for the Blaschke product is to solve for the condition $n(i\mu_n) - N_D = 0$ numerically (using eqn [18]) and dielectric function from the oscillator fit (eqn [1]). Another possibility is to apply the KK procedure self-consistently, by iteratively adjusting the Blaschke root μ_n.

2.13.3.2 Electronic Excitations

2.13.3.2.1 Extended excitations

Interband transitions are electronic excitations between bands, whereas intraband transitions are those within a band. An example of the latter is the damped frequency dependence of electronic excitations associated with itinerant electrons in a metal (which by definition has a partially filled band). The collective longitudinal excitations of the conducting electrons are known as plasma oscillations. Plasma oscillations (plasmons) can be excited by inelastic scattering techniques at high pressures. Plasmons can also be excited in materials with a bandgap (i.e., dielectrics), typically at higher energies. In olivines, the bandgap varies from 7.8 eV in forsterite to 8.8 eV in fayalite (Nitsan and Shankland, 1976).

2.13.3.2.2 Excitons

Electronic excitations may occur within the bandgap due to the creation of a bound electron–hole pair, called an exciton. The pair is characterized by a binding energy E_b, which is given by $E_g - E_{ex}$, where E_{ex} is the excitation energy. In some respects, these excitations are the equivalent of localized transitions in molecular spectroscopy, but they can propagate in a crystal and are characterized by a wavevector k. Continuing with the example of olivines at zero pressure, a prominent excitonic absorption is observed near the bandgap (Nitsan and Shankland, 1976). The absorption characteristics in this region in dense ferromagnesian silicates and oxides are important for assessing the heat transfer in the Earth, which is predominantly radiative at deep mantle temperatures.

2.13.3.2.3 Crystal field transitions

The color of many minerals arises from substitution of transition metals in the crystal structure. The substitution of transition metals in olivines at zero pressure results in a strong absorption beginning 1–2 eV below the bandgap, which is ascribed to transitions between widebands and the d-levels in the system (Nitsan and Shankland, 1976). The development and application of crystal field theory for understanding behavior of open-shell systems ions, such as partially filled d-shell of transition elements, in minerals have a long history. As discussed earlier in the text, a more fundamental quantum mechanical picture shows that orbital hybridization of the central ion and its neighbors (e.g., oxygen atoms) is significant and that the orbital splitting is not a purely electrostatic effect, but has a similar dependence on interatomic distances.

2.13.3.2.4 Charge transfer

Charge transfer represents another important class of excitations in these materials. Many of these transitions in minerals occur in the ultraviolet region (Burns, 1993). Intervalence charge transfer (e.g., metal–metal charge transfer) may occur between ions of different valence states, such as Fe^{+2}–Fe^{3+} or Fe^{2+} and Ti^{4+}. These transitions often give rise to bands in the

visible spectrum that show marked shifts with pressure (Mao, 1976).

2.13.3.2.5 Excitations from defects

Many defects are also associated with electronic properties or are electronic in origin. Electron–hole centers or defects can be produced by deformation or radiation, either naturally or in the laboratory. Examples of naturally occurring systems at ambient pressure that exhibit these properties are smoky quartz and numerous colored diamonds (see Rossman, 1988). Defect luminescence has been observed to be pressure-induced, and it may be connected with emission features observed in shock-wave experiments (see Hemley et al., 1998b).

2.13.3.2.6 Electrical conductivity

Electrical conductivity is another measure of the response of the system to an applied electric field (static or frequency-dependent). Electrical conductivity may be electronic or ionic and can be intrinsic or extrinsic. If there is a gap between the valence and conduction bands, the electronic conductivity can be thermally activated at finite temperature. This can also give rise to coupled distortions of the lattice as the electrons move through it, called small polarons (see Kittel, 1996). Naturally, electrical conductivity measurements provide a means for the direct identification of the insulator–metal transitions, induced by either pressure or temperature.

In general, electrical properties are also very sensitive to minor chemical impurities and defects in a given specimen (Tyburczy and Fisler, 1995), such as Fe content and volatile content. The conductivity can be written as a complex quantity, giving a real and an imaginary part (loss factor); this complex function is measured by impedance spectroscopy. Grain boundary conduction, for example, is observed to decrease under pressure as grain–grain contacts increase. Ionic conductivity may be especially noticeable at higher temperatures (e.g., premelting or sublattice melting). Such behavior has been proposed for silicate perovskites by analogy to other perovskites and theoretical calculations (Hemley and Cohen, 1992).

An exciting area now is understanding conductivity in correlated metals. Transition metal oxides are examples of Mott insulators (Mott, 1990), which are insulating because of local correlations not included in the conventional band picture. At high temperatures and pressures, these materials can become metallic. The computational technology has now developed to treat these materials with many-body theory, even to compute the frequency-dependent conductivity (Ohta et al., 2012). Measurements are in good agreement with experiment. Note that the conventional view of transport in wüstite, $Fe_{1-x}O$, was that the conductivity was caused by defects (Gartstein and Mason, 1982; Li and Jeanloz, 1990). Although this is true at ambient conditions, we now know that in the metallic state at high pressures and temperatures, the conductivity is a bulk effect and apparently little effected by defects, as can be seen from the good agreement between defect-free many-body calculations and experiments on real, defective, wüstite.

2.13.3.3 Magnetic Excitations

Magnons are excited magnetic states that can be excited in light scattering via direct magnetic dipole coupling or an indirect, electric dipole coupling together with spin orbit interaction (Fleury and Loudon, 1968). High-pressure measurements on mineral analogs have been performed to determine the metal–anion distance dependence of the superexchange interaction J (Struzhkin et al., 1993b). This interaction parameter is a measure of the coupling of metal anions through a (normally) diamagnetic anion, such as the O between two Fe atoms. Magnon excitations may also be observed by infrared absorption.

2.13.4 Overview of Experimental Techniques

An array of ambient pressure techniques can now be used to probe electronic and magnetic excitations in minerals. Band structure can be probed by photoemission, which involves interaction of electrons with the sample. Other such spectroscopies involving electron interactions include electron energy loss and auger (Cox, 1987), each of which have been used for studying high-pressure phases quenched to ambient conditions. Here, we focus on techniques that have been applied to deep Earth materials in situ at high pressure. Pressure generation techniques will not be discussed. A review of these methods, and specifically diamond anvil cells (DACs), is given elsewhere in this treatise. It is useful to point out briefly that new techniques, such as those based on chemical vapor-deposited diamond, are helping to advance these measurements (Hemley et al., 2005; Mao et al., 2003b; Yan et al., 2002). Cubic zirconia (Xu et al., 1996), moissanite (Xu and Mao, 2000; Xu et al., 2004), and other materials can be used as high P–T anvils. Variations on a number of these techniques can also be used for in situ measurements on dynamic compression (e.g., shock-wave) experiments (Ahrens, 1987).

2.13.4.1 Optical Spectroscopies

2.13.4.1.1 Optical absorption and reflectivity

Optical spectroscopies have been one of the principal techniques used for in situ high-pressure investigations of minerals with high-pressure devices having optical access (e.g., diamond anvil cells). A number of different types of absorption spectrometer systems, including double-beam instruments, have been designed and built for high-pressure mineral studies. In optical experiments on samples in high-pressure cells using refractive optics (lenses), there is a need in general to correct for the index of refraction of the diamond because of chromatic aberrations (wavelength dependence of the focusing). This problem can also be overcome by the use of reflecting optics (e.g., mirror objectives). Versatile UV–visible–near-IR absorption and reflectivity systems using conventional continuum light sources have been designed for high-pressure applications (Hemley et al., 1998a; Syassen and Sonneschein, 1982; **Figure 1**). Standard continuum sources and wide variety of laser sources that span the UV–visible and much of the IR regions are now available. Examples of optical absorption measurements on $(Mg,Fe)SiO_3$ perovskite are shown in **Figure 2(a)** and **2(b)** (Goncharov et al., 2008; Keppler et al., 2008).

The most straightforward is the measurement of the real part of the dielectric function (i.e., off-resonance), corresponding to the refractive index in the visible spectrum of

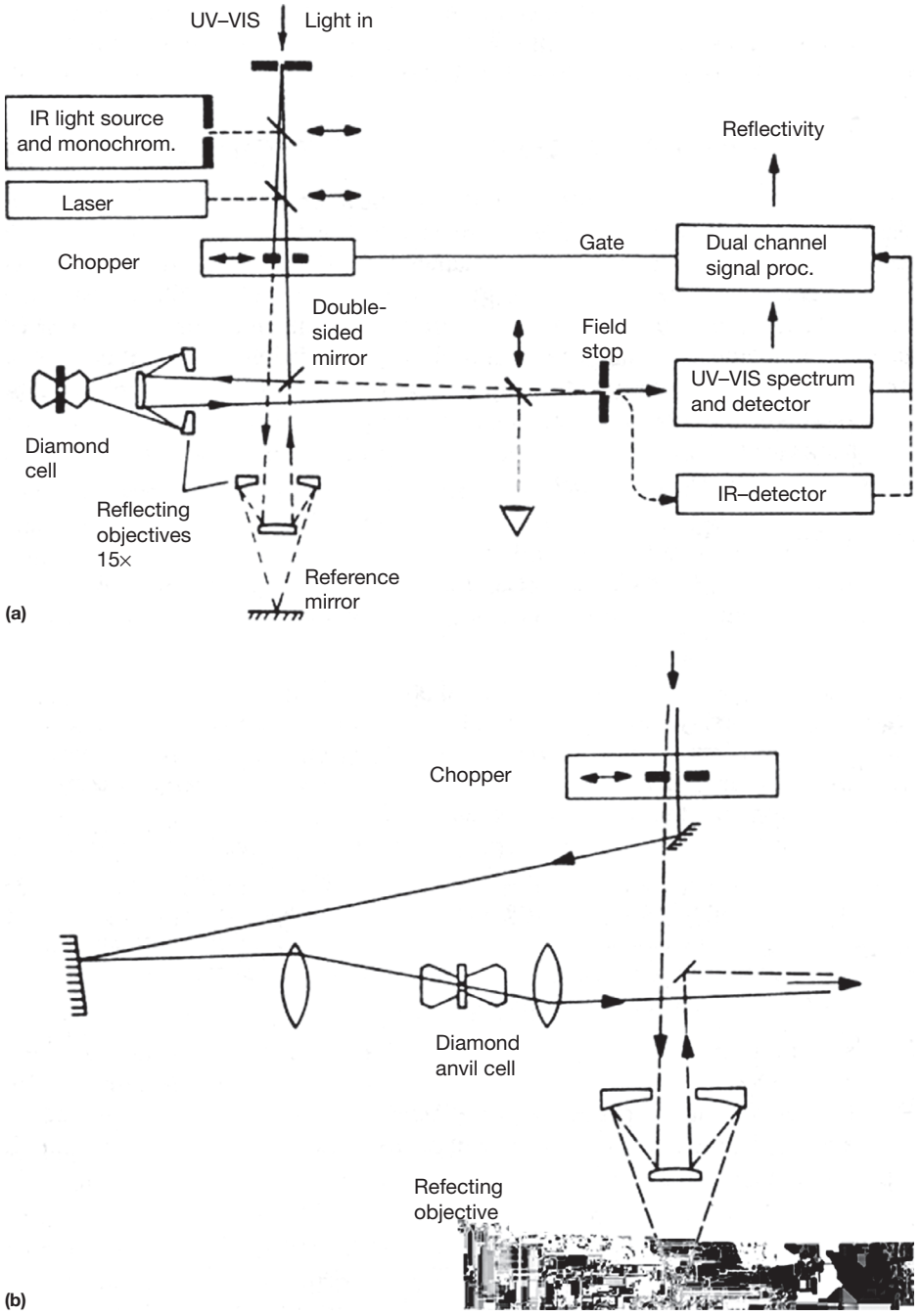

Figure 1 Example of a high-pressure UV–visible–near-IR optical setup. (a) Double-beam instrument for reflectivity measurements. Reflecting microscope optics are used to remove chromatic aberrations along with a grating spectrometer. (b) Modification of the double-beam system for absorption measurements. One of the reflecting objects is replaced by an achromatic lens. The system is capable of measurements from 0.5 to 5 eV; similar systems are in use in a number of high-pressure laboratories. Reproduced from Syassen K and Sonneschein R (1982) *Review of Scientific Instruments* 53: 644–650.

minerals that are transparent wide-bandgap insulators. Absorption (transmission) or reflectivity measurements with broadband light of thin samples of comparable thickness to the wavelength of light give rise to patterns of constructive and destructive interference in the spectrum. These fringes are straightforward to measure in a diamond anvil cell as shown in the measurements for H_2O ice (Zha et al., 2008; Figure 2(c)). The spacing is determined by the refractive index and the thickness of the platelike sample; each may be determined independently if the order of the fringe is known, and this can be found in several ways. Moreover, the wavelength dependence gives the dispersion of the index, which can be related to the higher-energy electronic excitations, as described in the preceding text.

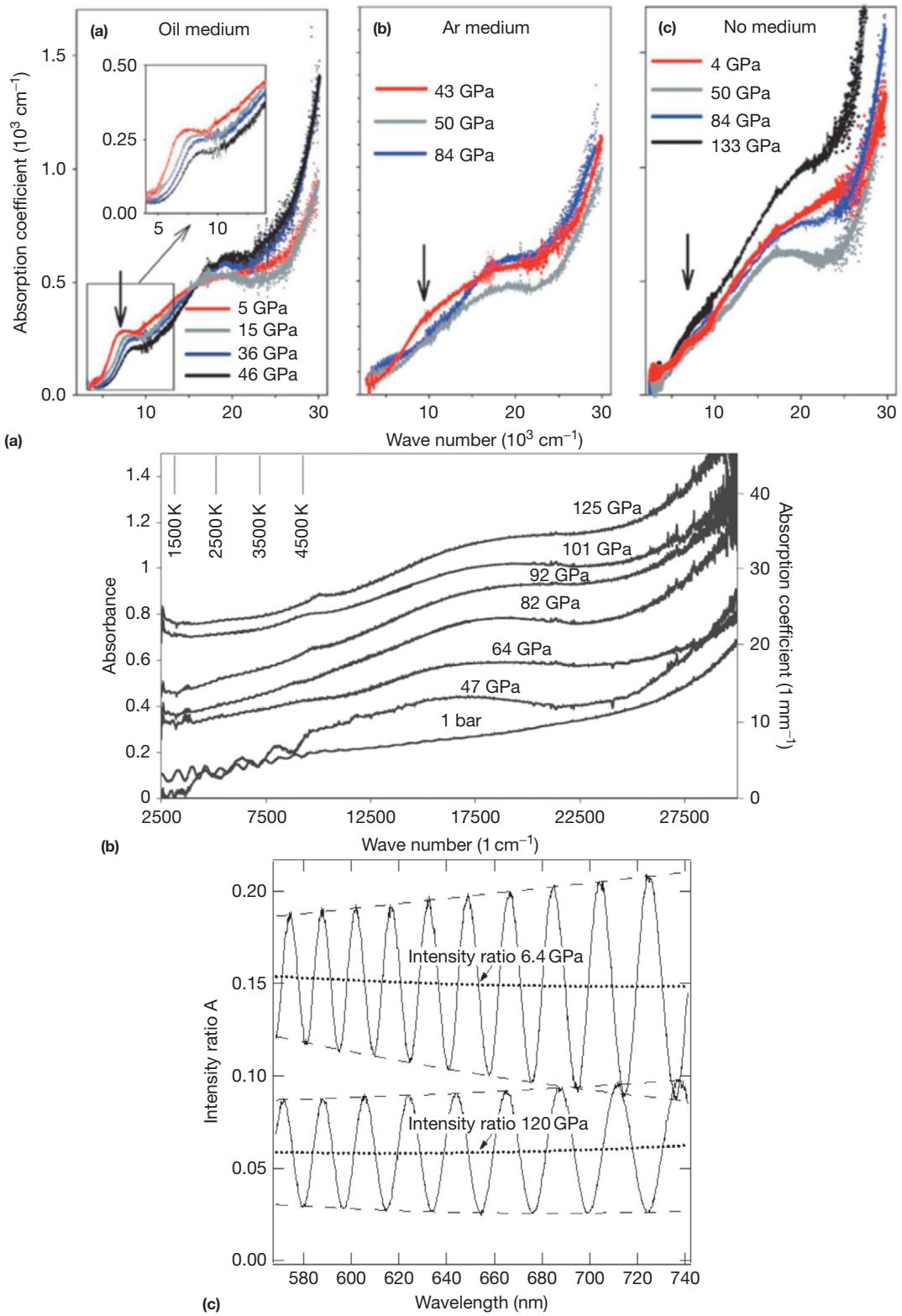

Figure 2 (a) Optical absorption spectra of silicate perovskite (10 mol% Fe) up to 133 GPa at room temperature in various pressure media. The sample thickness was measured from white-light interferometry at ambient pressure and calculated at high pressure using an isothermal equation of state. Ripples in the spectra at low pressures are interference fringes resulting from multiple reflections between the parallel polished sample surfaces. The interference patterns have been smoothed (thick solid lines) for clarity. Vertical arrows designate the Fe^{2+} crystal field transitions that are characteristic of the high-spin phase. The inset shows an enlarged view of the near-infrared spectral range. Reproduced from Goncharov AF, Haugen B, Struzhkin VV, Beck P, and Jacobsen SD (2008) *Nature* 456: 231–234. (b) Near-infrared and optical absorption spectra of silicate perovskite to 125 GPa. The 1 bar spectrum is shown as measured; the other spectra are offset vertically for clarity. Without offset, the low-frequency parts of the spectra below

Such measurements can be used to calculate effective oscillator frequencies that describe the behavior of the dielectric function as a function of pressure and temperature. For example, examples include H_2O and H_2 at megabar pressures (Hemley et al., 1991; Loubeyre et al., 2002; Zha et al., 2008). The results for H_2 are broadly compatible with direct observation of optical absorption of H_2 at pressures of >250 GPa (Loubeyre et al., 2002; Mao and Hemley, 1989, 1994). MgO and diamond both show a decrease in refractive index with pressure. From this, we infer that the bandgap of MgO increases with pressure, in agreement with theory (Mehl et al., 1988). A similar behavior is observed for hydrostatically compressed diamond (Eremets et al., 1992; Surh et al., 1992). In contrast, the bandgaps of many other materials decrease under pressure (Hemley and Mao, 1997). Also, both theory and experiment indicate that the diamond index can increase with nonhydrostatic stress. Brillouin scattering provides independent measurements of the refractive index; results for MgO are in good agreement with the interference fringe measurements (Zha et al., 1997).

2.13.4.1.2 Luminescence

High-pressure luminescence measurements give in principle the same information as does absorption and reflectivity. Luminescence includes fluorescence and phosphorescence, which correspond to shorter- and longer-lived excited states (generally defined as in the less than and greater than a nanosecond, respectively). The transitions are typically governed by dipole selection rules. For the case of atomic-like transitions, such as localized excitations of ions in crystal fields, this can be understood in terms of the Laporte selection rules (i.e., $\Delta l = \pm 1$, where l is the angular momentum quantum number). An early and particularly important application in mineralogy is the use of this technique in constraining the proportion of Fe^{2+} and Fe^{3+} in various sites in silicates from d-orbital excitations (Rossman, 1988). Charge transfer applications are described earlier in the text. Other applications include excitations near and across bandgaps and excitations associated with defects.

Luminescence measurements are of obvious importance in the calibration of pressure. This includes excitation of Cr^{3+} in ruby by UV–visible lasers (e.g., He–Cd, Ar^+ ion, and doubled Nd–YAG) and measurement of the calibrated shift of the R_1 line in luminescence, currently calibrated to 180 GPa (Bell et al., 1986; Mao et al., 1978, 1986). The recent use of tunable lasers (e.g., titanium–sapphire) and pulsed excitation techniques has allowed the extension of the measurements of ruby luminescence to above 250 GPa (Goncharov et al., 1998). Other luminescent materials, such as Sm-doped yttrium aluminum garnet, have been calibrated for this pressure range (Liu and Vohra, 1996) and for high temperatures at lower pressures (Hess and Schiferl, 1992). Other applications include the study of vibronic spectra, which are combined (coupled) electronic and vibrational excitations. Measurements at high pressure reveal the pressure dependence of both the electronic and vibrational levels in the system, which can be used to determine acoustic velocities (given the assumptions about the dispersion of the modes and correct assignment of typically complex spectra; e.g., Zhang and Chopelas, 1994). There has been continued work on pressure calibration with optical spectroscopic methods (Goncharov et al., 2005b).

2.13.4.1.3 Infrared spectroscopy

Infrared spectroscopy is an extension of optical spectroscopy that typically involves different techniques (e.g., Fourier transform spectroscopy). In addition, the use of synchrotron radiation for infrared spectroscopy has been shown to be particularly useful for small samples such as those in high-pressure cells (**Figure 3(a)**). The technique can be used to study electronic and magnetic excitations, insulator–metal transitions, crystal field and charge transfer transitions, and, for metals, interband and intraband transitions (Hemley et al., 1998a). Optical studies under pressure, especially reflectivity and absorbance, provide unique information important for understanding fundamental changes in the electronic structure of these systems close to the insulator–metal transition because of the broad spectral range that extends to long wavelengths (low wave numbers). It can also provide unique information on magnetic excitations (Struzhkin et al., 2000). This study showed how the pressure dependence of the IR and Raman modes can be used to distinguish between magnon and electronic excitations. In addition, infrared vibrational spectral profiles contain information on the electronic properties, that is, through the KK transformation. An example of reflection spectra and the transformed data is shown in **Figure 3(b)** and **3(c)**.

2.13.4.1.4 Raman scattering

Although most commonly used to study vibrational dynamics, laser light-scattering spectroscopies can also be used to investigate high-pressure electronic and magnetic properties (**Figure 4**). Raman and Brillouin spectroscopies are inelastic light-scattering techniques that measure transitions to an excited state from the ground state (Stokes scattering) and to the ground state from a thermally excited state (anti-Stokes scattering). Low-frequency crystal field excitations of the appropriate symmetry can be probed, and the pressure dependence of such transitions has been studied in a few cases (Goncharov et al., 1994). The conduction electrons in metals can also be probed by Raman scattering, which in general gives rise to weaker broader features in the light-scattering spectrum. High-pressure studies are complicated by the need of

7500 cm^{-1} would nearly coincide. Sample thickness at ambient pressure is 30 μm. The absorption coefficients are based on the decadic logarithm and normalized to this sample thickness. Because of the compression of the sample, the absorption coefficients increase by about 9% relative to these values at 125 GPa. To obtain absorption coefficients based on the natural logarithm (i.e., eqn [2]), the scale needs to be multiplied with ln 10 = 2.30. The position of the maxima of thermal blackbody radiation at different temperatures is also shown for reference. The slight oscillations at low frequency in some spectra are artifacts (interference fringes). The small peak seen in some spectra close to 10 000 cm^{-1} is probably not real; it is likely related to the change in detector close to this frequency. Reproduced from Keppler H, Dubrovinsky LS, Narygina O, and Kantor I (2008). (c) Pressure dependence of the reflectivity of H_2O ice relative to diamond. *Science* 322: 1529–1532; and from Zha CS, Hemley RJ, Gramsch SA, Mao HK, and Bassett WA (2008) *Journal of Chemical Physics* 126: 07450.

discriminating the spurious background contaminations from the true electronic contribution. Superconductivity in metals gives rise to structure in the electronic Raman spectrum, such as gap-like features at low frequency (Zhou et al., 1996).

Such studies include magnetic transitions in AFM materials such as transition metal oxides predicted to undergo high-pressure insulator–metal transitions. These materials have magnetic anomalies that may be difficult to study directly at

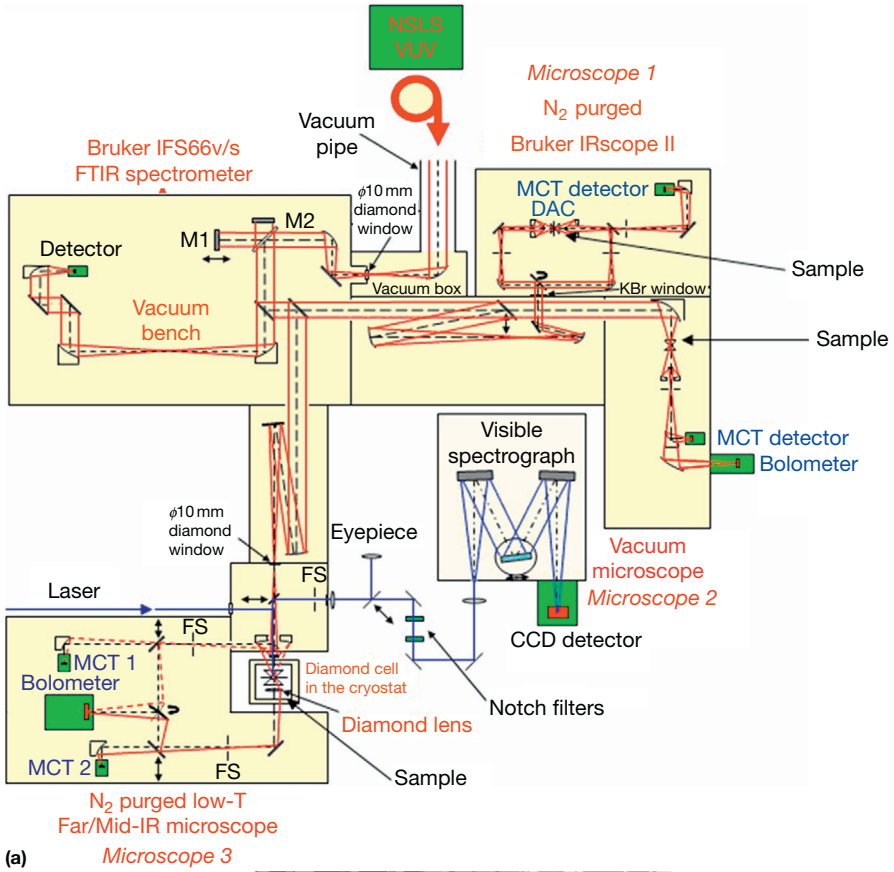

(a)

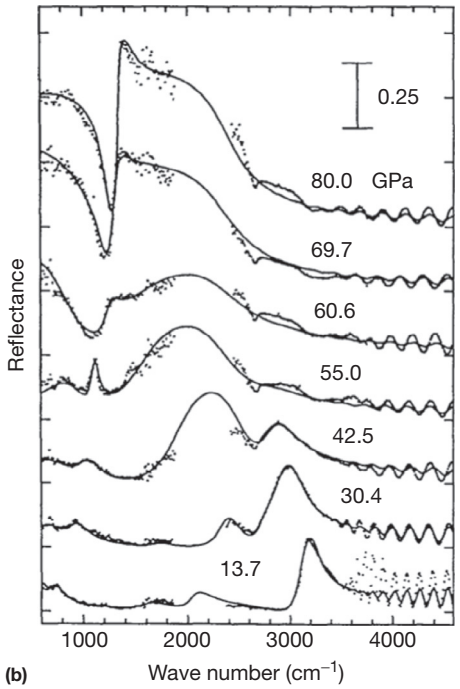

(b)

Figure 3 (continued)

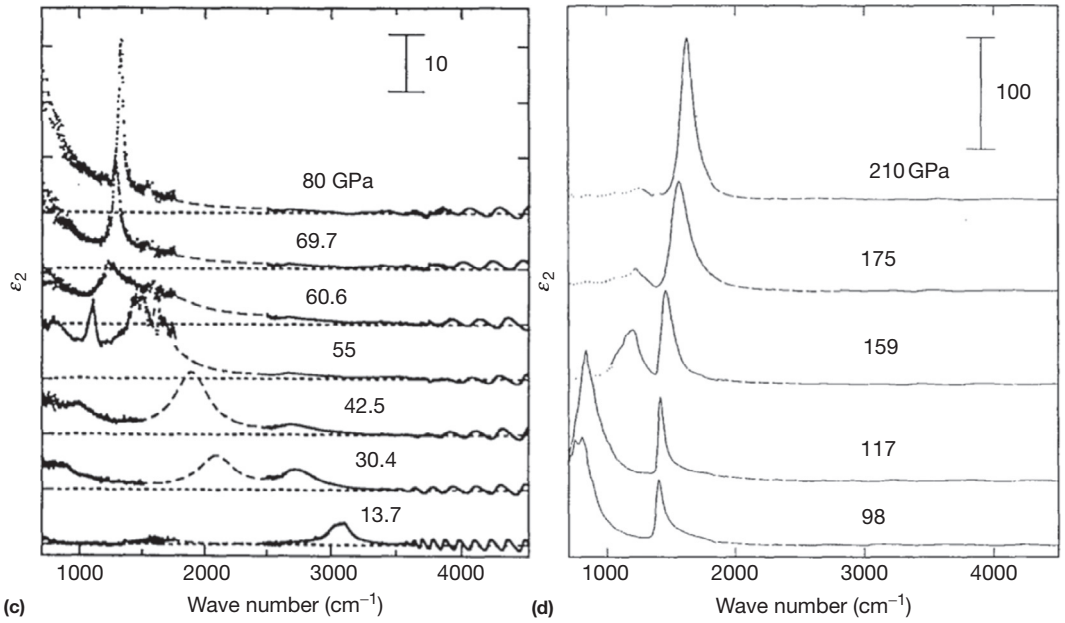

Figure 3 (a) Schematic of the high-pressure synchrotron infrared spectroscopy facility at the National Synchrotron Light Source (Beamline U2A). Three different microscopes are optically interfaced with the spectrometers. The sample is located within the high-pressure cell designated by diamond anvil cell or DAC. (b) Representative reflectivity spectra: points, experimental data; lines, oscillator model. Spectra are shifted with 0.25 unit increments in the vertical direction. There are no data in the range of the strong diamond absorption (1800–2400 cm^{-1}). Spurious oscillations at high frequencies originate from the Fabry–Pérot interference between the diamond anvil cells. The spectral region around 2600 cm^{-1} is complicated by the absorption of diamonds. Peculiarities in the spectra are due to incomplete cancellations of sharp features in reference and sample spectra. Reproduced from Goncharov AF, Struzhkin VV, Somayazulu M, Hemley RJ, and Mao HK (1996) *Science* 273: 218–220. (c) Imaginary part of the dielectric constant ε_2 of H_2O obtained from a Kramers–Kronig (KK) analysis of reflectivity spectra: points, KK transformation of experimental data; dashed lines, oscillator fit. The curves are offset in the vertical direction for clarity. Reproduced from Goncharov AF, Struzhkin VV, Somayazulu M, Hemley RJ, and Mao HK (1996) *Science* 273: 218–220. (d) ε_2 spectra of the H_2O (295 K) showing the positive pressure shift of the stretching mode to υ_s 210 GPa. Reproduced from Goncharov AF, Struzhkin VV, Somayazulu M, Hemley RJ, and Mao HK (1996) *Science* 273: 218–220.

high pressure, but these anomalies may be associated with pronounced changes in magnetic light-scattering spectra. These excitations have a strong temperature dependence because of the large temperature dependence of magnetic ordering (Struzhkin et al., 1993a). A large number of excitations are observed, including several very strong bands, all of which can be described by the appropriate Hamiltonian. Measurements of the two-magnon excitations in Fe_2O_3 and NiO by high-pressure Raman scattering constrain the magnetic properties of these materials at high density (Massey et al., 1990a,b). The pressure dependence of higher-order effects such as the coupling of the phonons with electron spin-pair excitations and the electronic structure of the material can also be probed (Massey et al., 1992). Although the higher-temperature behavior of such materials is of direct concern for the deep Earth (i.e., along the geotherm), detailed characterization of the low-temperature ground state is essential for understanding higher-temperature properties. The extremely low background signal in light-scattering experiments using ultrapure synthetic single-crystal diamond anvil cells (Goncharov et al., 1998) is enabling the extension of these light-scattering studies of electronic and magnetic excitations to a wider class of materials, including opaque minerals and metals. This is illustrated by high-pressure measurements on oxide superconductors, which can be considered analogs of dense oxide perovskite and perovskite-like planetary materials (Cuk et al., 2008; **Figure 5**).

2.13.4.1.5 Brillouin and Rayleigh scattering

In principle, other optical light-scattering techniques can be used to investigate electronic and magnetic phenomena at high pressure. Brillouin scattering involves the measurement of acoustic phonons; in metals, the measurements correspond to surface modes or plasmons. Brillouin scattering can also be used to determine the pressure dependence of the refractive index (dielectric function), usually in transparent materials. Rayleigh scattering is a quasi-elastic scattering spectroscopy; it has been used less in high-pressure studies of materials because of the difficulty of obtaining accurate measurements due to typically strong background scattering near the excitation wavelength (laser line) by the anvils in the high-pressure cell.

2.13.4.1.6 Nonlinear optical methods

One of the limitations of conventional one-photon absorption, reflectivity, and luminescence measurements is the fact that the absorption threshold of the anvils of the high-pressure cell precludes measurements on samples at higher energies (e.g., in the ultraviolet range), as mentioned in the preceding text. Nonlinear optical techniques can be used to access this region, however. For example, one can perform three-photon

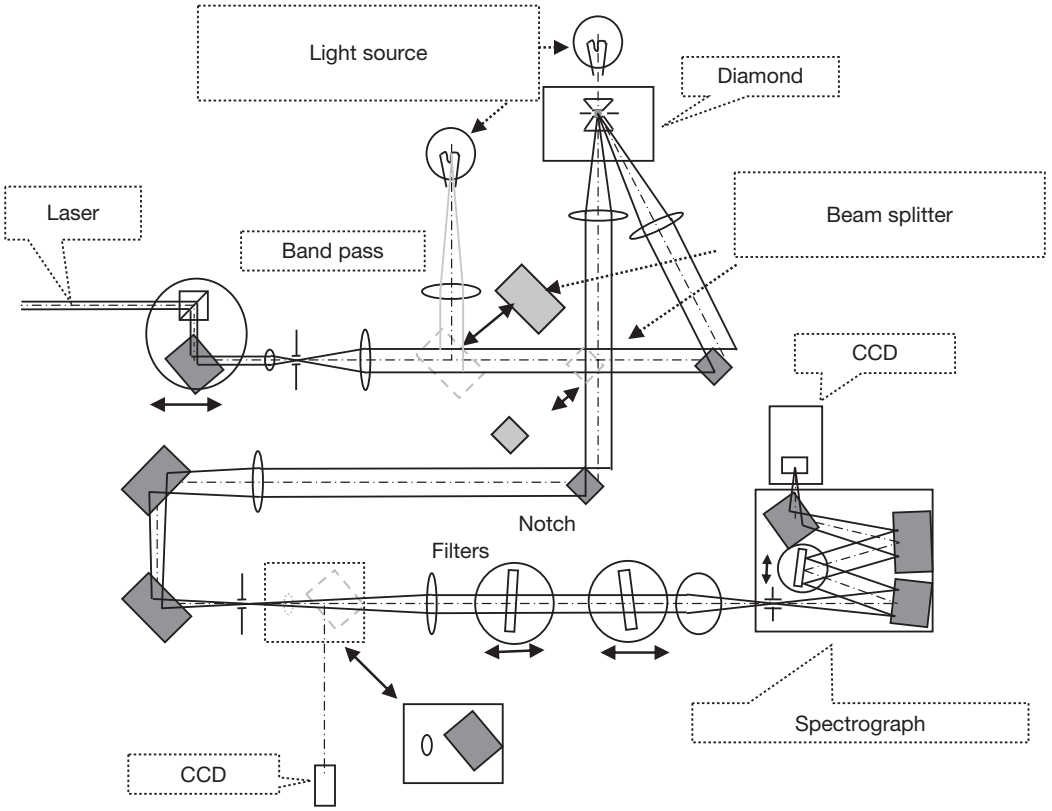

Figure 4 Schematic of a high-pressure Raman scattering system. The excitation wavelength can be easily tuned without changing the holographic optics and consequent realignment of the whole system; use of holographic transmission gratings (notch filters and band-pass filters) at wavelengths other than nominal does not typically result in a deterioration of the system's performance. Rapid changes in both the excitation wavelength and the spectral range are essential for high-pressure spectroscopy. The second important distinction of the system is that it allows rapid modifications of the scattering geometry to be made. In the case of a transparent sample or if the sample is heterogeneous or very small (e.g., at multimegabar pressures), the backscattering geometry in combination with a confocal spatial filter is probably the best choice. For nontransparent and highly reflective samples, a quasi-backscattering (or angular) geometry may be employed. This arrangement has the advantage that the specular reflection (or direct laser beam in the case of forward scattering) is directed away from the spectrometer. Compared with the backscattering geometry, this expedient reduces the overall background and allows the observation of lower-frequency excitations. In the case of metals, use of the angular excitation geometry can be crucial. To be compatible with this geometry, it was necessary to modify the DAC to allow off-axis entry of the incident light. Specially designed tungsten carbide seats having angular conical holes have been used for this purpose. Use of double-spatial filtering (one for the laser and one for the signal) effectively suppresses laser plasma lines and unwanted Raman/fluorescence signals. In this configuration, the laser spot can be made very small (e.g., 2 μm), and the depth of focus substantially reduced. Thus, the Raman signal from the diamond anvil cell is suppressed. Also, the effects of pressure inhomogeneity can also be substantially obviated. Use of synthetic ultrapure anvils can further reduce diamond fluorescence. This is crucial for studies of very weak scatters and/or materials at very high pressures (above 200 GPa), where strong stress-induced fluorescence of the diamond anvil cells can be a major obstacle to the acquisition of Raman or fluorescence spectra.

excitation of valence electrons to the conduction band or excitonic states in the vicinity of the conduction band, which is above the one-photon threshold of the anvil; this has been achieved in compressed salts in sapphire anvil cells (Lipp and Daniels, 1991). It is now possible to apply and extend these techniques to study to high-pressure minerals. Another category of techniques in this class is four-wave mixing experiments, such as coherent anti-Stokes Raman scattering (CARS). These rely on the third-order susceptibility and are enhanced when there are two-photon electronic resonances.

CARS is a nonlinear optical technique whereby a pump beam ω_P and a Stokes beam ω_S are mixed via third-order susceptibility to generate enhanced anti-Stokes emission. Enhanced anti-Stokes emission is observed when the narrowband pump and Stokes beams are detuned such that their difference frequency ($\omega_V = \omega_P - \omega_S$) corresponds to vibrational sideband. A resonantly enhanced signal is emitted in the presence of the second pump photon at the frequency $\omega_{CARS} = 2\omega_P - \omega_S$, subject to momentum conservation (phase matching) of the four-wave mixing process. Signal generation in CARS is coherent, with an intensity that grows quadratically with interaction length, unlike incoherent spontaneous Raman, where intensity grows linearly with interaction length. In order to achieve this enhancement, the pump and Stokes pulses must spatially and temporally overlap at the sample. Moreover, anti-Stokes emission is directional due to phase matching. The Stokes beam may be narrowband, which gives an anti-Stokes response at the difference between the pump and Stokes beams (which may be scanned), or broadband, where a broadband anti-Stokes spectrum may be detected in

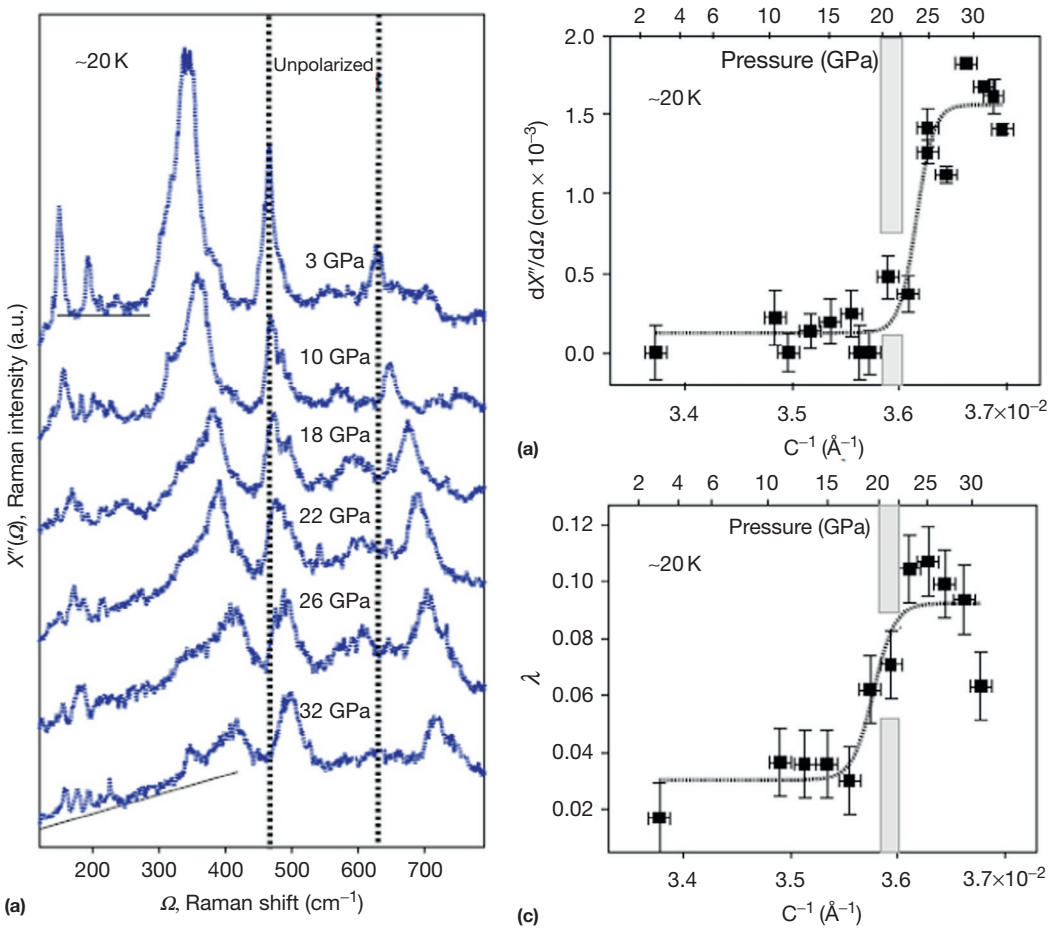

Figure 5 (a) Raman spectra of the B_{1g} phonon, O–Bi phonon in the Bi–O block layer, and the apical oxygen phonon at ~20 K with pressure. (b) Slope of the linear electronic background from 200 to 300 cm^{-1} at ~20 K. Spectra at each pressure were normalized to the intensity at 850 cm^{-1}. (c) The full Raman vertex, using a normal-state electronic background, was fit to 20 K data to derive the electron–phonon coupling parameter λ. Reproduced from Cuk T, Struzhkin VV, Devereaux TF, et al. (2008) *Physical Review Letters* 100: 217003.

a spectrometer. The previously mentioned considerations are important for choosing a correct experimental strategy in the case of the DAC. CARS spectroscopy has been used to study molecular materials under extreme conditions generated by shock waves. High-quality spectra have been obtained using a single (combined) laser pulse of several nanosecond duration. As described earlier in the text, in this experiment, the entire CARS spectrum is measured simultaneously using a broadband Stokes pulse. Similar techniques have been used in DAC studies. The overall CARS cross section is determined by the $\chi^{(3)}$ susceptibility, a nonlinear electronic property.

2.13.4.2 Mössbauer Spectroscopy

Mössbauer spectroscopy probes the recoilless emission and resonant absorption of γ-rays by nuclei (Mössbauer, 1958). The energy levels of the nuclei are sensitive to the electrostatic and magnetic fields present at the nuclei and thus to changes in chemical bounding, valence (i.e., the oxidation state of an atom, ferrous versus ferric), and magnetic ordering. Mössbauer spectroscopy reveals information on the hyperfine interactions and the local electronic and magnetic fields at a nucleus. Only a few nuclei exhibit the Mössbauer effect (e.g., ^{57}Fe, ^{119}Sn, ^{121}Sb, ^{153}Eu, and ^{197}Au), and the great majority of applications in Earth science (and in general) are with ^{57}Fe. The natural abundance of ^{57}Fe is 2.1%, so some studies require enrichment of ^{57}Fe to obtain a stronger signal. The technique has been used extensively in the mineralogy of deep Earth materials, including in situ high-pressure measurements. A typical probe for mineral systems is based on the reaction $^{57}Co + {}^{0}\beta^{57} \rightarrow Fe + \gamma$. In a conventional Mössbauer experiment, one modulates the energy of the γ-rays by continuously vibrating the parent source to introduce a Doppler shift of the radiation (see Dickson and Berry (1986) for an introduction to Mössbauer spectroscopy and McCammon (1995) for a review of applications to minerals).

The isomer shift is the shift in the nuclear energy level and corresponds to the source velocity at which maximum absorption appears. The electric quadrupole splitting arises from the interaction between the nuclear moment and quadrupole splitting and the local electric field gradient at the nucleus. This occurs for nuclei with spin quantum number $I > 1$ (i.e., for ^{57}Fe, $I = 3/2$). The hyperfine field is due primarily to the contact interaction between electrons at the nucleus and the nucleus, rather than to the macroscopic magnetic field in a material. A hyperfine field arises from different densities of spin up and down electrons at the nucleus.

Applications include determination of Curie and Neél transition temperatures, valence state, site occupancy, and local

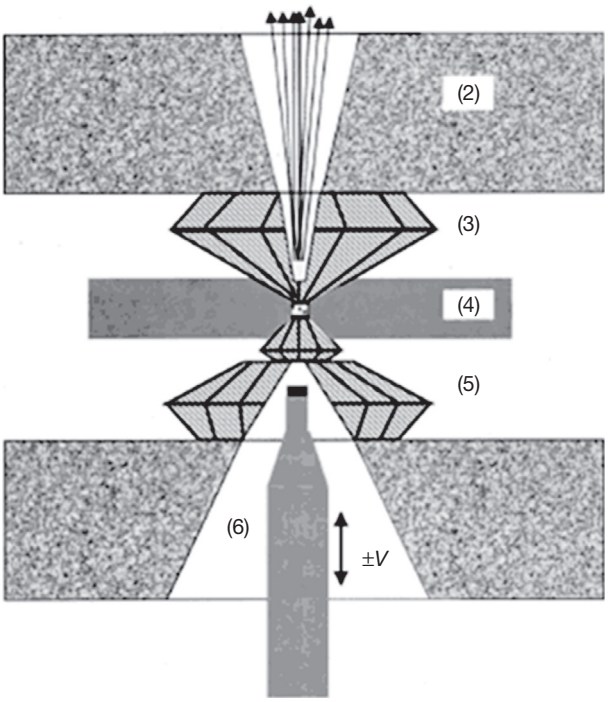

Figure 6 A sketch depicting the setup for high-pressure Mössbauer studies using perforated diamond anvil cells (see Dadashev et al. (2001) for details).

order. In studies of deep Earth materials at high pressure, each of these can be probed as a function of pressure (and temperature), including the measurement of changes across various transformations (crystallographic, electronic, and magnetic). Instrumentation consists of a radioactive source, vibrating drive, and detector (scintillator or proportional counter). Recent examples of high-pressure studies include measurements on a series of pyroxenes to 10 GPa (Zhang and Hafner, 1992) and measurements on $CaFeSi_2O_6$ to 68 GPa, which revealed evidence for a phase transition associated with a change in spin state. The Mössbauer technique has been extended into the megabar pressure range as discussed later in the text for FeO (Pasternak et al., 1997b; **Figure 6**). The Mössbauer studies on FeO along with acoustic sound velocity measurements show fascinating interplay between magnetic ordering and elasticity (Kantor et al., 2004b).

2.13.4.3 x-Ray and Neutron Diffraction

2.13.4.3.1 x-Ray diffraction

Crystal structures are determined by the system optimizing the interactions of electrons and nuclei and thus by details of bonding interactions between atoms; thus, crystallography is an essential mean for studying bonding and evolution of atomic interactions with pressure (Wyckoff, 1923). x-Ray diffraction relies on the interaction between x-rays and electron distributions in materials, so in principle, it can give the real-space charge density, but this requires high-quality crystals, corrections for absorption, and measurements to high q. The charge density includes smearing from atomic motions, which must be modeled and subtracted to obtain useful information. Few experimental charge densities have thus been obtained; one successful study was on stishovite (Spackman et al., 1987). Changes in electron density associated with crossing insulator–semiconductor–metal transitions can be identified (Fujii, 1996; Shen et al., 2012). Recently, a new method, the maximum entropy method (MEM), has been developed as a practical technique for solving crystal structures. Based on information theory and using Bayesian statistics, it builds electron density through constrained entropy maximization. The MEM statistically estimates the most reliable electron density distribution from the finite observed structure factors, removing the problem caused by the termination effect in the difference Fourier synthesis. Recent work has included studies of oxides by Yamanaka (2007) and changes in electron density across spin transition of Fe^{2+} in ferropericlase (Ikuta et al., to be published). The advent of third-generation synchrotron radiation sources and modern area detectors is potentially important for extending these measurements to deep Earth materials at very high pressures. As discussed in the preceding text, pressure can induce complex crystal structures in simple elements, in principle yielding detailed information about atomic interactions. Because this structural complexity is driven in part by bonding and electronic structure, detailed understanding of this real-space atomic structure of these phases provides insight into the electronic structure. The latest developments in single-crystal x-ray diffraction at high pressure and high temperature have benefited greatly from advances in large opening designs of DAC (Boehler et al., 2013) and high-energy x-ray sources, which allows collecting single-crystal diffraction data at pressures above 100 GPa and at temperatures above 1000 °C (Boffa Ballaran et al., 2013; Dera et al., 2013). In addition to the single-crystal diffraction, intensity information in powder diffraction is now widely used for structure refinement via the Rietveld (1966) method. It must be noted that the Rietveld method does not provide the initial model to be refined. Traditional methods of structure analysis, such as Patterson synthesis or direct methods, are often used to establish the basic features of the structure, after which the Rietveld refinement can be carried out. Recently, many successful structure predictions have been made by the first principles (e.g., Oganov, 2010; Wang and Ma, 2014). These theoretical predictions provide important basic models in further structure refinement with experimental data. With the developments in microbeam technology in synchrotron radiation, the minimal size needed for single-crystal diffraction has been reduced to around 1 μm. Traditional powder sample may be treated as multiple grains. A new tool of 'multigrain crystallography' has been recently developed with the quality of the resulting refinements comparable with single-crystal work (Sørensen et al., 2012). The multigrain approach holds great potentials for crystallographic studies of deep Earth materials, as demonstrated recently by a study of single-crystal structural determination of $(Mg,Fe)SiO_3$ postperovskite (Zhang et al., 2013).

2.13.4.3.2 Neutron diffraction

Neutron scattering is complementary to x-ray scattering, and it has the advantages relative to x-ray scattering by virtue of its sensitivity to low-Z elements, angle-independent form factor, high penetrating power, and sensitivity to magnetic order. Because the scattering amplitude of neutrons by an atom depends on the direction of its magnetic moment, neutron diffraction can be used to map out the orientation of the

magnetic moments in the unit cell of a crystal. There have been a growing number of in situ high-pressure measurements on minerals (Parise, 2006). Advances have been made possible by the development of new classes of high-pressure devices, notably the Paris–Edinburgh cell and various types of gem anvil cells (Figures 7 and 8). An example is the high-pressure polymorphism of FeS in which the transformation to FeS II at 3.4 GPa was found to be associated with a spin-reorientation transition (Marshall et al., 2000). A second example is Fe_2O_3, for which the AFM ordering can be tuned by pressure (Goncharenko et al., 1995; Parise, 2006). High-pressure neutron scattering of FeO carried out with gem anvil cells revealed a surprising absence of long-range magnetic order to 20 GPa (Ding et al., 2005).

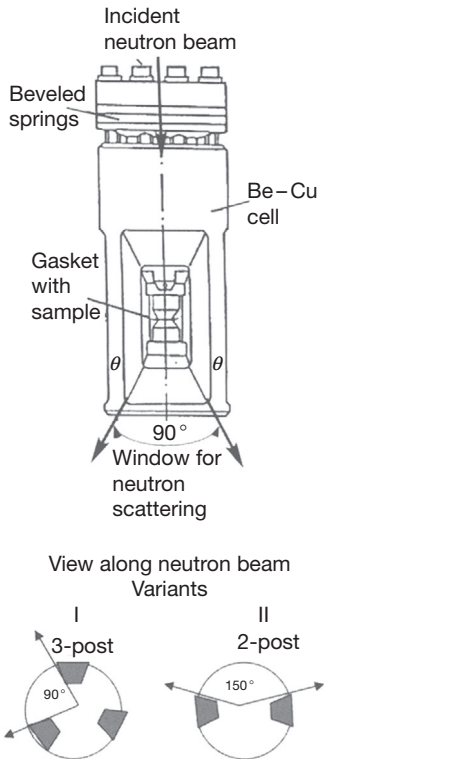

Figure 7 A variation of the 'gem cell.' Reproduced from Ivanov AS, Goncharenko IN, Somenkov VA, and Braden M (1995) *Physica B* 213: 1031–1033.

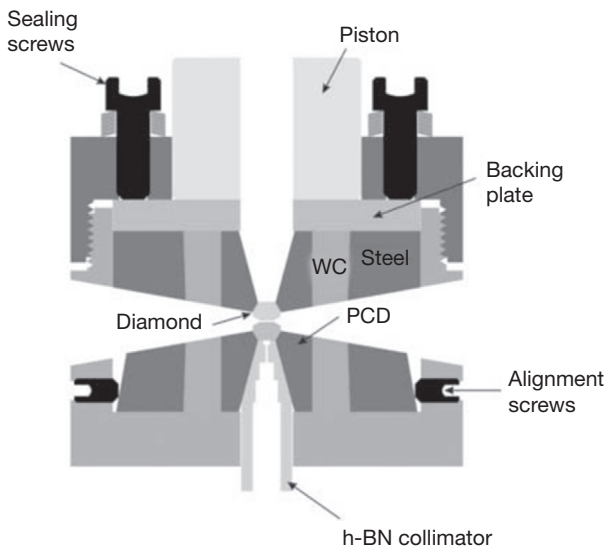

Figure 8 Schematic of a new diamond anvil cell accommodating binding ring supports for conical anvils for high-pressure neutron scattering. Reproduced from Boehler R, Guthrie M, Molaison JJ, et al. (2013) *High Pressure Research* 33: 546–554.

The coupling of phonons with the high-spin/low-spin transitions can be observed by x-ray techniques (Schwoerer-Bohning et al., 1996). Inelastic neutron scattering can also be used to excite magnetic transitions; it requires high energies and the measurement of low-momentum transfer. Measurements of crystal field transitions at zero pressure have been reported (Winkler et al., 1997). Given the intensity of current neutron sources, large samples are required.

2.13.4.4 Inelastic x-Ray Scattering and Spectroscopy

Advances in synchrotron radiation techniques have resulted in significant developments in x-ray spectroscopy, as well as diffraction, of minerals and related materials under pressure. x-Ray spectroscopies can be used as a probe of electronic structure; these techniques thus constitute an alternative to methods requiring the use or measurement of charged particles interacting with a sample (e.g., electrons in photoemission). As such, x-ray spectroscopies can be used for in situ study of properties such as band structures and local electronic structure.

Applications to mineralogy and geochemistry of Earth materials in the near-surface environment have been described previously (Brown et al., 1988). The applications at high pressure were reviewed since 1998 (Hemley et al., 1998b). Prior to this, very little x-ray spectroscopy had been conducted under pressure, and most of it has been limited to x-ray absorption spectroscopy (XAS). With new developments, the following methods are being used and/or developed for high-pressure studies of geophysically important materials: x-ray emission spectroscopy (XES), XAS, x-ray magnetic circular dichroism (XMCD), x-ray inelastic near-edge spectroscopy (XINES), electronic inelastic x-ray scattering (EIXS), resonant inelastic x-ray scattering (RIXS), Compton scattering (CS), nuclear resonant forward scattering (NRFS), nuclear resonant inelastic x-ray scattering (NRIXS), and phonon inelastic x-ray scattering (PIXS).

These x-ray intensity-limited techniques have become practical with the arrival of the third-generation high-energy synchrotron sources. Since higher pressures are reached at the expense of diminishing sample volume, the pressure limit of these experiments depends upon the ability of passing the maximum number of photons into a microscopic sample volume. The development of high-pressure x-ray spectroscopy has also been hindered by the opaqueness of high-pressure vessels. Recently, third-generation sources have greatly boosted the intensities, and new high-pressure techniques such as the development of high-strength but x-ray transparent Be gaskets have extended the window for measurements from 12 keV down to 4 keV. This extended x-ray energy range allows the study of pressure-induced effects on atomic coordination,

crystal structures, and electronic properties of a wider class of minerals using a variety of x-ray spectroscopies. The region below 4 keV (e.g., soft x-ray and vacuum ultraviolet) is still opaque in all kinds of high-pressure devices; however, inelastic scattering techniques provide a means to access states that cannot be probed by direct (one-photon) processes due to the opaqueness of the anvil and gasket (e.g., in the soft x-ray region).

2.13.4.4.1 x-Ray absorption spectroscopy

In XAS, incident x-ray is absorbed when its energy exceeds the excitation energy of deep-core electrons of a specific element in the sample, causing an atomic edge-like absorption spectrum. Near-edge x-ray absorption fine structure (XANES) (Ablett et al., 2003) provides information on symmetry-projected conduction band density of states (DOS), while the extended x-ray absorption fine structure (EXAFS) (Buontempo et al., 1998; Pascarelli et al., 2002) provides local structure information. XAS is typically monitored by broadband fluorescence. Different spectral regions in the vicinity of a core-level absorption edge are typically defined on the basis of the different information they contain. EXAFS arises from multiple scattering of electrons in the environment of an atom, from which local structural information (interatomic distances and coordination) is obtained. Spin-dependent XAS can reveal magnetic properties even in the absence of long-range magnetic order (Hämäläinen et al., 1992).

These element-specific probes reveal electronic and structural changes at high pressure (Itie et al., 1992). XAS was one of the first x-ray spectroscopy techniques applied at high pressure (Ingalls et al., 1978), but was previously limited to higher energies due to the absorption of diamond anvil cells. Both techniques extend XAS down to 4 keV that covers K-edges of first-row transition elements and L-edges of rare earth elements. XAS instrumentation is among the simplest in high-pressure x-ray experiments. Only the monochromator needs to be scanned across the specific energy edge of the element of interest. The monochromatic x-rays are focused by mirrors (e.g., meter-long K–B type) upon the sample in the cell. The absorption is measured by monitoring the intensity change of either the transmission or the fluorescence signals due to the absorption/reemission process and is normalized relative to a reference intensity measured before the sample. The large, high-demagnification, K–B mirrors provide sufficient intensity, with the beam diameter matching the small sample size at ultrahigh pressure.

High-pressure XAS has been used successfully for transition elements at moderate pressures with boron carbide anvils (Wang et al., 1998) and for higher-Z materials (Itie et al., 1992; Pasternak et al., 1997a; Zeng et al., 2010). EXAFS is now well developed for high-pressure studies (Hong et al., 2009; Ishimatsu et al., 2012; Itie et al., 1997) and can be measured by absorption or fluorescence. In addition, the Laue diffraction of single-crystal diamonds causes sharp absorption peaks that are detrimental to the EXAFS spectroscopy. To greatly reduce the diamond in the beam path, holes can be drilled in diamond anvil cells, as used in the Bassett-type hydrothermal diamond anvil cell for studying ions in aqueous solutions at moderate P–T conditions (Anderson et al., 2002; Bassett et al., 2000), and alternative beam path through high-strength beryllium and boron gaskets is used in megabar panoramic diamond anvil cells (Mao et al., 2003a). Early high-pressure work with diamond anvil cells was limited by the Bragg diffraction from the diamond and by the absorption edge of the diamond and the gasket. Because of the low energy of the Si edge, high-pressure studies of germanate analogs have been carried out (Itie et al., 1989). The development of more transparent gaskets has helped to overcome these problems. High-quality XANES (Zeng et al., 2010) and EXAFS (Mayanovic et al., 2007) data have been collected for transition metals in DAC experiments with energies between 5 and15 keV. In studying absorption edges over 30 keV, XAS data from a DAC are contaminated by diffraction from single-crystal diamond anvil cells. Using nanodiamond as anvil material, the contamination from single-crystal diffraction can be avoided (Ishimatsu et al., 2012). EXAFS is particularly useful for studying the pressure effects on the structures of liquids (Katayama et al., 1998; Ohtaka et al., 2004) and amorphous solids (Baldini et al., 2010; Mobilio and Meneghini, 1998). A notable example is the observation of the coordination change in crystalline and amorphous GeO_2 (Baldini et al., 2010; Itie et al., 1989). Mobilio and Meneghini (1998) provided a review of the variety of synchrotron-based x-ray techniques for studying amorphous materials, including techniques such as anomalous scattering that can be used in conjunction with EXAFS.

An energy-dispersive XAS technique has been developed (Pascarelli and Mathon, 2010), in which a focused polychromatic beam (~5 μm) of extremely high flux passes a sample and is collected by an energy-dispersive detector capable of fast capturing the XAS signals at microsecond level (Andrault et al., 2010; Boehler et al., 2009). The fast measurement and small beam size in this technique allow for mapping XAS images by scanning the sample position (Aquilanti et al., 2009).

2.13.4.4.2 x-Ray emission spectroscopy

In this technique, deep-core electrons in the sample are excited by x-rays. The core holes then decay through either radiative or nonradiative processes. For deep-core holes, the dominant decay channels are radiative processes, producing fluorescence, which is analyzed to provide information on the filled electronic states of the sample. The information provided by XES is complementary to that provided by XAS on valence electrons and unoccupied states. Moreover, the final state of the fluorescent process is a one-hole state, similar to the final state of a photoemission process. Thus, the most important information provided by photoelectron spectroscopy, that is, large chemical shifts in the core-level binding energies and the valence band DOS, is also available in XES.

The energies of the fluorescent photons are analyzed with subelectronvolt energy resolution of the emission spectral line shape to provide information on the filled electronic states of the sample. As for XAS, the development of panoramic diamond anvil cells has extended the low end of the high-pressure energy window down to 4 keV (Lin et al., 2003a; Mao et al., 1998). Deep-core electrons of all elements above Ca can now be studied at high pressure by a suitable choice of analyzer crystals. For instance, transition-element ions, with their variable valence and magnetic states, control major geochemical processes and geophysical behaviors, such as oxidation,

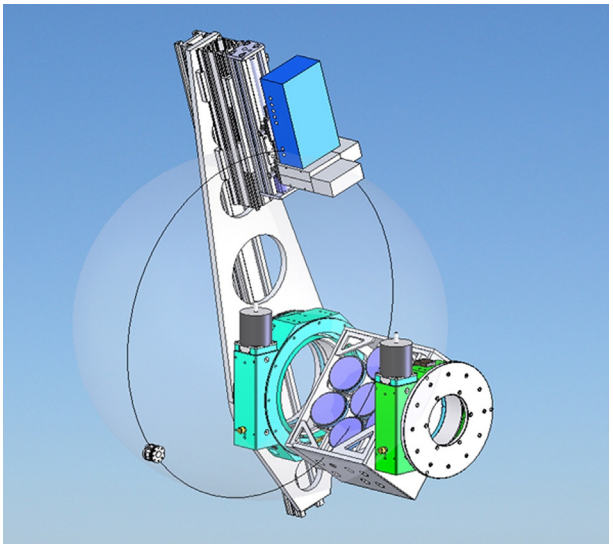

Figure 9 A 1 m Rowland circle spectrometer equipped with the 7-element analyzer system at High Pressure Collaborative Access Team (HPCAT) sector at the Advanced Photon Source. DAC, detector, and analyzers are along the circle, with precise controls of θ and 2θ for synchronized scans.

reduction, chemical differentiation, elasticity, geomagnetism, conductivity, and radiation heat transfer.

In XES experiments, the incident beam impinges on the sample, the emission x-radiation can be collected at any direction, and high-resolution emission spectra are obtained by a synchronized θ–2θ scan of the analyzer and the detector. A high-resolution Rowland circle spectrometer is often used. Because emission signals can be collected at any direction, multiple analyzers may be used to increase solid angle coverage in data collection and thus the signal level (Figure 9). Recently, a short-distance spectrometer of large solid angle coverage has been developed, with which data collection time in XES is reduced from hours to only several minutes (Pacold et al., 2012). The excitation x-ray source only needs to have a higher energy than that of the fluorescent photons; the energy bandwidth (resolution) of the x-ray source is inconsequential. In principle, white (a broad, smooth continuum of energy), pink (an unfiltered undulator beam with energy band path of hundreds of electronvolts), and monochromatic (a narrow, electronvolt band path of photon) x-rays can all be used as the source.

Examples of high-pressure XES include the study of predicted high-spin/low-spin transitions in iron oxides and sulfides. A schematic of the K_β emission process in Fe^{2+} is shown in Figures 10 and 11. In an atomic picture, the final state of the K_β is a whole state with $1s^2 3p^5 3d^5$. The measurement also reveals the XANES portion of the spectra, that is, including the pre-edge peak associated with transitions to unoccupied d-states (i.e., 3d in Fe). By measuring the absorption through selective monitoring of the fluorescence peaks, information on the contribution of different spins to the spectrum can be obtained.

XES of the Fe-K_β emission was first measured with a white x-ray source at a second-generation facility (NSLS); the high-spin to low-spin transition in troilite (FeS), coinciding with its I–II structural transition, was observed (Rueff et al., 1999). Subsequently, with higher source intensity, the technique has

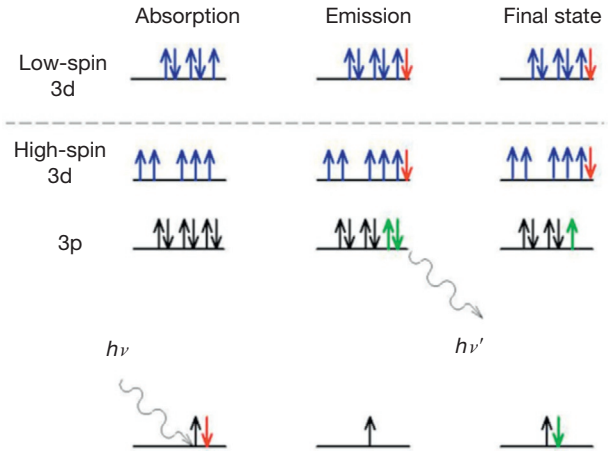

Figure 10 The schematic diagram of the K_β emission process.

been applied at APS and European Synchrotron Radiation Facility (ESRF) for studies of high-spin to low-spin transitions in wüstite (Badro et al., 1999), hematite (Badro et al., 2002), magnesiowüstite (Badro et al., 2003), perovskite (Li et al., 2004; Lin et al., 2012), and postperovskite (Yamanaka et al., 2012) to above 100 GPa pressures. The technique has been extended to high P–T conditions in combination with laser-heating techniques (Figure 12).

Resonant XES (RXES), or partial fluorescence yield (PFY), has also been successfully utilized in high-pressure studies. RXES may be viewed as a combination of XES and XAS. Instead of collecting transmitted x-rays as in XAS, emission spectra are measured at each step as the incident beam energy is changed or scanned across an absorption edge. This resonant method significantly enhances footprints of electron states and has a remarkable sharpening effect in projected spectra (RXES or PFY) (Rueff, 2010; Wang et al., 2010). Resonant x-ray emission spectra have allowed for resolving crystal field splitting of Fe^{3+} in Fe_2O_3 at HP (Wang et al., 2010) and intermediate-spin state of Fe_3O_4 at 15–16 GPa (Ding et al., 2008).

There have been significant developments in the ab initio treatment of such spectra, in particular, the electron–hole attraction, which requires going beyond a simple mean-field approach such as the local-density approximation (LDA) (Shirley, 1998). This is needed for x-ray absorption and RIXS. Measurements of the effect of pressure on plasmon excitations in metals (e.g., the high-pressure phase of Ge) suggest the potential for investigating the electronic structure of core materials at megabar pressures.

2.13.4.4.3 x-Ray inelastic near-edge spectroscopy

Near core-electron absorption edge features measured by soft x-ray absorption (XANES) or electron energy loss spectroscopy reveal information on chemical bonding. Such information is particularly pronounced and important for light elements but has been inaccessible for high-pressure studies as the pressure vessel completely blocks the soft x-ray and electron beams. With XINES, the high-energy incident x-ray penetrates the pressure vessel and reaches the sample. The scattered photon loses a portion of energy corresponding to the K-edge of the low-Z sample but can still exit the vessel to be registered on

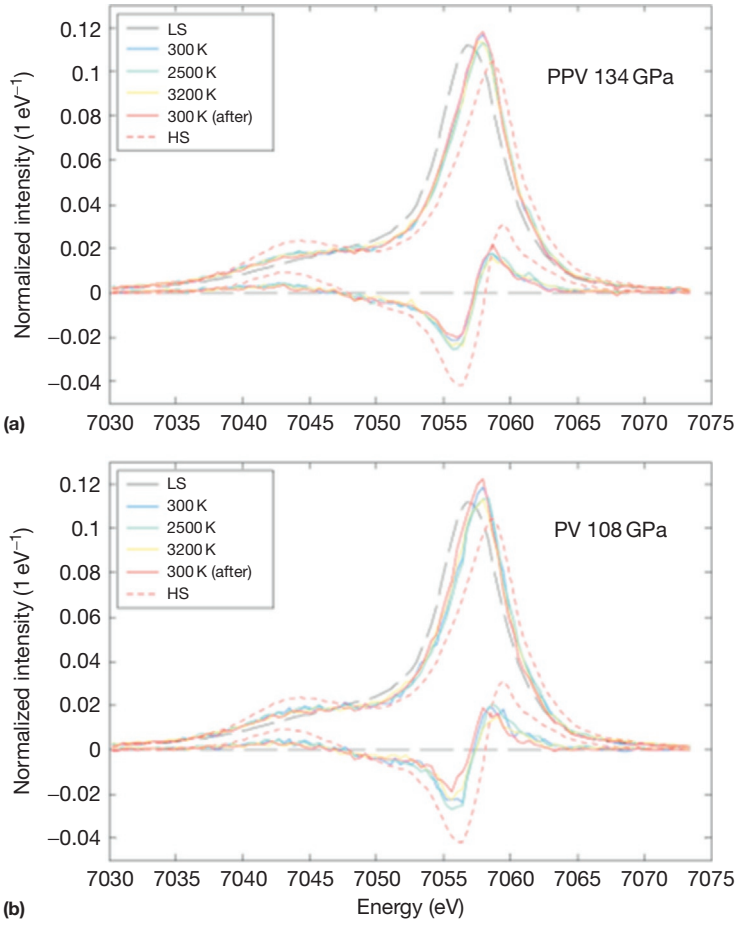

Figure 11 x-Ray emission spectra of $(Mg,Fe)SiO_3$ postperovskite at 134 GPa and perovskite at 108 GPa in laser-heated DAC. High-spin and low-spin references are used for the integrated absolute difference analysis, and differences from the low-spin line shape, shown below the spectra, are used to derive the average spin number of Fe^{2+}. An energy shift of 0.8 eV in the main K_β emission peak, which is approximately half of the energy shift in the high-spin to low-spin transition in ferropericlase, is also used to derive the total spin number, providing an additional evidence for the occurrence of the intermediate-spin state. Reproduced from Lin JF, Watson H, Vanko G, et al. (2008) *Nature Geoscience* 1: 688–691.

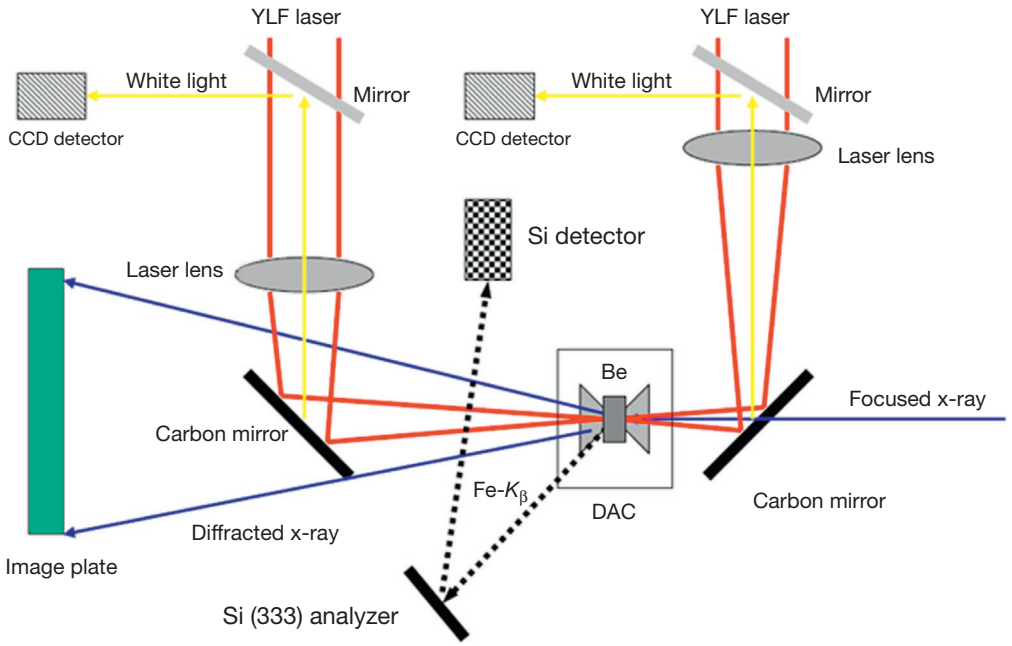

Figure 12 Schematic of the x-ray emission spectroscopy with laser-heated DACs. The YLF laser beam is focused to 25 μm onto the both sides of the sample surfaces. The diameter of the focused x-ray beam at 14 keV was approximately 7 μm (FWHM); the small beam size ensures that the x-ray emission signal from the sample is measured only within the laser-heated spot of 25 μm. The technique has been used to the study single-crystal magnesiowüstite $[(Mg_{0.76},Fe_{0.24})O]$ sample loaded into the sample chamber of a diamond anvil cell with flat diamonds with a culet size of 300 μm. The Fe-K_β fluorescence lines were collected through the Be gasket by an 1 m Rowland circle spectrometer in the vertical scattering geometry. An image plate (MAR345) is used to collect diffracted x-ray in the forward direction. Figure reproduced from Lin JF, Struzkhin VV, Jacobsen SD, et al. (2005d) *Journal of Synchrotron Radiation* 12: 637–641.

the analyzer–detector system. Inelastic K-edge scattering spectra of second-row elements from Li (56 eV) to O (543 eV) at high pressures opened a wide new field of near K-edge spectroscopy of the second-row elements, as in carbon in graphite (Lin et al., 2011; Mao et al., 2003a) and boron and oxygen in amorphous Earth materials (Lee et al., 2014).

In XINES experiments, spherically bent single-crystal analyzers collect scattered x-radiation and focus it to the detector at nearly backscattering geometry, thus fixing the energy at the elastic line. The incident x-ray energy is scanned relative to the elastic line to determine the inelastic (Raman) shift. Since XINES probes the core-electron energy level at hundreds of electronvolts, the undulator gap need to be changed to follow the energy scan of the double monochromator. For most high-pressure XINES measurements, the intrinsic peak width is of the order of electronvolts, and the direct beam without a high-resolution monochromator and 1 m analyzer-to-detector distance would usually suffice. The angle 2θ between the incident beam and the scattered x-radiation defines the momentum transfer ($q = 4\pi E \sin\theta$ where E is the scattered x-ray energy). XINES features are relatively insensitive to q, except for the extremely large and small q (Krisch et al., 1997). The 2θ angle for high-pressure XINES study can thus be set at an angle (e.g., 30°) to optimize the intensity, the collimation in the detection path, and multiple analyzers used to increase the count rate without discriminating q. Data collection efficiency can be increased by the use of an array of analyzers developed; such techniques were used for measurements for graphite (Lin et al., 2011; Mao et al., 2003a), boron (Lee et al., 2008a; Meng et al., 2004), hydrocarbons (Fister et al., 2007), oxygen in glasses (SiO_2, B_2O_3, GeO_2, and $MgSiO_3$) (Lee et al., 2008a; Lelong et al., 2012; Lin et al., 2007; Yi and Lee, 2012), and H_2O (Cai et al., 2005; Fister et al., 2009). Because the features in XINES are sensitive to local 'short-range' structure, the technique has been particularly useful in revealing structural changes in no-crystalline oxides and silicates at high pressure. For example, topological disorder tends to increase with pressure as shown by the increase in the width of the O K-edge absorption with increasing pressure (Lee et al., 2008b). The XINES data of shock-compressed oxide glasses provide strong geochemical implications for impact processes (Lee et al., 2012).

2.13.4.4.4 x-Ray magnetic circular dichroism

This technique measures the spin polarization of an electronic excitation on FM materials by the use of circularly polarized x-rays. It is therefore in principle identical to conventional optical magnetic circular dichroism (MCD) with visible light (magneto-optic Kerr effect). In synchrotron radiation experiments, an x-ray phase plate changes the x-rays from linearly to circularly polarized. XMCD can be observed in both XANES and EXAFS. XMCD in XANES can measure spin-resolved conduction band densities of states, whereas XMCD in EXAFS provides local magnetic structural information. The sign of the dichroism gives the FM coupling between atoms in a metal. High-pressure MCD measurements have been performed (Baudelet et al., 1997). For magnetic samples, magnetic circular dichroism is also observable in XES by exciting core holes with circularly polarized x-rays. With the low end of the high-energy window extended down to 4 keV by the high-strength Be gasket, all elements above Ca ($Z = 20$) in principle can be studied at high pressure with a suitable choice of analyzer crystals. Crystal analyzers have been developed for inelastic x-ray scattering (IXS) with subelectronvolt energy resolution of emission spectral line shapes for studies of oxidation states, electronic energy level, spin states, and trace element analysis. In particular, the important 3d and 4f emission bands can be studied to very high pressures (Fabbris et al., 2013; Gorria et al., 2009; Haskel et al., 2011; Iota et al., 2007; Souza-Neto et al., 2012).

XMCD is the technique of choice to study ferro(ferri)magnetic materials, yielding element and orbital-selective magnetization, which is of advantage in cases where more than one magnetic element is present. The selectivity is also beneficial for elucidating the role of selected electronic orbitals in mediating magnetic interactions. Neutron scattering techniques, on the other hand, probe the magnetic moment of all scattering atoms simultaneously. Similarly, SQUID magnetometry lacks element specificity and is limited to lower applied pressures due to restrictions in sample environment. Other x-ray probes of magnetism include XES and nuclear resonance x-ray scattering (Mössbauer) spectroscopy. Unlike XMCD, XES is a probe of local magnetic moment and is not sensitive to magnetic ordering, while Mössbauer spectroscopy can only be applied to selected isotopes.

2.13.4.4.5 Electronic inelastic x-ray scattering

Pressure has dramatic effects on the energy and dispersion of all electronic bands. Many electronic levels, including some of the most intriguing pressure-induced changes, occur above the intrinsic, 5 eV, bandgap of the diamond window and are thus inaccessible by the standard vacuum techniques such as electron and ultraviolet spectroscopy probes. Using 10 keV x-ray beam for excitation and 0.3–1 eV resolution, IXS can in principle probe the full range of high-energy electronic levels, that is, the electronic band structure (Caliebe et al., 2000), Fermi surface (Huotari et al., 2000), excitons (Arms et al., 2001; Mao et al., 2010), plasmons (Hill et al., 1996; Mao et al., 2011), and their dispersion at high pressure. The instrumentation of EIXS is similar to that of XINES, except both energy and q need to be scanned to obtain the dielectric function $\varepsilon(E, q)$ and the dynamic structure factor $S(E, q)$, EIXS probe valence, and conduction electronic structures at low energies up to a few tens of electronvolts from the elastic line. Many high-pressure EIXS can use the same 1 eV resolution setup as high-pressure XINES.

2.13.4.4.6 Resonant inelastic x-ray spectroscopy

Shallow core excitations are the same excitations probed by soft XAS and are rich in multiplet structures for these highly correlated electronic systems. There have been a growing number of RIXS studies of core excitations (Ament et al., 2011; Bartolome et al., 1997; Hill et al., 1998; Kao et al., 1996a; Kotani and Shin, 2001; Krisch et al., 1995; Rueff, 2010); that is, the final states of the inelastic scattering process in these studies are localized shallow core excitations. For magnetic samples, excitation with circularly polarized x-rays can also provide information on spin-resolved electronic structure (DeGroot et al., 1997; Krisch et al., 1996).

In RIXS experiments, both incident and scattered x-ray energies are scanned. The incident x-ray energy is scanned

across the core absorption similar to the procedures for XAS. For each monochromatic incident x-ray energy, fluorescence spectra are collected by scanning analyzers similar to the procedures of XES. One can obtain selected information connected directly with a specific intermediate state to which the incident photon energy is tuned. RIXS in transition metal and rare earth systems gives us important information on the electronic states, such as the intra-atomic multiplet coupling, electron correlation, and interatomic hybridization. Unusual phase transitions driven by electron correlation effects occur in many transition metals and transition metal compounds at high pressures, some accompanied with large volume collapses (e.g., 5–17% in rare earth metals and 10–15% in magnetic 3d transition metal oxides) (Bradley et al., 2012). Examples include Bradley et al. (2012), Maddox et al. (2006), and Ding et al. (2008). The nature of these transitions, including the relationships between the crystal and electronic structures and the role of magnetic moment and order, is an area of active study (e.g., Ament et al., 2011).

2.13.4.4.7 IXS spectroscopy

IXS spectroscopy (IXSS) measures the dynamical structure factor, and as such, it is similar to inelastic neutron scattering (Ghose, 1988). Formally, $S(q, \omega)$ is related to the space–time Fourier transform of the density correlation function, which provides information on the electronic band structure and elementary excitations (such as phonons and plasmons) and in turn thermal, optical, magnetic, and transport properties of the material (Ament et al., 2011; Hill et al., 1996). IXSS has a number of advantages in comparison with other scattering probes, such as those that use (optical) light, electrons, and neutrons (Kao et al., 1996b; Krisch et al., 1995). For example, light scattering can only probe zero-momentum transfer transitions; electron scattering suffers from multiple scattering effects and can only be used in high vacuum conditions; neutron scattering needs very large samples. On the other hand, IXSS covers wide length (momentum) and temporal (energy) scales that are potentially important in high-pressure mineral studies. Low-energy excitations have been studied with ultrahigh resolution ($\sim$1.5 meV or 12 cm^{-1}) IXSS techniques (Ruocco et al., 1996; Sampoli et al., 1997). The resolution that can be achieved is as good as or better than what has been achieved by the best angle-resolved photoemission spectrometer.

Another variation on these techniques is high-resolution resonant x-ray Raman scattering, which is in principle like the more familiar Raman scattering at optical wavelengths. It can be viewed as an instantaneous absorption and emission process where the initial and final states are electronic and magnetic (rather than vibrational) states. In such RIXS, one detects electronic excitations of $\omega = \omega_1 - \omega_2$ and monitors momentum transfer $q = q_1 - q_2$. Examples include the study of the metal–AFM insulator transitions (Isaacs et al., 1996), but the technique has not yet been used for high-pressure minerals. Studies at ambient pressure have shown that it is possible to measuring EXAFS-like spectra for K-edges of low-Z elements by x-ray Raman; similar studies in high-pressure cells could provide probes of local structure (e.g., of Si) that cannot be studied by direct EXAFS techniques.

2.13.4.4.8 Compton scattering

CS is an inelastic scattering at high momentum transfer that probes electron momentum distributions. The details of the momentum distribution reveal information about bonding type (e.g., covalency) and band structure, particularly in combination with electronic structure theory (Isaacs et al., 1999). The availability of intense synchrotron radiation sources, particularly the high brightness at very high energies ($\sim$50 keV), and the development of high-resolution spectrometers are opening up new classes of CS experiments on small samples and at high pressures. The method has been applied to elemental solids such as Na and Si in Paris–Edinburgh cells, but not yet to geophysical materials (Hämäläinen et al., 2000; Tse et al., 2005).

2.13.4.4.9 Nuclear resonance forward scattering

As described earlier in the text, Mössbauer spectroscopy has been used extensively in high-pressure mineralogy in laboratory studies with a radioactive parent source. High-pressure studies using a conventional Mössbauer source suffer from limited intensity for measurements on small samples, absorption by anvils, and background scattering. There have been major advances that exploit the temporal structure of synchrotron radiation to perform nuclear resonance spectroscopy in the time domain (Hastings et al., 1991; Sturhahn, 2004). With this technique, highly monochromatized x-rays from the synchrotron are used to excite narrow nuclear resonances, and the delayed photons are detected (**Figure 13**). Hyperfine splittings are reconstructed from the time-dependent intensity. The phonon densities of states around the nuclei can also be measured. Mössbauer spectroscopy has been used successfully to study Fe and Eu at second-generation synchrotron sources (Chefki et al., 1998; Nasu, 1996; Takano et al., 1991). The NRFS technique has been extended to probe magnetism up to megabar pressures (**Figure 14**).

Because of the high brilliance and highly focused beam, NRFS is well suited for, and has been extensively used in, high-pressure research of deep Earth materials. The NRFS hyperfine signals are very sensitive to internal magnetic fields, electric field gradients, and isomer shifts and are widely used in recent years to study magnetic collapse (Li et al., 2004; Lin et al., 2005b), site occupancy (Catalli et al., 2011; Lin et al., 2012), and valence and spin states (Chen et al., 2012; Jackson et al., 2005b; Shim et al., 2009; Speziale et al., 2005). Compared with other nuclear resonant techniques, NRFS measures the transmission signals that are relatively strong and may be collected in a fast manner. For example, fast NRFS experiments have been performed to determine high-pressure melting temperatures of iron by measuring the Lamb–Mössbauer factor, which describes the probability of recoilless absorption (Jackson et al., 2013).

2.13.4.4.10 Nuclear resonant inelastic x-ray scattering

Nuclear resonant scattering yields information on the phonon DOS through an inelastic scattering process (**Figure 13**). In principle, the DOS provides constraints on dynamic, thermodynamic, and elastic information of a material, including vibrational kinetic energy, zero-point vibrational energy, vibrational entropy, vibrational heat capacity, Debye temperature, Grüneisen parameter, thermal expansivity, longitudinal velocity, shear velocities, bulk modulus, and shear modulus. By

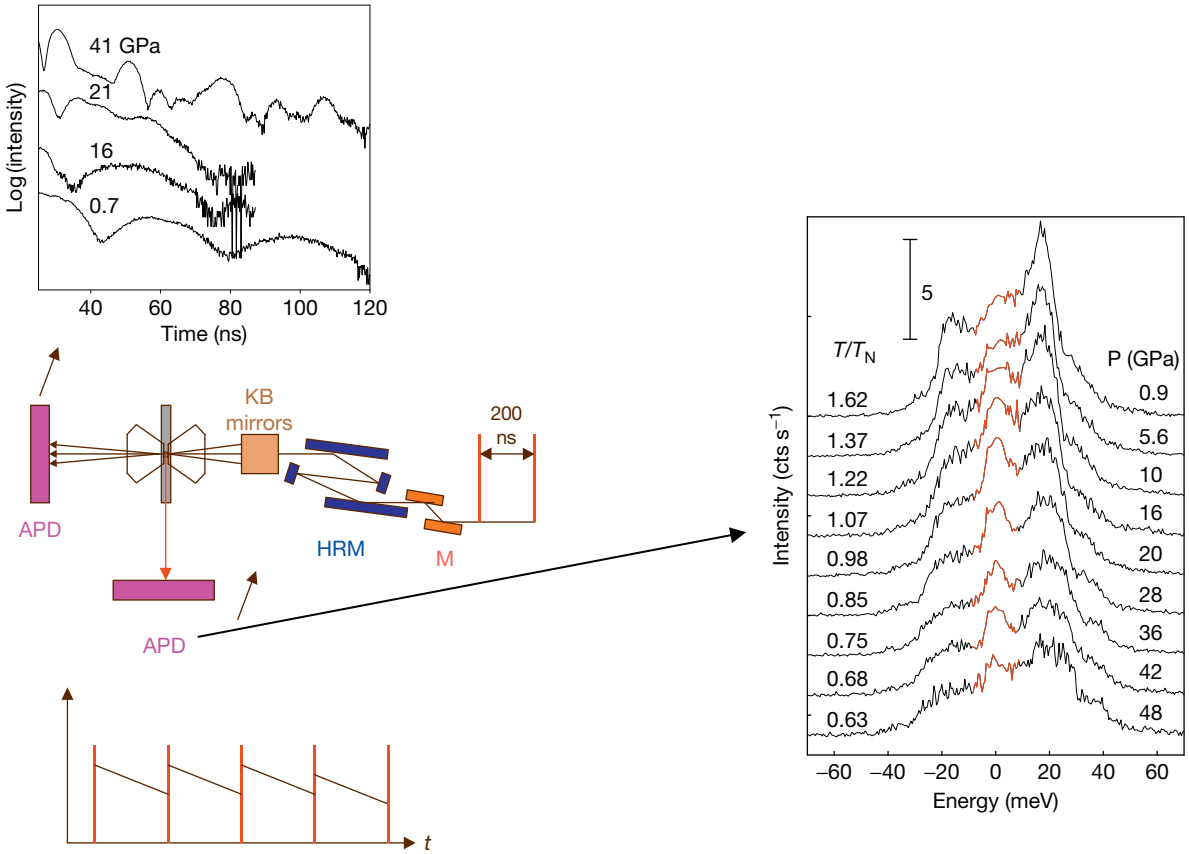

Figure 13 High-pressure nuclear resonant inelastic x-ray scattering. In-line high-resolution monochromator used to narrow down the photon energy to millielectronvolt resolution and fine-tune the monochromatic x-ray near the narrow nuclear resonant (elastic) line. Avalanche photodiodes (APDs) are used to collect only signals from nuclear resonance absorption and reject all nonresonantly scattered radiation. An APD directly downstream of the sample collects nuclear forward scattering and the APDs surrounding the sample collect nuclear resonant inelastic x-ray scattering (NRIXS) spectroscopy (Hu et al., 2003; Sturhahn et al., 1995). Nuclear resonant forward scattering spectra of FeO (top) and NRIXS spectra of FeO (right) through the pressure-driven transition from the paramagnetic (NaCl structure) to the antiferromagnetic (AFM) (rhombohedral structure) phase above 17 GPa. Reproduced from Struzhkin VV, Mao HK, Hu J, et al. (2001) *Physical Review Letters* 87: 255501.

using time discrimination electronics, the delayed signals caused by the narrow nuclear absorption provide NRIXS data (Sturhahn, 2004). Measurements were first carried out on ^{57}Fe in its bcc metallic iron at ambient conditions (Seto et al., 1995; Sturhahn et al., 1995). The NRIXS technique has been extended to high pressure and obtained the DOS of ε-Fe up to 153 GPa (Mao et al., 2001) and as a function of pressure and temperature with laser-heating techniques (Lin et al., 2005c; Zhao et al., 2004). The measurement of the Debye sound velocity (Murphy et al., 2011; Wicks et al., 2010) distinguishes compression and shear wave velocities and their temperature and pressure dependence. This technique also allows the determination of anisotropy of sound velocities and mode Grüneisen constants (Murphy et al., 2011). High-pressure studies have been carried out on iron (Gleason and Mao, 2013; Lin et al., 2005b; Mao et al., 2001), (Mg,Fe)O (Chen et al., 2012; Struzhkin et al., 2001); Fe–Ni, Fe–C, and Fe–Si alloys (Lin et al., 2003b; Mao et al., 2012); (Mg,Fe)SiO_3 glass (Gu et al., 2012); (Mg,Fe)SiO_3 enstatite (Jackson et al., 2009a); (Mg,Fe)SiO_3 perovskite (Catalli et al., 2011); and (Mg,Fe)SiO_3 post-perovskite (Catalli et al., 2010; Jackson et al., 2009b).

2.13.4.4.11 Phonon inelastic x-ray scattering

PIXS is used for studying lattice dynamics. Because nonresonant PIXS requires high-energy resolution (meV) and the double differential scattering cross section of phonon IXS is very small, such an experiment is very demanding even with the brilliance of third-generation synchrotron undulator sources. Additional challenges posed by high-pressure studies are limitations in sample size. Nonresonant PIXS has been applied to studying the high-pressure elasticity anisotropy of ε-Fe and of d- and f-electron metals (Manley et al., 2003; Wong et al., 2003). Sound velocities of materials to over 1 Mbar have been measured (Antonangeli et al., 2010, 2011; Fiquet et al., 2001) using this technique. With single-crystal samples, complete phonon dispersions in the Brillouin zone may be mapped by PIXS at high pressures (Farber et al., 2006). However, lattice dynamical data at high pressure are still limited, largely due to constraints by the strict requirements of sample quality, hydrostaticity, and, to some extent, beam time availability.

Recently, a compact laser-heated DAC has been integrated with the PIXS technique (Fukui et al., 2013). Sound velocities of iron and iron alloys have been measured at high pressure

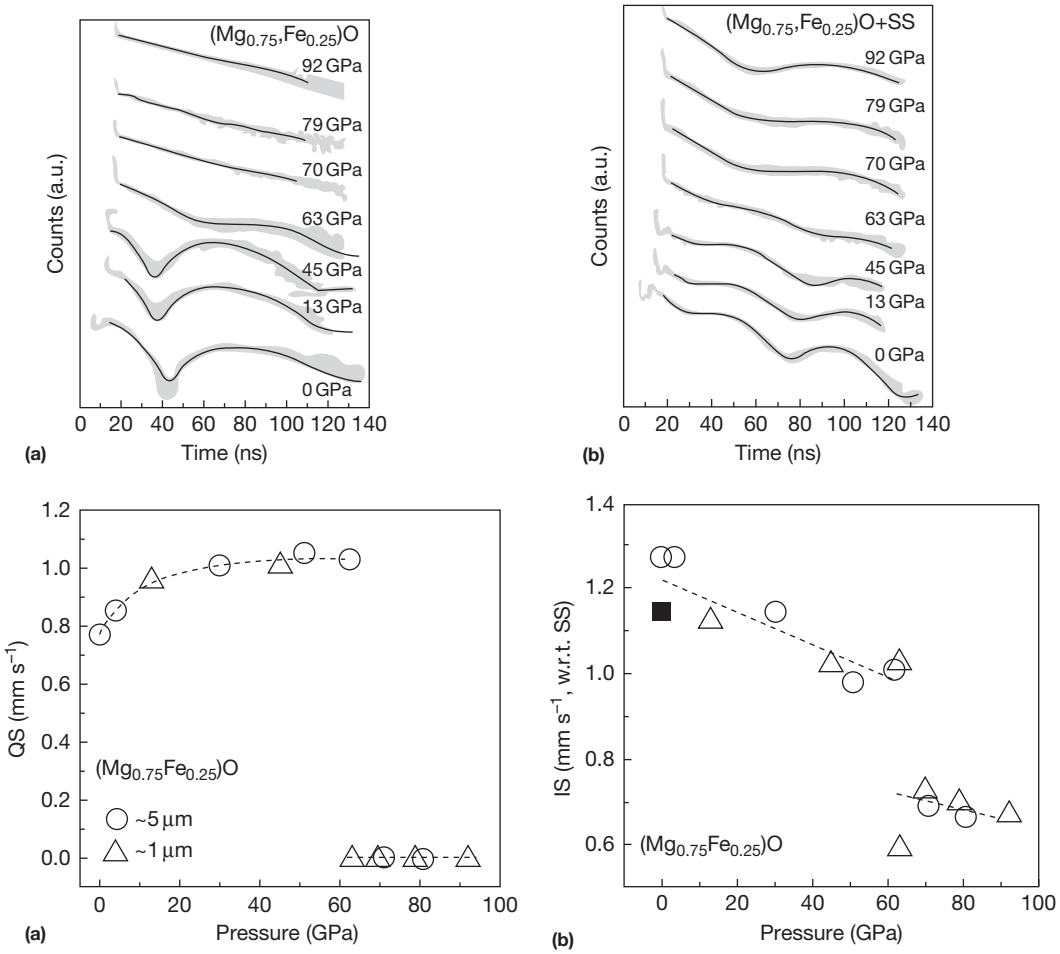

Figure 14 Representative nuclear resonant forward scattering (NRFS) spectra. Top: $(Mg_{0.75},Fe_{0.25})O$ (a) and $(Mg_{0.75},Fe_{0.25})O$ with stainless steel (b) as a function of pressure at room temperature. Black line, modeled spectrum with the MOTIF (Shvyd'ko, 1999) program. The sample thickness was approximately 1 μm, and the stainless steel foil of ~0.5 μm was used outside the diamond anvil cell to generate quantum bits in synchrotron Mössbauer spectra (SMS) spectra for isomer shift (IS) measurements. Evolution of the NRFS spectra of $(Mg_{0.75},Fe_{0.25})O$ with the stainless steel as a reference enables derivation of the IS of the sample as a function of pressure. The quantum bits at 0, 13, and 45 GPa generated from the quadrupole splitting (QS) of the high-spin state of iron in the sample, whereas the flat feature of the spectra at 70, 79, and 92 GPa indicates disappearance of the QS. The spectrum at 63 GPa is modeled with two states, a state with a QS and a state with QS, which may explain the pressure gradient in the sample chamber. Bottom: pressure dependence of (a) QS and in $Mg_{0.75}Fe_{0.25}O$ as revealed from the modeling of the NRFS spectra. The disappearance of the QS and the significant drop of the IS at above 63 GPa are consistent with the high-spin to low-spin electronic transition of iron in the sample occurring between 51 and 70 GPa. A least-squares fit to the IS (short dashed lines) gives d(IS)/dP of −0.0037 (±0.0007) mm s^{-1} GPa^{-1} for the high-spin state and d(IS)/dP of −0.0021 (±0.0010) mm s^{-1} GPa^{-1} for the low-spin state, respectively. At 63 GPa, modeling of the NRFS spectrum indicates coexistence of two states, high-spin state and low-spin state of Fe^{2+}.

and high-temperatures conditions (Kamada et al., 2014; Ohtani et al., 2013; Shibazaki et al., 2012).

2.13.4.5 Transport Measurements

2.13.4.5.1 Electrical conductivity

Electrical conductivity has been measured under pressure in a wide variety of apparatus since the pioneering work of Bridgman (1949). The principal technique is the four-probe method. The method has been used in multianvil presses for studies of upper and lower mantle minerals, including studies of the $(Mg,Fe)SiO_4$ polymorphs of the upper mantle (Xu et al., 1998a) and $(Mg,Fe)SiO_3$ perovskite (Xu et al., 1998b). The method has also been extensively applied in diamond anvil cells that provide the opportunity to access higher pressures (Mao and Bell, 1981). A modified pseudo-four-probe technique has been applied at megabar pressures (see Hemley et al., 2002). The technique has been extended to above 200 GPa at room temperature down to 0.05 K (Eremets et al., 1998). The technique was early on used in conjunction with high P–T laser heating (e.g., Li and Jeanloz, 1987) and resistive heating (e.g., Peyronneau and Poirier, 1989).

A large number of studies of conductivity of Earth materials have now been done in the diamond anvil cell. Gomi et al. measured conductivity of hcp iron to 100 GPa at room temperature (Gomi et al., 2013). Conductivities of perovskite, postperovskite, and bulk mantle compositions have also been measured (Ohta et al., 2008, 2010a,b).

Microlithographic techniques are allowing still smaller leads to be attached to or actually built into the surface of the anvils for achieving both higher pressure and higher accuracy. The technique can also be coupled with a radiation field for carrying out photoconductivity measurements under pressure. Extensions of these techniques are benefiting from the development of designer anvil methods (Patterson et al., 2000, 2004).

The multianvil experiments mentioned in the preceding text used a complex impedance method commonly used at ambient pressure (Poe et al., 1998). In this technique, the frequency of the current is varied over a wide range (from 0.01 Hz to 1 MHz); measurements on $(Mg,Fe)_2SiO_4$ polymorphs to 20 GPa as a function of temperature indicate that the conductivity in the high-pressure phases (wadsleyite and ringwoodite) is a factor of 10^2 higher than that in olivine (Poe et al., 1998), consistent with previous low-pressure studies. Another useful example is conductivity measured along the Hugoniot in shock-wave experiments (Knittle et al., 1986), including the more recent reverberation approach (Weir et al., 1996).

2.13.4.5.2 Magnetic susceptibility

The magnetic susceptibility χ describes the response of a system to an applied magnetic field. Diamagnetic materials have negative χ. Paramagnetic and FM materials have positive χ. For paramagnetic materials, $\chi \sim 10^{-6}$–$10^{-5}\,m^3\,G^{-1}$, and for FM materials, χ is several orders of magnitude higher. Typically, one reports the differential magnetic susceptibility, $\chi_\alpha = d\chi/dH$. For example, $\chi_\alpha = 1100$ for Fe at external magnetic field $H = 0$. Several classes of high-pressure techniques have been developed. One involves measurement with SQUIDs (Webb et al., 1976). A second is an inductive technique developed by Tissen and Ponyatovskii (1987) and later extended by Timofeev (1992). Originally applied to study superconductivity under pressure, it has been extended to investigate other pressure-induced magnetic transitions, including those in Fe (Timofeev et al., 2002; **Figure 15**). The designer anvil technique continues to be used for studies of magnetic transitions, for example, in FM rare earth materials (Jackson et al., 2005a). More recently, these methods have been extended with the use of focused ion beam techniques for precise lithography of diamond anvil cells

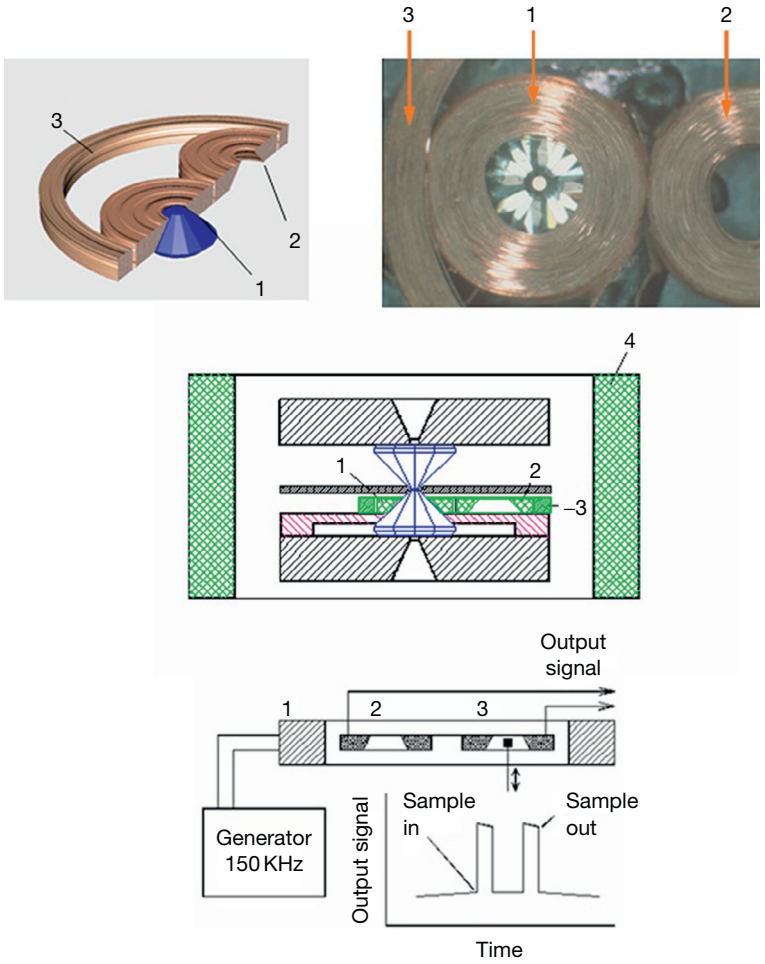

Figure 15 High-pressure magnetic susceptibility technique. Top: double-frequency modulation setup – coil 4 is used to apply low-frequency magnetic field to modulate the amplitude response from the high-frequency pickup coil 2 due to the superconducting sample. The setup includes two signal generators and two lock-in amplifiers, operating at low (20–40 Hz) and high (155 KHz) frequencies. Bottom: schematic representation of the background subtraction principle in magnetic susceptibility measurements – 1, primary coil; 2, secondary compensating coil; 3, secondary signal coil. Removal of the sample from the signal coil produces measurable changes in the total output signal.

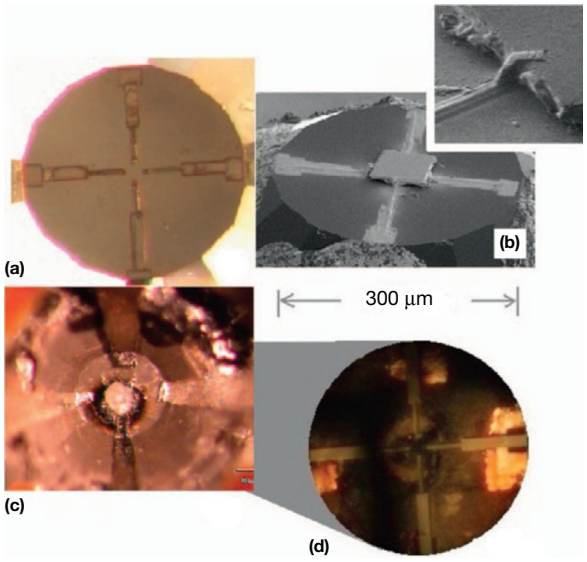

Figure 16 Anvils with an electrical probe assembly. (a) The flat diamond culet with the probes produced with a focused ion beam (FIB) before the attachment of the sample. (b) The same diamond with the sample attached. The inset shows one probe running over the edge of the crystal sample. (c) The Pt metal leads inside the indented boron nitride (BN) that will carry the signal from the sample to FIB electrical probes further to the electronics. (d) The culet after closure of the DAC with the attached sample and FIB probes in contact with the outer Pt-foil leads. Reproduced from Rotundu C, Cuk T, Greene RL, Shen ZX, Hemley RJ, and Struzhkin VV (2013) *Review of Scientific Instruments* 84: 063903.

and samples, with experiments performed in inert gas pressure media (Rotundu et al., 2013; **Figure 16**).

2.13.4.6 Resonance Methods

2.13.4.6.1 Electron paramagnetic and electron spin resonance

Various techniques have been developed for electron pragmatic resonance (EPR) and electron spin resonance (ESR), which involves resonant microwave absorption between spin levels split in a magnetic field (the Zeeman effect). This requires coupling of the microwave field, with the sample, which can be challenging at high pressure because of the small sample size (dimensions less than the wavelength of the radiation; **Figure 17**). Studies to ~8 GPa have been reported. Measurements on mantle silicates have been carried out at ambient pressures (e.g., Sur and Cooney, 1989).

2.13.4.6.2 Nuclear magnetic resonance

Nuclear magnetic resonance (NMR) is similar to EPR in that it too involves splitting of magnetic levels (Kirkpatrick, 1988; Stebbins, 1988). Because the magnetic moments of the nuclei are three orders of magnitude smaller than that of the electron, the level splitting is much lower in energy (radio-frequency range, or ~100 MHz) at typical laboratory magnetic fields ($H \sim 5$–10 T). NMR studies of high-pressure phases recovered at zero pressure include ^{1}H and ^{29}Si NMR studies of quenched high-pressure hydrous phase (Phillips et al., 1997) and magic angle spinning ^{29}Si relaxation techniques for characterizing naturally shocked samples (e.g., silica phases from Coconino Sandstone) (Meyers

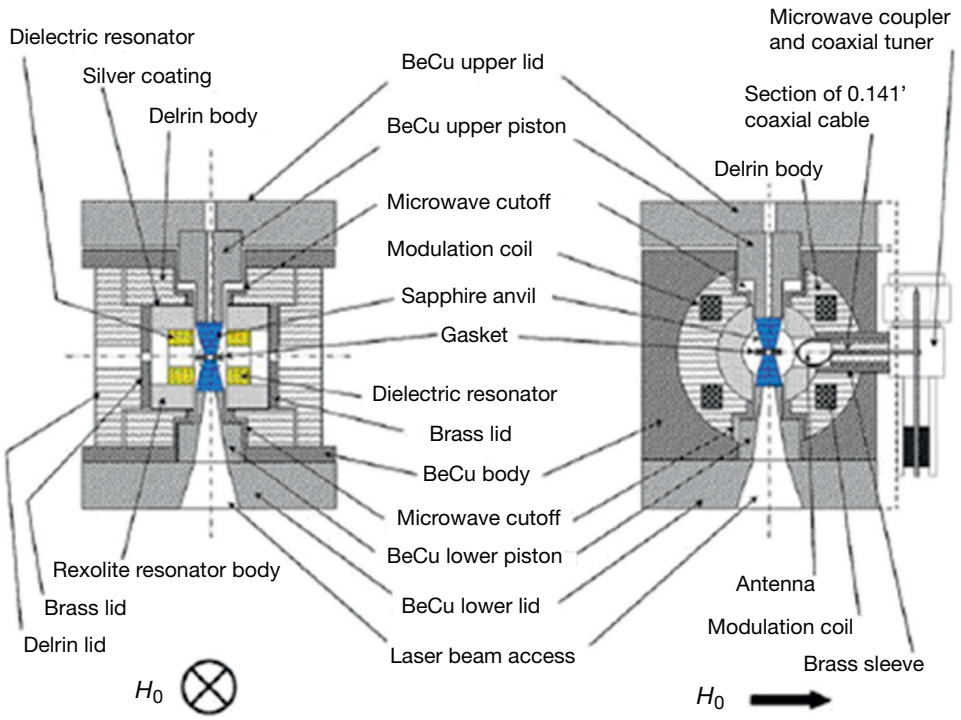

Figure 17 Cross-sectional view of the high-pressure electron spin resonance probe including the microwave coupler and coaxial tuner (see Sienkiewicz et al. (2005) for further details).

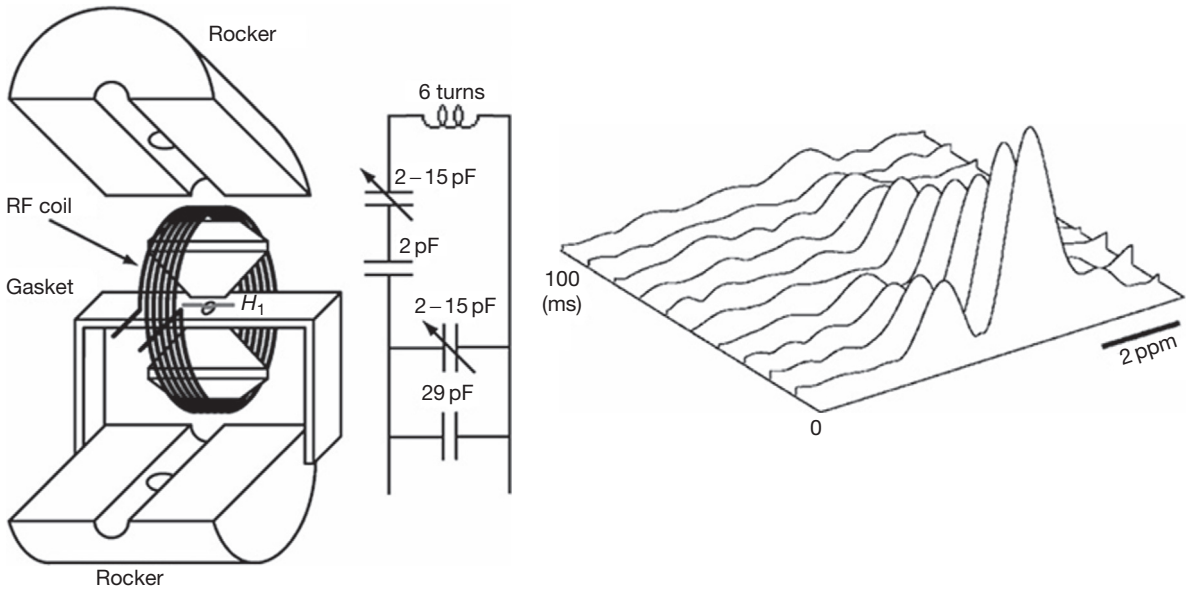

Figure 18 Technique for in situ nuclear magnetic resonance (NMR) in DACs (Okuchi et al., 2005a). Left: schematic illustration of the single-solenoid r.f. probe and its circuit. Right: magnetization of CH_3OH observed at 2.7 GPa.

et al., 1998). The technique has been applied to investigate glasses under pressure (Poe et al., 1993; Yarger et al., 1995). Most recently, two-dimensional NMR experiments applied to pressure-quenched glasses reveal details of the changes in bonding associated with pressure densification (Lee et al., 2004, 2005).

There has been important progress in high-pressure NMR techniques (**Figure 18**). Proton NMR measurements have been carried out to 17 GPa (Pravica and Silvera, 1998a,b; Ulug et al., 1991). In situ high-pressure NMR measurements on H_2, H_2O, and H_2O clathrates reveal information on the effect of compression on local bonding properties (e.g., H bonding) (Okuchi et al., 2005a,b,c). A related measurement is nuclear quadrupolar resonance, which is similar to NMR but consists of measuring nuclear resonances in zero field. Measurements of the quadrupolar resonance ^{63}Cu in Cu_2O have been performed to 6 GPa (Reyes et al., 1992). The numerous double-resonance techniques employed for years in condensed matter and chemical physics generally require larger sample volumes but potentially can be employed at high pressure with continued increases in sample size under pressure.

2.13.4.6.3 de Haas–van Alphen

This is a now standard technique for measuring Fermi surfaces of metals under ambient pressures, but it generally requires large, perfect single crystals. The advent of high-field magnets used in conjunction with new classes of diamond anvil cells offers the possibility of extending these measurements to high pressures. Again, such studies of iron alloys under pressure could provide important constraints on the evolution of fundamental electronic properties of core materials with pressures. Other extensions of magnetic susceptibility methods are described earlier in the text.

2.13.5 Selected Examples

We now discuss selected examples, focusing on systems where the combination of techniques discussed previously in the text has been key to uncovering information on the electronic and magnetic properties of geophysically important materials.

2.13.5.1 Olivine

The electronic properties of $(Mg,Fe)SiO_4$ olivine and its polymorphs can be considered a textbook problem in high-pressure mineral physics. In olivines, the bandgap varies from 7.8 eV in forsterite to 8.8 eV in fayalite (Nitsan and Shankland, 1976). A prominent excitonic absorption is observed near the bandgap (Nitsan and Shankland, 1976). Large changes in the optical absorption spectra under pressure were documented in the first in situ visible spectroscopy of minerals under pressure (Mao and Bell, 1972). As described earlier in the text, high-temperature measurements to 20 GPa indicate that the conductivity in the high-pressure phases (wadsleyite and ringwoodite) is a factor of 10^2 higher than that in olivine (Poe et al., 1998).

More recent work on olivine has included high P–T shock compression studies of olivine in which the optical absorption and emission spectra of the material have been used to constrain the emissivity and temperature on shock compression (Luo et al., 2004). The electrical conductivity of olivine containing 0.01–0.08 wt% water up to 1273 K and 4 GPa indicates that the conductivity is strongly dependent on water content and only modestly dependent on pressure and can be explained by the motion of free protons (Wang et al., 2006). Recent single-crystal measurements of electrical conductivity under pressure reveal a strong dependence on oxygen fugacity (Dai et al., 2006) and the mechanism of hydrogen incorporation and diffusion has been examined (Demouchy and Mackwell, 2006). The radiative heat transfer under pressure has been modeled based on high-pressure vibrational spectra (Hofmeister, 2005). These results have been complemented by subsequent laser flash measurements on olivine at zero pressure (Pertermann and Hofmeister, 2006).

The zero-pressure absorption edge of fayalite (Nitsan and Shankland, 1976) shifts from the UV to the near IR with pressure such that samples became opaque to visible light above 15–18 GPa; concomitantly, the electrical resistivity decreases by five orders of magnitude over this range (Lacam, 1983; Mao and Bell, 1972; Smith and Langer, 1982). A similar decrease in resistivity is also observed on shock-wave compression (Mashimo et al., 1980). The low-temperature AFM to paramagnetic transition has been tracked to at least 16 GPa by Mössbauer spectroscopy (Hayashi et al., 1987). First-principles calculations of the electronic structure and optical and magnetic properties of fayalite are consistent with the redshift of the absorption edge and decrease in electrical resistivity on compression (Jiang and Guo, 2004). Optical, electrical, and x-ray measurements extended to much higher pressures provided evidence that fayalite undergoes amorphization near 40 GPa with a further decrease in the bandgap (Williams et al., 1990).

2.13.5.2 Magnesiowüstite

We consider the high-pressure behavior of magnesiowüstite (Mg,Fe)O and its end-member phases MgO and FeO. Several examples of the changes in electronic and magnetic properties of these materials have been discussed already. Periclase (MgO) remains in the cubic rock-salt (B1) structure and remains electronically simple to at least 227 GPa (Duffy et al., 1995a), whereas wüstite ($Fe_{1-x}O$) exhibits complex polymorphism under pressure. Wüstite is nonstoichiometric and contains some ferric iron even in equilibrium with iron metal. The vacancies in wüstite form complex defect clusters (Hazen and Jeanloz, 1984). With increasing pressure, more stoichiometric wüstite can be stabilized. At room temperature and pressure, wüstite has the cubic rock salt (B1) structure. As temperature is lowered, it passes the Néel temperature T_N and becomes antiferromagnetically ordered and simultaneously assumes a distorted rhombohedral structure. As pressure is increased, T_N increases (Zou et al., 1980), so that pressure promotes the rhombohedral phase. Isaak et al. (1993) showed that pressure promotes the rhombohedral distortion even in the absence of magnetism. Theory reveals the origin of the rhombohedral distortion with pressure. Visualization of the charge density as a function of rhombohedral angle (Hemley and Cohen, 1996; Isaak et al., 1993) indicated that Fe–Fe bonding causes the rhombohedral strain, and the increase in Fe–Fe bonding with pressure is associated with the increased angle with pressure.

First-principles density functional theory (DFT) computations predicted that FeO and other transition metal monoxides would undergo magnetic collapse at high pressures (Cohen et al., 1997, 1998). Both LDA and the generalized gradient approximation give 100 GPa for a first-order high-spin to low-spin transition in AFM FeO for a cubic lattice with a 7–9% volume collapse and a continuous transition for FM cubic FeO (Cohen et al., 1998) and for rhombohedrally strained FeO (Cohen et al., 1997). The Mössbauer experiments show evidence for a transition at about 90 GPa to a low-spin phase and also a transition to a nonmagnetic phase with increasing temperature (Pasternak et al., 1997b), consistent with the DFT computations. On the other hand, XES shows no magnetic collapse up to 143 GPa and reinterprets the 90 GPa transition observed by Mössbauer as a Néel transition (spin disordering) as opposed to magnetic collapse (Badro et al., 1999). LDA+U computations, which model local Coulomb repulsions not included in normal DFT calculations, predict high-spin behavior for AFM FeO to very high pressures (over 300 GPa), consistent with the XES measurements, but show metallization at lower pressures, depending on the value of U (Gramsch et al., 2003). A U of 4.6 eV, found by a self-consistent method (Pickett et al., 1998) and close to another recent estimate of 4.3 eV (Cococcioni and de Gironcoli, 2005), gives a pressure of only 60 GPa for metallization. (Gramsch et al., 2003); the lowest energy structure is predicted to be monoclinic (Gramsch et al., 2003) and was rediscovered by Cococcioni and de Gironcoli (2005). Neutron diffraction shows a monoclinic ground state at 10 K and zero pressure (Fjellvag et al., 2002), but single-crystal x-ray diffraction at high pressures has not resolved the monoclinic distortion (Jacobsen et al., 2005), perhaps because of the lack of high-angle data and/or twinning. LDA+U computations have now been performed for magnesiowüstite (Persson et al., 2006; Tsuchiya et al., 2006), which show reasonable agreement with experiments. An analysis of high-spin to low-spin transitions from a crystal field perspective predicts a continuous magnetic collapse at high temperatures as a function of pressure (Sturhahn et al., 2005; Tsuchiya et al., 2006). However, when the PV term is included in the free energy, it is possible to obtain a different behavior (Persson et al., 2006), including possibly a first-order transition.

At high temperature, the transition originally identified by shock-wave experiments (Jeanloz and Ahrens, 1980) was found to be to a metallic phase (Knittle and Jeanloz, 1986), which was identified as the NiAs (B8) structure by in situ diffraction (Fei and Mao, 1994). The phase diagram indicates that it should occur at low temperatures as well. Subsequent analysis of the diffraction data suggested the formation of a polytype or superlattice between B8 and anti-B8, with Fe in the As-site and O in the Ni-site (Mazin et al., 1998). These B8 and anti-B8 structures can be joined together smoothly, and the boundary between them is the rhombohedrally distorted B1 structure. This phase could form due to lack of equilibrium or could even form a unique continuous structure transition between the different phases. This interpretation of the behavior of FeO has been confirmed by experiments (Kantor et al., 2004a; Murakami et al., 2004a,b). The phase diagram has been extended to higher P–T conditions and metallic B1 phase has been found (Ohta et al., 2012; **Figure 19**).

Recent studies of (Mg,Fe)O illustrate the importance of using multiple techniques. Theoretical studies indicate that the high-spin to low-spin transitions in a number of structures are dominated by the size of the local coordination polyhedron (Cohen et al., 1997). Thus, a transition metal ion in a smaller site will transform at lower pressures than one in a larger site. Thus, ferric iron in solid solution substituting for Mg^{2+}, which is a smaller ion than Fe^{2+}, transforms at lower pressures than in the pure ferrous iron compound. After being predicted theoretically, this has now been seen in a series of studies. XES shows a high-spin transition at 54–67 GPa in $(Mg_{0.75}Fe_{0.25})O$ and 84–102 GPa in $(Mg_{0.40}Fe_{0.60})O$, again suggesting that the transition in pure FeO is much greater than 100 GPa. Optical absorption spectra have been measured up to 80 GPa for the lower mantle oxide, (Mg,Fe)O. Upon

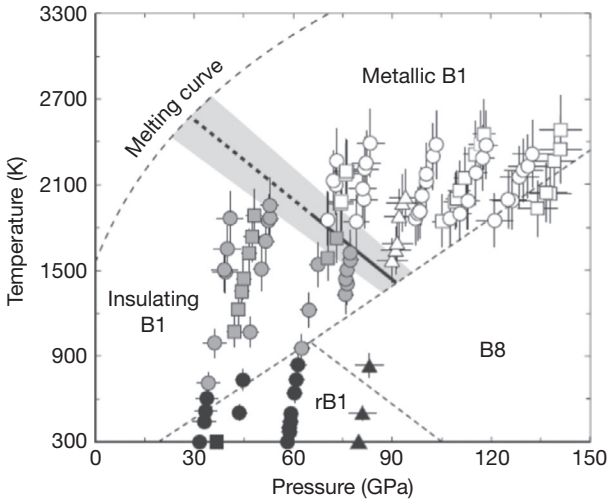

Figure 19 *P–T* phase diagram of FeO. The stability fields of rB1, insulating B1, and metallic B1 phases are represented by solid, gray solid, and open symbols, respectively. Circles, squares, and triangles indicate different sets of experiments. A metal–insulator transition boundary shown as bold line was determined from the data and linearly extrapolated to the melting condition (broken bold line). The estimated uncertainty in the location of the transition is shown by gray band. The melting curve and the phase boundaries of FeO shown as broken lines are from previous studies. Reproduced from Ohta K, Cohen RE, Hirose K, Haule K, Shimizu K, and Ohishi Y (2012) *Physical Review Letters* 108: 026403.

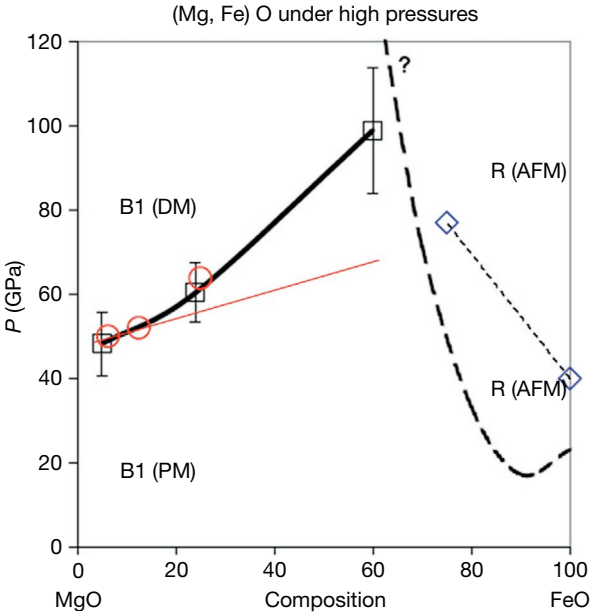

Figure 20 Phase diagram of the magnesiowüstite–(Mg,Fe)O system under high pressures. An isosymmetric transition from the paramagnetic state (PM) to the diamagnetic state (DM) occurs in MgO-rich magnesiowüstite (ferropericlase) (Badro et al., 2003; Lin et al., 2005b), and addition of FeO in MgO stabilizes the high-spin state to much higher pressures (Lin et al., 2005b). On the other hand, addition of MgO in FeO stabilizes the B1 structure relative to the AFM rhombohedral phase to much higher pressures (Lin et al., 2003c). Potential electronic and structural transitions in FeO-rich region remain to be further understood. Red-dashed line represents the calculated high-spin to low-spin transition boundary based on the assumption that the spin transition occurs at the same Fe–O bond length and the iron–iron exchange interaction could be neglected. Figure reproduced from Lin JF, Gavriliuk AG, Struzhkin VV, et al. (2006) *Physical Review B* 73: 113107.

reaching the high-spin to low-spin transition of Fe^{2+} at about 60 GPa, there is enhanced absorption in the mid- and near-infrared spectral range, whereas absorption in the visible–ultraviolet is reduced. The observed changes in absorption are attributed to d–d-orbital charge transfer transitions in the Fe^{2+} ion (Figure 2). The results indicate that low-spin (Mg,Fe)O will exhibit considerably lower radiative thermal conductivity than the lower pressure high-spin (Mg,Fe)O (Goncharov et al., 2006). A schematic phase diagram is shown in Figure 20.

The Mössbauer data for high-pressure magnesiowüstite are less clear; they show hyperfine field split spectra coexisting with a paramagnetic peak over large pressure ranges (Speziale et al., 2005). The authors interpret the first appearance of a paramagnetic peak at the transition, but the data seem more consistent with coexisting high-spin and low-spin iron, perhaps in different local environments. In any case, these data are consistent with solid solution in which Mg^{2+} decreases the transition pressure, consistent with earlier predictions. Theory suggests that ferrous iron in the B8 or anti-B8 structures will remain high spin to much higher pressures. This also makes clear the distinction between magnetic collapse and metal–insulator transitions, since normal B8 FeO is predicted to be a high-spin metal and anti-B8 is predicted to be a high-spin insulator.

2.13.5.3 Silicate Perovskite and Postperovskite

The electronic properties of the silicate perovskite $(Mg,Fe)SiO_3$ have been the focus of considerable study. UV–visible spectra indicate the presence of crystal field splitting (Shen et al., 1994), although subsequent measurements showed similar results for perovskite and magnesiowüstite (Keppler et al., 1994). A broad feature in the optical spectrum near 14 900 cm^{-1} has been assigned to the $Fe^{2+} \rightarrow Fe^{3+}$ charge transfer transition (Keppler et al., 1994). Zhang (1997) measured the Lamb–Mössbauer factor on $(Mg,Fe)SiO_3$ perovskites and clinoenstatite. The thermally activated electron delocalization found earlier in quenched samples in Mössbauer measurements with a conventional radioactive source (Fei et al., 1994) was suppressed at high pressure. Li and Jeanloz (1987) measured the electrical conductivity of $(Mg,Fe)SiO_3$ perovskite at high pressures and temperatures by laser heating; subsequent measurements were carried out at lower maximum temperatures by Peyronneau and Poirier (1989) using a resistively heated cell. The latter results fit a hopping conductivity model. Katsura et al. (1998) reported that the temperature dependence of the conductivity differed significantly between samples measured at high pressure in its stability field and samples quenched to ambient pressure.

The strong partitioning of Fe^{2+} in magnesiowüstite relative to ferromagnesium silicate perovskite has been attributed to crystal field stabilization; that is, it arises from the stabilization of Fe^{2+} in the octahedral site of the oxide as compared with the (pseudo)dodecahedral site of the perovskite (Burns, 1993; Yagi et al., 1979). The apparent crystal field stabilization has been used to estimate (or rationalize) partitioning between the two

phases. Malavergne et al. (1997) found that partitioning results are consistent with observations for inclusions thought to have originated in the lower mantle and proposed to be representative of a pyrolite composition (Kesson and FitzGerald, 1992). McCammon used Mössbauer measurements to show that a significant fraction of the iron in (Mg, Fe, Al)SiO_3 perovskite produced in multianvil experiments is Fe^{3+} (McCammon, 1997). The incorporation of Fe^{3+} is strongly coupled with the Al^{3+}; this result does not, however, mean that the lower mantle is oxidized as pressure stabilized the Fe^{3+} ion (Frost et al., 2004; McCammon, 2005).

Both crystallographic and Mössbauer studies indicate that Fe^{2+} in silicate perovskite resides in the octahedral site (see Hemley and Cohen, 1992). Attempts have been made to determine the site occupancy of Fe^{2+} and Fe^{3+} from Mössbauer spectroscopy (McCammon, 1998). The spectra of $(Mg_{0.95}Fe_{0.95})SiO_3$ reportedly synthesized at low f_{O_2} indicate that the Fe^{3+} goes in the octahedral site, whereas higher f_{O_2} conditions result in Fe^{3+} on both sites. First-principles theoretical computations show that ferrous iron remains high spin in perovskite and is on the A-site (Caracas and Cohen, 2005a), but ferric iron undergoes a high-spin to low-spin transition in the pressure range of 100–125 GPa (Li et al., 2005).

A revolution in our understanding of the deepest mantle and high-pressure mineral physics was the discovery of the postperovskite phase in $MgSiO_3$ (Murakami et al., 2004a; Oganov and Ono, 2004; Tsuchiya et al., 2004), which appears to be stable for a wide range of compositions at pressures in the megabar range (Caracas and Cohen, 2005a,b). The application of the previously mentioned electronic and magnetic techniques to silicate postperovskite is challenging because of the need to carry out the experimental in situ at very high pressures (e.g., ~100 GPa and above), and much input on the properties of postperovskite has come from theoretical computations. Nevertheless, a number of measurements are being carried out, including NRIXS and XES, which are providing acoustic velocities and identification of the iron as low spin (**Figure 21**). A growing number of experimental studies are being performed in spite of the challenges (Mao et al., 2006b). Experiments show that most iron in Al-bearing postperovskite is ferric iron (Sinmyo et al., 2006), consistent with first-principles theory (Li et al., 2005). First-principles DFT calculations show ferrous iron to be unstable to disproportionation to ferric iron (in postperovskite) and metallic iron in an hcp-Fe phase (Zhang and Oganov, 2006), consistent with experiment (McCammon, 2005). Theory predicts ferrous iron to be high spin to pressures well above the highest pressures in the mantle in both perovskite and postperovskite (Caracas and Cohen, 2005a; Stackhouse et al., 2006).

2.13.5.4 Volatiles

Volatile uptake and recycling in high-pressure phases provide important constraints on the Earth's history (Bercovici and Karato, 2003; Brooker et al., 2003; Kerrick and Connolly, 2001; Sanloup et al., 2002b,c). Under pressure, volatiles can become structurally bound components, either as stoichiometric compounds or as soluble components in nominally anhydrous phases (Williams and Hemley, 2001). Dense hydrous silicates present different degrees of hydrogen bonding under ambient conditions. The prototype system is H_2O, which is discussed further later in the text.

Pressure-induced disordering of crystals may be intimately associated with the behavior of the hydrogen through sublattice amorphization or melting (e.g., Duffy et al., 1995b; Nguyen et al., 1997; Parise et al., 1998). The pressure dependence of OH stretching modes shows a tendency toward increased hydrogen bonding, but decreased hydrogen bonding is also observed (Faust and Williams, 1996; Hemley et al., 1998a). These results, together with the evidence for disordering, point toward the importance of hydrogen–hydrogen repulsions. Finally, an example of the change in bonding affinities is the formation of iron hydride at high pressure. It produces a dhcp structure at 3.5 GPa, which is stable to at least 60 GPa (Badding et al., 1992).

There is growing evidence for pressure-induced chemical interactions in rare gases. The low abundance of xenon in the atmosphere (relative to cosmochemical abundances) is a long-standing problem in geochemistry and has given rise to the proposal that the element may be sequestered at depth within the Earth. Near-IR spectroscopy and electrical conductivity measurements show that solid Xe becomes metallic at 130–150 GPa (Eremets et al., 2000; Goettel et al., 1989; Reichlin et al., 1989). Prior to metallization, the material

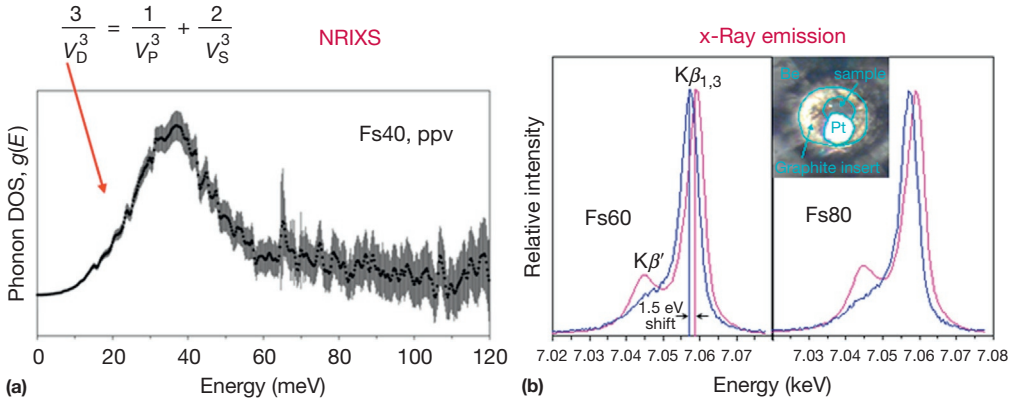

Figure 21 (a) NRIXS spectra showing the phonon DOS for postperovskite phase of Fs40 at 130 GPa after temperature quench from 2000 K. Reproduced from Mao WL, Mao HK, Sturhahn W, et al. (2006) *Science* 312: 564–565. (b) x-Ray emission spectroscopy (XES) of the material measured in situ at high pressure. Reproduced from Mao WL, Mao HK, Sturhahn W, et al. (2006) *Science* 312: 564–565.

transforms from the fcc to the hcp structure (Jephcoat et al., 1987). Recent studies have shown that the equilibrium transition pressure is as low as 21 GPa (Caldwell et al., 1997). Experiments to 30 GPa and theoretical calculations to inner core pressures reported in this study show (surprisingly) no evidence for chemical affinity for Xe and Fe (Caldwell et al., 1997). The melting points of Xe and Ar increase initially with pressure (Jephcoat, 1998) but then flatten out; this has been interpreted as arising from s–p–d hybridization (Ross et al., 2005).

We also briefly mention planetary gases and ices at high pressure. Dense hydrogen is the most abundant element in the solar system. Accurate determinations of its electronic and magnetic properties to multimegabar pressures (>300 GPa) over a wide temperature range and ultimately to the high-density plasma are crucial for planetary geophysics. Both optical spectra and direct measurements of the electrical conductivity show that solid hydrogen remains insulating to at least 230 GPa at low temperatures (<200 K) (Hemley et al., 2002). On the other hand, the dense hot fluid exhibits metallic conductivity 140–200 GPa (Collins et al., 2001; Nellis et al., 1996). Recent developments have made it possible to contain hydrogen at 1000 K at static megabar pressures, allowing measurements to be performed on the dense hot fluid over this P–T range (Gregoryanz et al., 2003).

The changes in bonding and electronic structure of various ices are particularly important for planetary science. The symmetrical hydrogen bond state of ice at 60 GPa reveals intriguing quantum mechanical tunneling effects associated with the transition (Goncharov et al., 1996). There is a steep increase in melting temperature of the ionic symmetrical ice phase (Goncharov et al., 2005a; Lin et al., 2005a). Sublattice melting has also been explored (Cavazzoni et al., 1999; Katoh et al., 2002). There are predictions to other high-pressure forms above 0.3 TPa (Benoit et al., 1996; Cavazzoni et al., 1999). Most recently, it has been found that the combination of x-ray irradiation and high pressure can break down H_2O to form an alloy H_2 and O_2 at pressures up to at least ~50 GPa and stable relative to H_2O to ~500 K (Mao et al., 2006a).

2.13.5.5 Iron and Iron Alloys

The Earth's core plays a central role in the evolution and dynamic processes within the planet. As the major constituents of the core, iron and its alloys hold the key to understanding the nature of this most enigmatic region of the planet (Hemley and Mao, 2001). Geophysical observations have uncovered surprising inner core properties, such as seismic anisotropy, super rotation, and magnetism (Glatzmaier and Roberts, 1996; Niu and Wen, 2001; Romanowicz et al., 1996; Song and Helmberger, 1998; Song and Richards, 1996; Su et al., 1996; Tromp, 2001). These observations are supplemented by geodynamic simulations (Buffett, 2000, 2003; Buffett and Wenk, 2001; Karato, 1999; Olson and Aurnou, 1999). Ab initio theoretical calculations have been applied to examine and predict melting, phase stabilities, elastic anisotropy, and magnetism of iron beyond experimental capabilities (Alfé et al., 1999, 2000; Belonoshko et al., 2003; Laio et al., 2000; Steinle-Neumann et al., 2001; Stixrude and Cohen, 1995; Vocadlo et al., 2003). Theory shows that the bcc phase is stabilized by magnetism. There had been much discussion of bcc as the possible structure for iron in the Earth's inner core, but calculations showed that bcc iron is mechanically unstable at high pressures due to the loss of magnetism with pressure (Stixrude and Cohen, 1995). On the other hand, the hexagonal phase (ε-Fe) is nonmagnetic. The reflectivity of iron decreases markedly across the bcc–hcp transition; measurements to 300 GPa showed that this low reflectivity continues to much higher pressure (Reichlin et al., unpublished).

Pressure effects on the valence band densities of states and magnetic properties of Fe are being measured with the new synchrotron x-ray techniques described in the preceding text. Large differences in DOS are predicted between bcc Fe and the two closed-packed phases (hcp and fcc). Spin-dependent K_β emission fine structure can be used to probe localized magnetic properties with XMCD. The element-specific nature of XES and XMCD will be particularly important in the study of transition metal and rare earth alloys. High P–T XAS and XRD are providing electronic and structure information for iron melt and crystals (Jackson et al., 1993; Sanloup et al., 2002a). High P–T NRFS is providing information on Mössbauer effect and magnetism (Jackson et al., to be published), and high P–T NRIXS coupled with hydrostatic equation of state data yields phonon densities of state, bulk longitudinal and shear wave velocities, heat capacity, entropy, Debye temperature, and Grüneisen parameter (Lübbers et al., 2000; Mao et al., 2001; Struzhkin et al., 2001).

2.13.6 Conclusions

A range of high-pressure techniques are now available to investigate changes in bonding electronic and magnetic structures induced by pressure in the Earth and planetary materials. In general, recent work has shown that a variety of techniques are required to understand the evolution of these complex systems under pressure. This includes the use of newly developed theoretical methods, which are providing increasingly accurate predictions for energetic properties of these materials under extreme conditions. There is much to be learned about the origin of the behavior of transition metal compounds and solid solutions at high pressures. The study of transitions in Mott insulators is a particularly important current problem, with implications for condensed-matter theory as well. Future work should also focus on both defect properties and polyphase aggregates at high P–T conditions: Rocks are composite material, yet most mineral physics studies assume that the electronic and magnetic properties of the rock can be determined by adding up the contributions from the component mineral phases. An important question is the extent to which the electronic properties of the composite need to be considered (i.e., from interfacial, nanophase properties (Maxwell-Garnet, 1904)). The effects of such large changes in pressure on chemical properties are established. In general, the large perturbation of pressure on the electronic structure of materials suggests that the partitioning among different phases may be difficult to predict from ambient pressure measurements.

Acknowledgment

We thank M. Phillips Hoople for his help with the preparation of the manuscript and E. Rod for Figure 9. This work was supported

by NSF-EAR(1119504), DOE-BES, and DOE-NNSA (CDAC, DE-NA-0002006). R.E.C. acknowledges support from NSF grant EAR-0310139. G.S. acknowledges support from DOE-NNSA grant (DE-NA0001974) and DOE-BES grant (DE-FG02-99ER45775).

References

Ablett JM, Kao CC, Shieh SR, Mao HK, Croft M, and Tyson TA (2003) *High Pressure Research* 23: 471–476.

Ahrens TJ (1987) In: Sammis CG and Henyey TL (eds.) *Methods of Experimental Physics*, vol. 24, pp. 185–235. San Diego, CA: Academic Press.

Alfé D, Gillan MJ, and Price GD (1999) *Nature* 401: 462–463.

Alfé D, Gillan MJ, and Price GD (2000) *Nature* 405: 172–175.

Ambrosch-Draxl C and Sofo JO (2006) *Computer Physics Communications* 175: 1–14.

Ament LJP, van Veenendaal M, Devereaux TP, Hill JP, and van den Brink J (2011) *Reviews of Modern Physics* 83: 705–767.

Anderson PW (1958) *Physical Review* 109: 1492–1505.

Anderson AJ, Jayanetti S, Mayanovic RA, Bassett WA, and Chou I-M (2002) *American Mineralogist* 87: 262–268.

Andrault D, Munoz M, Bolfan-Casanova N, et al. (2010) *Earth and Planetary Science Letters* 293: 90–96.

Antonangeli D, Siebert J, Aracne CM, et al. (2011) *Science* 331: 64–67.

Antonangeli D, Siebert J, Badro J, et al. (2010) *Earth and Planetary Science Letters* 295: 292–296.

Aquilanti G, Pascarelli S, Mathon O, Munoz M, Narygina O, and Dubrovinsky L (2009) *Journal of Synchrotron Radiation* 16: 376–379.

Arms DA, Simmons RO, Schwoerer-Bohning M, Macrander AT, and Graber TJ (2001) *Physical Review Letters* 87: 156402-1–156402-4.

Ashcroft NW and Mermin ND (1976) *Solid State Physics*. New York: Holt Rinehart and Winston.

Badding JV, Mao HK, and Hemley RJ (1992) In: Syono Y and Manghnani MH (eds.) *High Pressure Research in Mineral Physics: Application to Earth and Planetary Sciences*. Washington, DC: Terra Scientific Publishing Co (TERRAPUB).

Badro J, Fiquet G, Guyot F, et al. (2003) *Science* 300: 789–791.

Badro J, Fiquet G, Struzhkin VV, et al. (2002) *Physical Review Letters* 89: 205504.

Badro J, Struzhkin VV, Shu J, et al. (1999) *Physical Review Letters* 83: 4101–4194.

Baldini M, Aquilanti G, Mao HK, et al. (2010) *Physical Review B* 81: 024201.

Bartolome F, Tonnerre JM, Seve L, et al. (1997) *Physical Review Letters* 79: 3775–3778.

Bassani F and Altarelli M (1983) In: Koch EE (ed.) *Handbook on Synchrotron Radiation*, vol. 1, pp. 463–605. Amsterdam: North-Holland.

Bassett WA, Anderson AJ, Mayanovic RA, and Chou IM (2000) *Chemical Geology* 167: 3–10.

Baudelet F, Odin S, Itie JP, et al. (1997) *Crystallography at High Pressure Using Synchrotron Radiation: The Next Steps*. Grenoble, France: ESRF.

Bell PM, Xu J, and Mao HK (1986) In: Gupta Y (ed.) *Shock Waves in Condensed Matter*, pp. 125–130. New York: Plenum.

Belonoshko AB, Ahuja R, and Johansson B (2003) *Nature* 424: 1032–1034.

Benoit M, Bernasconi M, Focher P, and Parrinello M (1996) *Physical Review Letters* 76: 2934–2936.

Bercovici D and Karato S (2003) *Nature* 425: 39–44.

Boehler R, Guthrie M, Molaison JJ, et al. (2013) *High Pressure Research* 33: 546–554.

Boehler R, Musshoff HG, Ditz R, Aquilanti G, and Trapananti A (2009) *Review of Scientific Instruments* 80: 045103.

Boffa Ballaran T, Kurnosov A, and Trots D (2013) *High Pressure Research* 33: 453–465.

Born M and Wolf E (1980) *Principles of Optics*. Oxford: Pergamon Press.

Bradley JA, Moore KT, Lipp MJ, et al. (2012) *Physical Review B* 85: 100102.

Bridgman PW (1949) *The Physics of High Pressure*. London: G. Bell and Sons.

Brooker RA, Du Z, Blundy JD, et al. (2003) *Nature* 423: 738–741.

Brown GE, Calas G, Waychunas GA, and Petiau J (1988) In: Hawthorne FC (ed.) *Spectroscopic Methods in Mineralogy and Geology. Reviews in Mineralogy*, vol. 18, pp. 431–512. Washington, DC: Mineralogical Society of America.

Buffett BA (2000) *Science* 288: 2007–2012.

Buffett BA (2003) *Science* 299: 1675–1677.

Buffett BA and Wenk H-R (2001) *Nature* 413: 60–62.

Buontempo U, Filipponi A, Martinez-Garcia D, Postorino P, Mezouar M, and Itie JP (1998) *Physical Review Letters* 80: 1912–1915.

Burns RG (1993) *Mineralogical Applications of Crystal Field Theory*. Cambridge: Cambridge University Press.

Cai YQ, Mao HK, Chow PC, et al. (2005) *Physical Review Letters* 94: 025502.

Caldwell WA, Nguyen JH, Pfrommer BG, Mauri F, Louie SG, and Jeanloz R (1997) *Science* 277: 930–933.

Caliebe WA, Soininen JA, Shirley E, Kao C-C, and Hämäläinen K (2000) *Physical Review Letters* 24: 3907–3910.

Caracas R and Cohen RE (2005a) *Geophysical Research Letters* 32: L16310.

Caracas R and Cohen RE (2005b) *Geophysical Research Letters* 32: L06303.

Catalli K, Shim S-H, Prakapenka VB, Zhao J, and Sturhahn W (2010) *American Mineralogist* 95: 418–421.

Catalli K, Shim S-H, Prakapenka VB, Zhao J, and Sturhahn W (2011) *American Mineralogist* 95: 418–421.

Cavazzoni C, Chiarotti GL, Scandolo S, Tosatti E, Bernasconi M, and Parrinello M (1999) *Science* 283: 44–46.

Chefki M, Abd-Elmeguid MM, Micklitz H, Huhnt C, and Schlabitz W (1998) *Physical Review Letters* 80: 802–805.

Chen B, Jackson JM, Sturhahn W, et al. (2012) *Journal of Geophysical Research: Solid Earth* 117: B08208.

Cococcioni M and de Gironcoli S (2005) *Physical Review B* 71: 035105.

Cohen RE, Fei Y, Downs R, Mazin II, and Isaak DG (1998) In: Wentzcovitch R, Hemley RJ, Nellis WJ, and Yu P (eds.) *High-Pressure Materials Research*, vol. 499. Pittsburgh, PA: Materials Research Society.

Cohen RE, Gramsch S, Mukherjee S, Steinle-Neumann G, and Stixrude L (2002) In: Hemley RJ, Bernasconi M, Ulivi L, and Chiarotti G (eds.) *Proceedings of the International School of Physics "Enrico Fermi". High-Pressure Phenomena*, vol. CXLVII, pp. 215–238. Washington, DC: IOS Press.

Cohen RE, Mazin II, and Isaak DG (1997) *Science* 275: 654–657.

Cohen RE and Mukherjee S (2004) *Physics of the Earth and Planetary Interiors* 143–144: 445–453.

Cohen RE, Naumov II, and Hemley RJ (2013) *Proceedings of the National Academy of Sciences of the United States of America* 110: 13757–13762.

Collins GW, Celliers PM, DaSilva LB, et al. (2001) *Physical Review Letters* 87: 165504.

Cox PE (1987) *The Electronic Structure and Chemistry of Solids*. Oxford: Oxford Science Publications.

Cuk T, Struzhkin VV, Devereaux TF, et al. (2008) *Physical Review Letters* 100: 217003.

Dadashev A, Pasternak MP, Rozenberg GK, and Taylor RD (2001) *Review of Scientific Instruments* 72: 2633–2637.

Dai L, Li H, Liu C, et al. (2006) *Progress in Natural Science* 4: 387–393.

DeGroot FMF, Nakazawa M, Kotani A, Krisch MH, and Sette F (1997) *Physical Review B* B56: 7285.

Demouchy S and Mackwell S (2006) *Physics and Chemistry of Minerals* 33: 347–355.

Dera P, Zhuravlev K, Prakapenka V, et al. (2013) *High Pressure Research* 33: 466–484.

Dickson DPE and Berry FJ (eds.) (1986) *Mossbauer Spectroscopy*. New York: Cambridge University Press.

Ding Y, Haskel D, Ovchinnikov SG, et al. (2008) *Physical Review Letters* 100: 045508.

Ding Y, Xu J, Prewitt CT, et al. (2005) *Applied Physics Letters* 86: 052505.

Drickamer HG and Frank CW (1973) *Electronic Transition and the High Pressure Chemistry and Physics of Solids*. London: Chapman and Hall.

Duffy TS, Hemley RJ, and Mao HK (1995a) *Physical Review Letters* 74: 1371–1374.

Duffy TS, Meade C, Fei Y, Mao HK, and Hemley RJ (1995b) *American Mineralogist* 80: 222–230.

Eremets M (1996) *High Pressure Experimental Methods*. New York: Oxford University Press.

Eremets MI, Gregoryanz E, Mao HK, Hemley RJ, Mulders N, and Zimmerman NM (2000) *Physical Review Letters* 83: 2797–2800.

Eremets MI, Shimizu K, Kobayashi TC, and Amaya K (1998) *Science* 281: 1333–1335.

Eremets MI, Struzhkin VV, Timofeev JA, Utjuzh AN, and Shirokov AM (1992) In: Singh AK (ed.) *Recent Trends in High Pressure Research*, pp. 362–364. New Delhi: Oxford & IBH.

Fabbris G, Matsuoka T, Lim J, et al. (2013) *Physical Review B* 88: 245103.

Farber DL, Krisch M, Antonangeli D, et al. (2006) *Physical Review Letters* 96: 115502.

Faust J and Williams Q (1996) *Geophysical Research Letters* 23: 427–430.

Fei Y (1996) In: Dyar MD, McCammon C, and Shaefer MW (eds.) *Mineral Spectroscopy: A Tribute to Roger G. Burns*, pp. 243–254. St. Louis, MO: Geochemical Society, Special Publication No. 5.

Fei Y and Mao H-K (1994) *Science* 266: 1668–1680.

Fei Y, Virgo D, Mysen BO, Wang Y, and Mao HK (1994) *American Mineralogist* 79: 826–837.

Fiquet G, Badro J, Guyot F, Requardt H, and Krisch M (2001) *Science* 291: 468–471.

Fister TT, Nagle KP, Vila FD, et al. (2009) *Physical Review B* 79: 174117.

Fister TT, Vila FD, Seidler GT, Svec L, Linehan JC, and Cross JO (2007) *Journal of the American Chemical Society* 130: 925–932.

Fjellvag H, Hauback BC, Vogt T, and Stolen S (2002) *American Mineralogist* 87: 347–349.

Fleury PA and Loudon R (1968) *Physics Review* 166: 514–530.

Frost DJ, Liebske C, Langenhorst F, McCammon CA, Trønnes RG, and Rubie DC (2004) *Nature* 428: 409–412.

Fujii Y (1996) *International Union of Crystallography: XVII Congress and General Assembly*, Seattle, Washington, C-1.

Fukui H, Sakai T, Sakamaki T, et al. (2013) *Review of Scientific Instruments* 84: 113902.

Gartstein E and Mason TO (1982) *Journal of the American Ceramic Society* 65: C24–C26.

Ghose S (1988) In: Hawthorne FC (ed.) *Spectroscopic Methods in Mineralogy and Geology. Reviews in Mineralogy*, vol. 18, pp. 161–192. Washington, DC: Mineralogical Society of America.

Glatzmaier GA and Roberts PH (1996) *Science* 274: 1887–1891.

Gleason AE and Mao WL (2013) *Nature Geoscience* 6: 571–574.

Goettel KA, Eggert JH, Silvera IF, and Moss WC (1989) *Physical Review B* 62: 665–668.

Gomi H, Ohta K, Hirose K, et al. (2013) *Physics of the Earth and Planetary Interiors* 224: 88–103.

Goncharenko IN, Mignot JM, Andre G, Larova OA, Mirebeau I, and Somenkov VA (1995) *High Pressure Research* 14: 41–53.

Goncharov AF, Goldman N, Fried LE, et al. (2005a) *Physical Review Letters* 94: 125508.

Goncharov AF, Haugen B, Struzhkin VV, Beck P, and Jacobsen SD (2008) *Nature* 456: 231–234.

Goncharov AF, Hemley RJ, Mao HK, and Shu J (1998) *Physical Review Letters* 80: 101–104.

Goncharov AF, Struzhkin VV, Hemley RJ, Mao HK, and Liu Z (2000) In: Manghnani MH, Nellis WJ, and Nicol M (eds.) *Science and Technology of High Pressure*, pp. 90–95. Hyderabad, India: Universities Press.

Goncharov AF, Struzhkin VV, and Jacobsen SD (2006) *Science* 312: 1205–1208.

Goncharov AF, Struzhkin VV, Ruf T, and Syassen K (1994) *Physical Review B* 50: 13841–13844.

Goncharov AF, Struzhkin VV, Somayazulu M, Hemley RJ, and Mao HK (1996) *Science* 273: 218–220.

Goncharov AF, Zaug JM, Crowhurst JC, and Gregoryanz E (2005b) *Journal of Applied Physics* 97: 094917.

Gorria P, Martinez-Blanco D, Perez MJ, et al. (2009) *Physical Review B* 80: 064421.

Gramsch SA, Cohen RE, and Savrasov SY (2003) *American Mineralogist* 88: 257–261.

Gregoryanz E, Goncharov AF, Matsuishi K, Mao HK, and Hemley RJ (2003) *Physical Review Letters* 90: 175701.

Gu C, Catalli K, Grocholski B, et al. (2012) *Geophysical Research Letters* 39: L24304.

Hämäläinen K, Huotari S, Laukkanen J, et al. (2000) *Physical Review B* 62: R735–R738.

Hämäläinen K, Kao CC, Hastings JB, et al. (1992) *Physical Review B* 46: 14274–14277.

Harrison WA (1980) *Electronic Structure and the Properties of Solids: The Physics of the Chemical Bond*. San Francisco, CA: W.H. Freeman and Company.

Haskel D, Fabbris G, Souza-Neto NM, et al. (2011) *Physical Review B* 84: 100403.

Hastings JB, Siddons DP, van Bürck U, Hollatz R, and Bergmann U (1991) *Physical Review Letters* 66: 770–773.

Hayashi M, Tamura I, Shimomura O, Sawamoto H, and Kawamura H (1987) *Physics and Chemistry of Minerals* 14: 341–344.

Hazen RM and Jeanloz R (1984) *Reviews of Geophysics and Space Physics* 22: 37–46.

Hemley RJ, Chen YC, and Yan CS (2005) *Elements* 1: 39–43.

Hemley RJ and Cohen RE (1992) *Annual Review of Earth and Planetary Sciences* 20: 553–600.

Hemley RJ and Cohen RE (1996) *Philosophical Transactions of the Royal Society of London, Series A* 354: 1461–1479.

Hemley RJ, Eremets MI, and Mao HK (2002) In: Hochheimer HD, Kuchta B, Dorhout PK, and Yarger JL (eds.) *Frontiers of High Pressure Research II*, pp. 201–216. Amsterdam: Kluwer.

Hemley RJ, Goncharov AF, Lu R, Li M, Struzhkin VV, and Mao HK (1998a) *Il Nuovo Cimento D* 20: 539–551.

Hemley RJ, Hanfland M, and Mao HK (1991) *Nature* 350: 488–491.

Hemley RJ and Mao HK (1997) In: Trigg GL (ed.) *Encyclopedia of Applied Physics*, vol. 18, pp. 555–572. New York: VCH Publishers.

Hemley RJ and Mao HK (2001) *International Geology Review* 43: 1–30.

Hemley RJ, Mao HK, and Cohen RE (1998b) In: Hemley RJ (ed.) *Ultrahigh-Pressure Mineralogy. Reviews in Mineralogy*, vol. 37, pp. 591–638. Washington, DC: Mineralogical Society of America.

Hess NJ and Schiferl D (1992) *Journal of Applied Physics* 71: 2082–2085.

Hill JP, Kao CC, Caliebe WAC, Gibbs D, and Hastings JB (1996) *Physical Review Letters* 77: 3665–3668.

Hill JP, Kao C-C, Caliebe WA, et al. (1998) *Physical Review Letters* 80: 4967–4970.

Hofmeister AM (2005) *Journal of Geodynamics* 40: 51–72.

Hong X, Newville M, Prakapenka VB, Rivers ML, and Sutton SR (2009) *Review of Scientific Instruments* 80: 073908.

Hu MY, Sturhahn W, Toellner TS, et al. (2003) *Physical Review B* 67: 094304.

Huotari S, Hämäläinen K, Laukkanen J, et al. (2000) In: Manghnani MH, Nellis WJ, and Nicol MF (eds.) *Proceeding of AIRAPT 17*, vol. 2, pp. 1017–1020. Honolulu, HI: Universities Press (India) Limited.

Huscroft C, McMahan AK, and Scalettar RT (1999) *Physical Review Letters* 82: 2342–2345.

Ingalls R, Garcia GA, and Stern EA (1978) *Physical Review Letters* 40: 334–336.

Iota V, Klepeis JHP, Yoo CS, Lang J, Haskel D, and Srajer G (2007) *Applied Physics Letters* 90: 042505.

Isaacs ED, Platzman PM, Metcalf P, and Honig JM (1996) *Physical Review Letters* 76: 4211–4214.

Isaacs ED, Shukla A, Platzman PM, Hamann DR, Barbiellini B, and Tulk CA (1999) *Physical Review Letters* 83: 4445.

Isaak DG, Cohen RE, Mehl MJ, and Singh DJ (1993) *Physical Review B* 47: 7720.

Ishimatsu N, Matsumoto K, Maruyama H, et al. (2012) *Journal of Synchrotron Radiation* 19: 768–772.

Itie J, Baudelet F, Dartyge E, Fontaine A, Tolentino H, and San-Miguel A (1992) *High Pressure Research* 8: 697–702.

Itie J, Polian A, Calas G, Petiau J, Fontaine A, and Tolentino H (1989) *Physical Review Letters* 63: 398–401.

Itie JP, Polian A, Martinez D, et al. (1997) *Journal de Physique IV France, Supplement au Journal de Physique III* 7: 31–38.

Ivanov AS, Goncharenko IN, Somenkov VA, and Braden M (1995) *Physica B* 213: 1031–1033.

Jackson WE, Deleon JM, Brown GE, and Waychunas GA (1993) *Science* 262: 229–233.

Jackson JM, Hamecher EA, and Sturhahn W (2009a) *European Journal of Mineralogy* 21: 551–560.

Jackson DD, Malba V, Weir ST, Baker PA, and Vohra YK (2005a) *Physical Review B* 71: 184416.

Jackson JM, Sturhahn W, Lerche M, et al. (2013) *Earth and Planetary Science Letters* 362: 143–150.

Jackson JM, Sturhahn W, Shen GY, et al. (2005b) *American Mineralogist* 90: 199–205.

Jackson JM, Sturhahn W, Tschauner O, Lerche M, and Fei Y (2009b) *Geophysical Research Letters* 36: L10301.

Jacobsen SD, Lin JF, Dera P, et al. (2005) *Journal of Synchrotron Radiation* 12: 577.

Jeanloz R and Ahrens T (1980) *Geophysical Journal of the Royal Astronomical Society* 62: 505–528.

Jephcoat AP (1998) *Nature* 393: 355–358.

Jephcoat AP, Mao HK, Finger LW, Cox DE, Hemley RJ, and Zha CS (1987) *Physical Review Letters* 59: 2670–2673.

Jiang X and Guo GY (2004) *Physical Review B* 69: 155108.

Kamada S, Ohtani E, Fukui H, et al. (2014) *American Mineralogist* 99: 98–101.

Kantor AP, Jacobsen SD, Kantor IY, et al. (2004a) *Physical Review Letters* 93: 215502.

Kantor IY, McCammon CA, and Dubrovinsky LS (2004b) *Journal of Alloys and Compounds* 376: 5.

Kao CC, Caliebe WA, Hastings JB, and Gillet J-M (1996a) *Physical Review B* 54: 16361–16364.

Kao CC, Caliebe WA, Hastings JB, Hämäläinen L, and Krisch MH (1996b) *Review of Scientific Instruments* 67: 1–5.

Karato S (1999) *Nature* 402: 871–873.

Katayama Y, Tsujii K, Oyanagi H, and Shimomura O (1998) *Journal of Non-Crystalline Solids* 232–234: 93–98.

Katoh E, Yamawaki H, Fujihisa H, Sakashita M, and Aoki A (2002) *Science* 295: 1264–1266.

Katsura T, Sato K, and Ito E (1998) *Nature* 395: 493–495.

Keppler H, Dubrovinsky LS, Narygina O, and Kantor I (2008) *Science* 322: 1529–1532.

Keppler H, McCammon CA, and Rubie DC (1994) *American Mineralogist* 20: 478–482.

Kerrick DM and Connolly JAD (2001) *Nature* 411: 293–296.

Kesson SE and FitzGerald JD (1992) *Earth and Planetary Science Letters* 111: 229–240.

Kirkpatrick RJ (1988) In: Hawthorne FC (ed.) *Spectroscopic Methods in Mineralogy and Geology. Reviews in Mineralogy*, vol. 18, pp. 341–403. Washington, DC: Mineralogical Society of America.

Kittel C (1996) *Introduction to Solid State Physics*. New York: Wiley.

Knittle E and Jeanloz R (1986) *Geophysical Research Letters* 13: 1541–1544.

Knittle E, Jeanloz R, Mitchell AC, and Nellis WJ (1986) *Solid State Communications* 59: 513–515.

Kotani A and Shin S (2001) *Reviews of Modern Physics* 73: 203–246.

Krisch MH, Kao CC, Sette F, Caliebe WA, Hämäläinen L, and Hastings JB (1995) *Physical Review Letters* 74: 4931–4934.

Krisch MH, Sette F, Bergmann U, et al. (1996) *Physical Review B* 54: R12673–R12676.

Krisch M, Sette F, Masciovecchio C, and Verbeni R (1997) *Physical Review Letters* 78: 2843–2846.
Lacam A (1983) *Physics and Chemistry of Minerals* 9: 127–132.
Laio A, Bernard S, Chiarotti G, Scandolo S, and Tosatti E (2000) *Science* 287: 1027–1030.
Landau LD and Lifshitz IM (1977) *Quantum Mechanics: Non-Relativistic Theory*. Oxford: Pergamon Press.
Lee SK, Cody GD, Fei Y, and Mysen BO (2004) *Geochimica et Cosmochimica Acta* 68: 4189–4200.
Lee SK, Eng PJ, and Mao HK (2014) *Reviews in Mineralogy and Geochemistry* 78: 139–174.
Lee SK, Eng PJ, Mao HK, and Shu JF (2008a) *Physical Review B* 78: 214203.
Lee SK, Lin J-F, Cai YQ, et al. (2008b) *Proceedings of the National Academy of Sciences of the United States of America* 105: 7925–7929.
Lee SK, Mibe K, Fei Y, Cody GD, and Mysen BO (2005) *Physical Review Letters* 94: 165507.
Lee SK, Park SY, Kim H-I, et al. (2012) *Geophysical Research Letters* 39: L05306.
Lelong G, Cormier L, Ferlat G, et al. (2012) *Physical Review B* 85: 134202.
Li L, Brodholt JP, Stackhouse S, Weidner DJ, Alfredsson M, and Price GD (2005) *Geophysical Research Letters* 32: L17307.
Li X and Jeanloz R (1987) *Geophysical Research Letters* 14: 1075–1078.
Li X and Jeanloz R (1990) *Journal of Geophysical Research: Solid Earth* 95: 21609–21612.
Li J, Struzhkin VV, Mao HK, et al. (2004) *Proceedings of the National Academy of Sciences of the United States of America* 101: 14027–14030.
Lin JF, Alp EE, Mao Z, et al. (2012) *American Mineralogist* 97: 592–597.
Lin JF, Fukui H, Prendergast D, et al. (2007) *Physical Review B* 75: 012201.
Lin JF, Gavriliuk AG, Struzhkin VV, et al. (2006) *Physical Review B* 73: 113107.
Lin JF, Shu J, Mao HK, Hemley RJ, and Shen G (2003a) *Review of Scientific Instruments* 74: 4732–4736.
Lin JF, Struzhkin VV, Sturhahn W, et al. (2003b) *Geophysical Research Letters* 30: 2112–2115.
Lin JF, Heinz DL, Mao HK, et al. (2003c) *Proceedings of the National Academy of Sciences* 100: 4405–4408.
Lin JF, Gregoryanz E, Struzhkin VV, Somayazulu M, Mao HK, and Hemley RJ (2005a) *Geophysical Research Letters* 32: L11306.
Lin JF, Struzhkin VV, Jacobsen SD, et al. (2005b) *Nature* 436: 377–380.
Lin JF, Sturhahn W, Zhao J, Shen G, Mao HK, and Hemley RJ (2005c) *Science* 308: 1892–1894.
Lin JF, Struzkhin VV, Jacobsen SD, et al. (2005d) *Journal of Synchrotron Radiation* 12: 637–641.
Lin JF, Watson H, Vanko G, et al. (2008) *Nature Geoscience* 1: 688–691.
Lin Y, Zhang L, Mao HK, et al. (2011) *Physical Review Letters* 107: 175504.
Lipp M and Daniels WB (1991) *Physical Review Letters* 67: 2810–2813.
Liu J and Vohra YK (1996) *Journal of Applied Physics* 79: 7978–7982.
Loubeyre P, Ocelli F, and LeToullec R (2002) *Nature* 416: 613–617.
Lübbers R, Grünsteudel HF, Chumakov AI, and Wortmann G (2000) *Science* 287: 1250–1253.
Luo SN, Akins JA, Ahrens TJ, and Asimow PD (2004) *Journal of Geophysical Research, B: Solid Earth* 109: B05205.
Maddox BR, Lazicki A, Yoo CS, et al. (2006) *Physical Review Letters* 96: 215701.
Malavergne V, Guyot F, Wang Y, and Martinez I (1997) *Earth and Planetary Science Letters* 146: 499–509.
Manley ME, Lander GH, Sinn H, et al. (2003) *Physical Review B* 67: 052302.
Mao HK (1976) In: Strens RGJ (ed.) *The Physics and Chemistry of Rocks and Minerals*, pp. 573–581. New York: Wiley.
Mao HK and Bell PM (1972) *Science* 176: 403–406.
Mao HK and Bell PM (1981) *Review of Scientific Instruments* 52: 615–616.
Mao HK, Bell PM, Shaner JW, and Steinberg DJ (1978) *Journal of Applied Physics* 49: 3276–3283.
Mao HK, Ding Y, Xiao Y, et al. (2011) *Proceedings of the National Academy of Sciences of the United States of America* 108: 20434–20437.
Mao HK and Hemley RJ (1989) *Science* 244: 1462–1465.
Mao HK and Hemley RJ (1994) *Reviews of Modern Physics* 66: 671–692.
Mao Z, Lin J-F, Liu J, et al. (2012) *Proceedings of the National Academy of Sciences of the United States of America* 109: 10239–10244.
Mao WL, Mao HK, Eng P, et al. (2003a) *Science* 302: 425–427.
Mao WL, Mao HK, Meng Y, et al. (2006a) *Science* 314: 636–638.
Mao WL, Mao HK, Sturhahn W, et al. (2006b) *Science* 312: 564–565.
Mao WL, Mao HK, Yan CS, Shu J, Hu J, and Hemley RJ (2003b) *Applied Physics Letters* 83: 5190–5192.
Mao HK, Shen G, and Hemley RJ (1997) *Science* 278: 2098–2100.
Mao HK, Shirley EL, Ding Y, et al. (2010) *Physical Review Letters* 105: 186404.
Mao HK, Shu J, Shen G, Hemley RJ, Li B, and Singh AK (1998) *Nature* 396: 741–743.
Mao HK, Xu J, and Bell PM (1986) *Journal of Geophysical Research* 91: 4673–4676.
Mao HK, Xu J, Struzhkin VV, et al. (2001) *Science* 292: 914–916.
Marshall WG, Nelmes RJ, Loveday JS, et al. (2000) *Physical Review B* 61: 11201–11204.
Mashimo T, Kondo KI, Sawaoka A, Syono Y, Takei H, and Ahrens TJ (1980) *Journal of Geophysical Research* 85: 1876–1881.
Massey MJ, Baier U, Merlin R, and Weber WH (1990a) *Physical Review B* 41: 7822–7827.
Massey MJ, Chen NH, Allen JW, and Merlin R (1990b) *Physical Review B* 42: 8776–8779.
Massey MJ, Merlin R, and Girvin SM (1992) *Physical Review Letters* 69: 2299–2302.
Mattheiss LF (1972) *Physical Review B* 5: 290–306.
Maxwell-Garnet JC (1904) *Philosophical Transactions of the Royal Society of London* 203: 385.
Mayanovic RA, Anderson AJ, Bassett WA, and Chou IM (2007) *Review of Scientific Instruments* 78: 053904.
Mazin II, Fei Y, Downs R, and Cohen RE (1998) *American Mineralogist* 83: 451–457.
McCammon CA (1995) In: Ahrens TJ (ed.) *Mineral Physics and Crystallography. AGU Reference Shelf 2*, pp. 332–347. Washington, DC: American Geophysical Union.
McCammon CA (1997) *Nature* 387: 694–696.
McCammon CA (1998) *Physics and Chemistry of Minerals* 25: 292–300.
McCammon CA (2005) *Science* 308: 807–808.
McMahon MI and Nelmes RJ (2004) *Zeitschrift fur Kristallographie* 219: 742–748.
Mehl MJ, Cohen RE, and Krakauer H (1988) *Journal of Geophysical Research* 93: 8009–8022.
Meng Y, Mao HK, Eng PJ, et al. (2004) *Nature Materials* 3: 111–114.
Meyers SA, Cygan RT, Assink RA, and Boslough MB (1998) *Physics and Chemistry of Minerals* 25: 313–317.
Mobilio S and Meneghini C (1998) *Journal of Non-Crystalline Solids* 232–234: 25–37.
Mössbauer RL (1958) *Zeitschrift für Physik* 151: 124.
Mott NF (1990) *Metal-Insulator Transitions*. New York: Taylor & Francis.
Murakami M, Hirose K, Kawamura K, Sata N, and Ohishi Y (2004a) *Science* 304: 855–858.
Murakami M, Hirose K, Ono S, Tsuchiya T, Isshiki M, and Watanuki T (2004b) *Physics of the Earth and Planetary Interiors* 146: 273–282.
Murphy CA, Jackson JM, Sturhahn W, and Chen B (2011) *Geophysical Research Letters* 38: L24306.
Nasu S (1996) *High Pressure Research* 14: 405–412.
Neaton JB and Ashcroft NW (1999) *Nature* 400: 141.
Neaton JB and Ashcroft NW (2001) *Physical Review Letters* 86: 2830.
Nellis WJ, Weir ST, and Mitchell AC (1996) *Science* 273: 936–938.
Nguyen J, Kruger MB, and Jeanloz R (1997) *Physical Review Letters* 78: 1936–1939.
Nitsan U and Shankland TJ (1976) *Geophysical Journal of the Royal Astronomical Society* 45: 59–87.
Niu F and Wen L (2001) *Nature* 410: 1081–1084.
Oganov AR (2010) *Modern Methods of Crystal Structure Prediction*. Berlin: Wiley-VCH.
Oganov AR and Ono S (2004) *Nature* 430: 445.
Ohta K, Cohen RE, Hirose K, Haule K, Shimizu K, and Ohishi Y (2012) *Physical Review Letters* 108: 026403.
Ohta K, Hirose K, Ichiki M, Shimizu K, Sata N, and Ohishi Y (2010a) *Earth and Planetary Science Letters* 289: 497–502.
Ohta K, Hirose K, Shimizu K, Sata N, and Ohishi Y (2010b) *Physics of the Earth and Planetary Interiors* 180: 154–158.
Ohta K, Onoda S, Hirose K, et al. (2008) *Science* 320: 89–91.
Ohtaka O, Arima H, Fukui H, Utsumi W, Katayama Y, and Yoshiasa A (2004) *Physical Review Letters* 92: 155506.
Ohtani E, Shibazaki Y, Sakai T, et al. (2013) *Geophysical Research Letters* 40: 2013GL057667.
Okuchi T, Cody GD, Mao HK, and Hemley RJ (2005a) *Journal of Chemical Physics* 122: 244509.
Okuchi T, Hemley RJ, and Mao HK (2005b) *Review of Scientific Instruments* 76: 026111.
Okuchi T, Mao HK, and Hemley RJ (2005c) In: Chen J, Wang Y, Duffy T, Shen G, and Dobrzhinetskaya L (eds.) *Advances in High-Pressure Technology for Geophysical Applications*, pp. 503–509. Amsterdam: Elsevier.
Olson P and Aurnou J (1999) *Nature* 402: 1701173.
Pacold JI, Bradley JA, Mattern BA, et al. (2012) *Journal of Synchrotron Radiation* 19: 245–251.
Parise JB (2006) In: Wenk HR (ed.) *Reviews in Mineralogy and Geochemistry: Neutron Scattering in Earth Sciences*, vol. 63, pp. 205–231. Geochemical Society and Mineralogical Society of America.

Parise JB, Theroux B, Li R, Loveday JS, Marshall WG, and Klotz S (1998) *Physics and Chemistry of Minerals* 25: 130–137.
Parker L and Badding JV (1996) *Science* 273: 95–97.
Pascarelli S, Aquilanti G, Crichton W, et al. (2002) *High Pressure Research* 22: 331–335.
Pascarelli S and Mathon O (2010) *Physical Chemistry Chemical Physics* 12: 5535–5546.
Pasternak MP, Rozenberg GK, Milner AP, et al. (1997a) *Physical Review Letters* 79: 4409–4412.
Pasternak MP and Taylor RD (2001) *Physica Status Solidi B: Basic Research* 223: 65–74.
Pasternak MP, Taylor RD, Jeanloz R, Li X, Nguyen JH, and McCammon C (1997b) *Physical Review Letters* 79: 5046–5049.
Patterson JR, Aracne CM, Jackson DD, et al. (2004) *Physical Review Letters* 69: 220101.
Patterson JR, Catledge SA, Vohra YK, Akella J, and Weir ST (2000) *Physical Review Letters* 85: 5364–5367.
Pauling L (1960) *The Nature of the Chemical Bond*. Ithaca, NY: Cornell University Press.
Persson K, Ceder G, Bengtson A, and Morgan D (2006) *Geophysical Research Letters* 33: L16306.
Pertermann M and Hofmeister AM (2006) *American Mineralogist* 91: 1747–1760.
Peyronneau J and Poirier JP (1989) *Nature* 342: 537–539.
Phillips BL, Burnley PC, Worminghaus K, and Navrotsky A (1997) *Physics and Chemistry of Minerals* 24: 179–190.
Pickett WE, Erwin SC, and Ethridge EC (1998) *Physical Review Letters* 58: 1201–1209.
Poe BT, McMillan PF, Coté B, Massiot D, and Coutures JP (1993) *Science* 259: 786–788.
Poe BT, Xu Y, and Rubie DC (1998) In: Nakahara M (ed.) *Review of High-Pressure Science and Technology*, vol. 7, pp. 22–24. Kyoto: Japan Society High-Pressure Science and Technology.
Pravica MG and Silvera IF (1998a) *Review of Scientific Instruments* 69: 479–484.
Pravica MG and Silvera IF (1998b) *Physical Review Letters* 81: 4181–4183.
Reichlin R, Brister K, McMahan AK, et al. (1989) *Physical Review Letters* 62: 669–672.
Resta R (2002) *Journal of Physics: Condensed Matter* 14: R625–R656.
Reyes AP, Ahrens ET, Heffner RH, Hammel PC, and Thompson JD (1992) *Review of Scientific Instruments* 63: 3120–3122.
Rietveld HM (1966) *Acta Crystallographica* S21: A228.
Romanowicz B, Li XD, and Durek J (1996) *Science* 274: 963–966.
Ross M, Boehler R, and Söderlind P (2005) *Physical Review Letters* 95: 257801.
Rossman GR (1988) In: Hawthorne FC (ed.) *Spectroscopic Methods in Mineralogy and Geology. Reviews in Mineralogy*, vol. 18, pp. 207–254. Washington, DC: Mineralogical Society of America.
Rotundu C, Cuk T, Greene RL, Shen ZX, Hemley RJ, and Struzhkin VV (2013) *Review of Scientific Instruments* 84: 063903.
Rueff JP (2010) In: Beaurepaire E, Bulou H, Scheurer F, and Kappler JP (eds.) *Magnetism and Synchrotron Radiation*, p. 263. Berlin, Heidelberg: Springer-Verlag.
Rueff JP, Kao CC, Struzhkin VV, et al. (1999) *Physical Review Letters* 83: 3343.
Ruocco G, Sette F, Bergmann U, et al. (1996) *Nature* 379: 521–523.
Sampoli M, Ruocco G, and Sette F (1997) *Physical Review Letters* 79: 1678–1681.
Sanloup C, Guyot F, Gillet P, and Fei Y (2002a) *Journal of Geophysical Research* 107. http://dx.doi.org/10.1029/2001JB000808.
Sanloup C, Mao HK, and Hemley RJ (2002b) *Geophysical Research Letters* 29. http://dx.doi.org/10.1029/2002GL014973.
Sanloup C, Mao HK, and Hemley RJ (2002c) *Proceedings of the National Academy of Sciences of the United States of America* 99: 25–28.
Schwarz K, Blaha P, and Madsen GKH (2002) *Computer Physics Communications* 147: 71–76.
Schwoerer-Bohning M, Klotz S, Besson JM, Burkel E, Braden M, and Pintschovius L (1996) *Europhysics Letters* 33: 679–682.
Seto M, Yoda Y, Kikuta S, Zhang XW, and Ando M (1995) *Physical Review Letters* 74: 3828–3831.
Sharma S, Dewhurst JK, and Ambrosch-Draxl C (2003) *Physical Review B* 68: 014111.
Shen G, Fei Y, Halenius U, and Wang Y (1994) *Physics and Chemistry of Minerals* 20: 478–482.
Shen G, Ikuta D, Sinogeikin S, Li Q, Zhang Y, and Chen C (2012) *Physical Review Letters* 109: 205503.
Shibazaki Y, Ohtani E, Fukui H, et al. (2012) *Earth and Planetary Science Letters* 313–314: 79–85.
Shim S-H, Bengtson A, Morgan D, et al. (2009) *Proceedings of the National Academy of Sciences of the United States of America* 106: 5508–5512.
Shirley EL (1998) *Physical Review Letters* 80: 794–797.
Sienkiewicz A, Vileno B, Garaj S, Jaworski M, and Forro L (2005) *Journal of Magnetic Resonance* 177: 278–290.
Sinmyo R, Hirose K, O'Neill HSC, and Okunishi E (2006) *Geophysical Research Letters* 33: L12S13.
Smith HG and Langer K (1982) *American Mineralogist* 67: 343–348.
Song X and Helmberger DV (1998) *Science* 282: 924–927.
Song XD and Richards PG (1996) *Nature* 382: 221–224.
Sørensen HO, Schmidt S, Wright JP, et al. (2012) *Zeitschrift für Kristallographie* 227: 63.
Souza-Neto NM, Zhao J, Alp EE, et al. (2012) *Physical Review Letters* 109: 026403.
Spackman MA, Hill RJ, and Gibbs GV (1987) *Physics and Chemistry of Minerals* 14: 139–150.
Speziale S, Lee VE, Jeanloz R, Milner A, Pasternak MP, and Clark SM (2005) *Proceedings of the National Academy of Sciences of the United States of America* 102: 17918.
Stackhouse S, Brodholt JP, Dobson DP, and Price GD (2006) *Geophysical Research Letters* 33: L12S03.
Stebbins JF (1988) In: Hawthorne FC (ed.) *Spectroscopic Methods in Mineralogy and Geology. Reviews in Mineralogy*, vol. 18, pp. 405–429. Washington, DC: Mineralogical Society of America.
Steinle-Neumann G, Cohen RE, and Stixrude L (2004a) *Journal of Physics: Condensed Matter* 16: S1109–S1119.
Steinle-Neumann G, Stixrude L, and Cohen RE (2003) In: Dehant V, Creger K, Karato S-I, and Zatman S (eds.) *Earth's Core Dynamics, Structure, Rotation. Geodynamics Series*, vol. 31, pp. 137–162. Washington, DC: American Geophysical Union.
Steinle-Neumann G, Stixrude L, and Cohen RE (2004b) *Proceedings of the National Academy of Sciences of the United States of America* 101: 33–36.
Steinle-Neumann G, Stixrude L, Cohen RE, and Gülseren O (2001) *Nature* 413: 57–60.
Stern F (1963) In: Seitz F and Turnbull D (eds.) *Solid State Physics*, pp. 299–408. New York and London: Academic Press.
Stixrude L (2001) *Reviews in Mineralogy and Geochemistry* 42: 319–343.
Stixrude L and Cohen RE (1995) *Science* 267: 1972–1975.
Struzhkin VV, Goncharov AF, Hemley RJ, et al. (2000) *Physical Review B* 62: 3895–3899.
Struzhkin VV, Goncharov AF, and Syassen K (1993a) *Materials Science and Engineering* A168: 107–110.
Struzhkin VV, Mao HK, Hu J, et al. (2001) *Physical Review Letters* 87: 255501.
Struzhkin VV, Schwarz U, Wilhelm H, and Syassen K (1993b) *Materials Science and Engineering* A168: 103–106.
Sturhahn W (2004) *Journal of Physics: Condensed Matter* 16: S497–S530.
Sturhahn W, Jackson JM, and Lin JF (2005) *Geophysical Research Letters* 32: L12307.
Sturhahn W, Toellner TS, Alp EE, et al. (1995) *Physical Review Letters* 74: 3832–3835.
Su W, Dziewonski AM, and Jeanloz R (1996) *Science* 274: 1883–1887.
Sur S and Cooney TS (1989) *Physics and Chemistry of Minerals* 16: 693–696.
Surh MP, Louie SG, and Cohen ML (1992) *Physical Review B* 45: 8239–8247.
Syassen K and Sonneschein R (1982) *Review of Scientific Instruments* 53: 644–650.
Takano M, Nasu S, Abe T, et al. (1991) *Physical Review Letters* 67: 3267–3270.
Timofeev YA (1992) *Pribory i Tekhnika Eksperimenta* 5: 186–189.
Timofeev YA, Struzhkin VV, Hemley RJ, Mao HK, and Gregoryanz EA (2002) *Review of Scientific Instruments* 73: 371–377.
Tissen VG and Ponyatovskii EG (1987) *JETP Letters* 46: 287–289.
Titchmarsh EC (1937) *Introduction to the Theory of Fourier Integrals*. Oxford: Clarendon Press.
Tromp J (2001) *Annual Review of Earth and Planetary Sciences* 29: 47–69.
Tse JS, Klug DD, Jiang DT, et al. (2005) *Applied Physics Letters* 87: 191905.
Tsuchiya T, Tsuchiya J, Umemoto K, and Wentzcovitch RM (2004) *Earth and Planetary Science Letters* 224: 241–248.
Tsuchiya T, Wentzcovitch RM, da Silva CRS, and de Gironcoli S (2006) *Physical Review Letters* 96: 198501.
Tyburczy JA and Fisler DK (1995) In: Ahrens TJ (ed.). *Mineral Physics and Crystallography: A Handbook of Physical Constants*, vol. 185–208. Washington, DC: American Geophysical Union.
Ulug AM, Conradi MS, and Norberg RE (1991) In: Hochheimer HD and Etters RD (eds.) *Frontiers of High Pressure Research*, pp. 131–141. New York: Plenum.
Vocadlo L, Alfe D, Gillan MJ, Wood IG, Brodholt JP, and Price GD (2003) *Nature* 424: 536–539.
Vos WL, Finger LW, Hemley RJ, Hu J-Z, Mao HK, and Schouten JA (1992) *Nature* 358: 46–48.
Wang Y and Ma Y (2014) *Journal of Chemical Physics* 140: 040901.
Wang S, Mao WL, Sorini AP, et al. (2010) *Physical Review B* 82: 144428.
Wang D, Mookherjee M, Xu Y, and Karato SI (2006) *Nature* 443: 977–980.

Wang Y, Weidner DJ, and Meng Y (1998) In: Manghnani MH and Yagi T (eds.) *Properties of the Earth and Planetary Materials at High Pressure and Temperature*, pp. 365–372. Washington, DC: American Geophysical Union.
Webb AW, Gubser DU, and Towle LC (1976) *Review of Scientific Instruments* 47: 59–62.
Weir S, Mitchell AC, and Nellis WJ (1996) *Physical Review Letters* 76: 1860–1863.
Wicks JK, Jackson JM, and Sturhahn W (2010) *Geophysical Research Letters* 37: L15304.
Williams Q and Hemley RJ (2001) *Annual Review of Earth and Planetary Sciences* 29: 365–418.
Williams Q, Knittle E, Reichlin R, Martin S, and Jeanloz R (1990) *Journal of Geophysical Research* 95: 21549–21563.
Winkler B, Harris MJ, Eccleston RS, and Knorr K (1997) *Physics and Chemistry of Minerals* 25: 79–82.
Wong J, Krisch M, Farber DL, et al. (2003) *Science* 301: 1078–1080.
Wu Z and Cohen RE (2005) *Physical Review Letters* 95: 037601.
Wyckoff RWG (1923) *Proceedings of the National Academy of Sciences of the United States of America* 9: 33–38.
Xu J and Mao HK (2000) *Science* 290: 783–785.
Xu J, Mao HK, Hemley RJ, and Hines E (2004) *Review of Scientific Instruments* 75: 006404RSI.
Xu Y, Poe BT, Shankland TJ, and Rubie DC (1998a) *Science* 280: 1415–1418.
Xu Y, McCammon C, and Poe BT (1998b) *Science* 282: 922–924.
Xu J, Yen J, Wang Y, and Huang E (1996) *High Pressure Research* 15: 127–134.
Yagi T, Mao HK, and Bell PM (1979) *Carnegie Institution of Washington Yearbook* 78: 612–614.
Yamanaka T (2007) Geological Society of America, Special Papers 421, pp. 175–188.
Yamanaka T, Hirose K, Mao WL, et al. (2012) *Proceedings of the National Academy of Sciences of the United States of America* 109: 1035–1040.
Yan CS, Vohra YK, Mao HK, and Hemley RJ (2002) *Proceedings of the National Academy of Sciences of the United States of America* 99: 12523–12525.
Yarger JL, Smith KH, Nieman RA, et al. (1995) *Science* 270: 1964–1967.
Yi YS and Lee SK (2012) *American Mineralogist* 97: 897–909.
Yoo CS, Maddox B, Klepeis JHP, et al. (2005) *Physical Review Letters* 94: 115502.
Zeng QS, Ding Y, Mao WL, et al. (2010) *Physical Review Letters* 104: 105702.
Zha CS, Hemley RJ, Gramsch SA, Mao HK, and Bassett WA (2008) *Journal of Chemical Physics* 126, 074506.
Zha CS, Mao HK, Hemley RJ, and Duffy TS (1997) *EOS Transaction American Geophysical Union* 78: F752.
Zhang L (1997) *Crystallography at High Pressure Using Synchrotron Radiation: The Next Steps*. Grenoble, France: ESRF.
Zhang L and Chopelas A (1994) *Physics of the Earth and Planetary Interiors* 87: 77–83.
Zhang L and Hafner SS (1992) *American Mineralogist* 77: 462–473.
Zhang L, Meng Y, Dera P, Yang W, Mao WL, and Mao HK (2013) *Proceedings of the National Academy of Sciences of the United States of America* 110: 6292–6295.
Zhang FW and Oganov AR (2006) *Earth and Planetary Science Letters* 249: 436–443.
Zhao J, Sturhahn W, Lin JF, Shen G, Alp EE, and Mao HK (2004) *High Pressure Research* 24: 447–457.
Zhou T, Syassen K, Cardona M, Karpinski J, and Kaldis E (1996) *Solid State Communications* 99: 669–673.
Zou G, Mao HK, Bell PM, and Virgo D (1980) *Carnegie Institution of Washington Yearbook* 79: 374–376.